JPL Publication 86-31

Electricity from Photovoltaic Solar Cells

Flat-Plate Solar Array Project Final Report

Volume VII: Module Encapsulation

11 Years of Progress

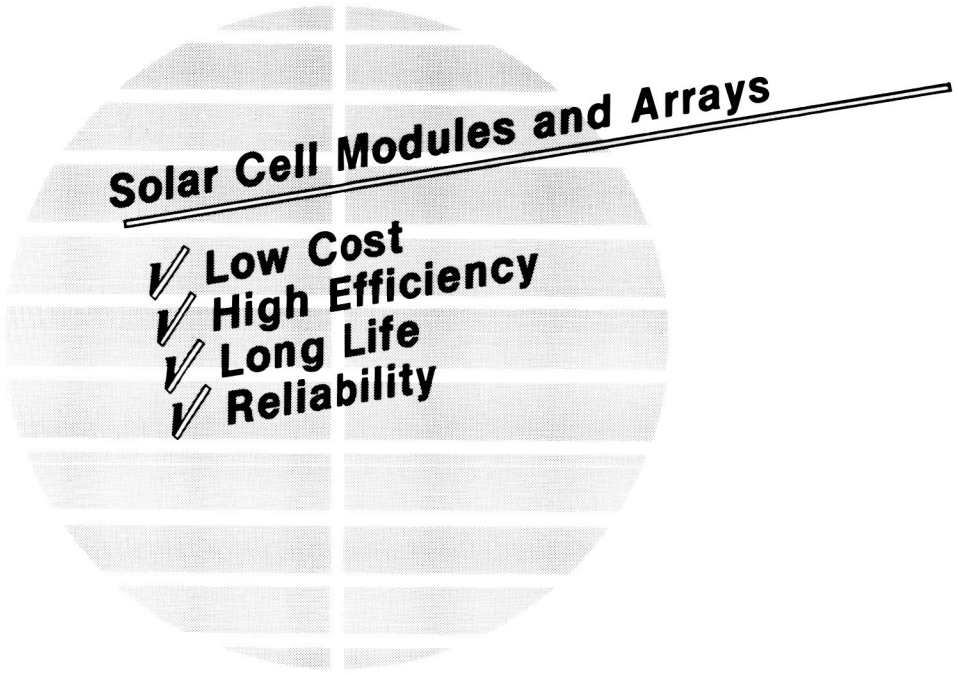

October 1986

Project Managed by the Jet Propulsion Laboratory for the U.S. Department of Energy

Photovoltaic Module Progress

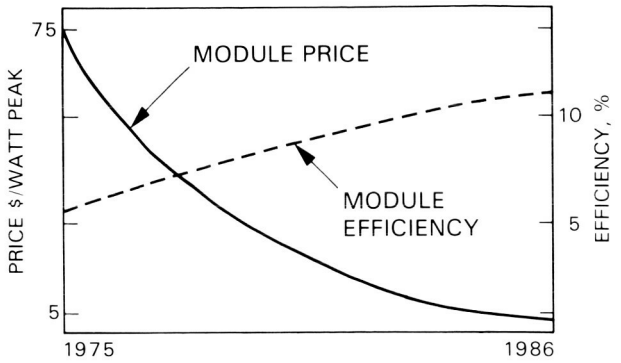

Flat or non-concentrating module prices have dropped as module efficiencies have increased. Prices are in 1985 dollars for large quantities of commercial products.

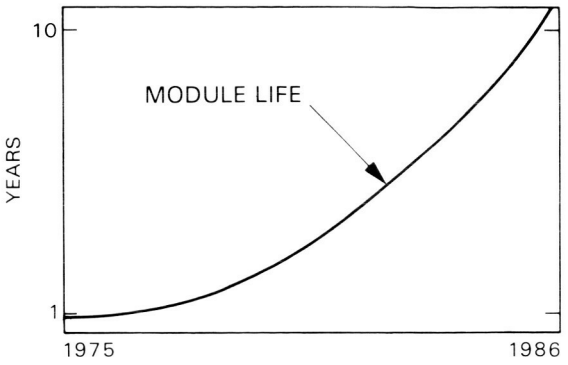

Typical module lifetimes were less than 1 year but are now estimated to be greater than 10 years. (Ten-year warranties are now available.)

Technology advancement in crystalline silicon solar cells and modules (non-concentrating).

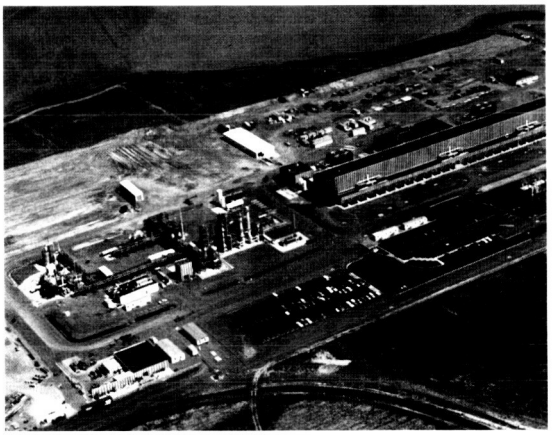

Union Carbide Corporation (UCC) funded the now operational silicon refinement production plant with 1200 MT/year capacity. DOE/FSA-sponsored efforts were prominent in the UCC process research and development.

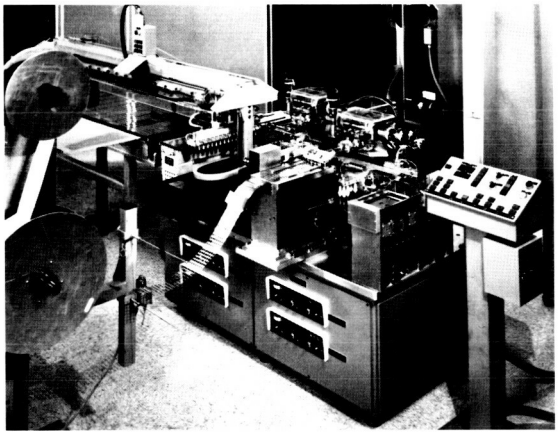

The automated machine interconnects solar cells and places them for module assembly. The second-generation machine made by Kulicke and Soffa was cost shared by Westinghouse Corporation and DOE/FSA.

A Block I module (fabricated in 1975), held in front of four Block V modules, represents the progress of an 11-year effort. The modules, designed and manufactured by industry to FSA specifications and evaluated by FSA, rapidly evolved during the series of module purchases by DOE/FSA.

More technology advancements of the cooperative industry/university/ DOE/FSA efforts are shown on the inside back cover. Use of modules in photovoltaic power systems are shown on the outside back cover.

5101-289
Flat-Plate
Solar Array Project

DOE/JPL-1012-125
Distribution Category UC-63b

Electricity from Photovoltaic Solar Cells

Flat-Plate Solar Array Project Final Report

Volume VII: Module Encapsulation

E. Cuddihy
C. Coulbert
A. Gupta
R. Liang

11 Years of Progress

October 1986

Prepared for
U.S. Department of Energy
Through an Agreement with
National Aeronautics and Space Administration
by
Jet Propulsion Laboratory
California Institute of Technology
Pasadena, California

Project Managed
by the
Jet Propulsion Laboratory
for the
U.S. Department of Energy's
National Photovoltaics Program

JPL Publication 86-31

Final Report Organization

This FSA Final Report (JPL Publication 86-31, 5101-289, DOE/JPL 1012-125, October 1986) is composed of eight volumes, consisting of an Executive Summary and seven technology reports:

Volume I: Executive Summary.

Volume II: Silicon Material.

Volume III: Silicon Sheet: Wafers and Ribbons

Volume IV: High-Efficiency Solar Cells.

Volume V: Process Development.

Volume VI: Engineering Sciences and Reliability.

Volume VII: Module Encapsulation.

Volume VIII: Project Analysis and Integration.

Two supplemental reports included in the final report package are:

FSA Project: 10 Years of Progress, JPL Document 400-279, 5101-279, October 1985.

Summary of FSA Project Documentation: Abstracts of Published Documents, 1975 to 1986, JPL Publication 82-79 (Revision 1), 5101-221, DOE/JPL-1012-76, September 1986.

Upon request, this FSA Final Report (JPL Publication 86-31) and the two supplemental reports (JPL Document 400-279 and JPL Publication 82-79) are individually available in print from:

National Technical Information Service
U.S. Department of Commerce
5285 Port Royal Road
Springfield, VA 22161

Abstract

The Flat-Plate Solar Array (FSA) Project, funded by the U.S. Government and managed by the Jet Propulsion Laboratory, was formed in 1975 to develop the module/array technology needed to attain widespread terrestrial use of photovoltaics by 1985. To accomplish this, the FSA Project established and managed an Industry, University, and Federal Government Team to perform the needed research and development.

The objective of the Encapsulation Task was to develop, demonstrate, and qualify photovoltaic (PV) module encapsulation systems that would provide 20-year (later increased to 30-year) life expectancies in terrestrial environments, and which would be compatible with the cost and performance goals of the FSA Project. The scope of the Encapsulation Task included the identification, development, and evaluation of material systems and configurations required to support and protect the optically and electrically active solar cell circuit components in the PV module operating environment. Encapsulation material technologies summarized in this report include the development of low-cost ultraviolet protection techniques, stable low-cost pottants, soiling resistant coatings, electrical isolation criteria, processes for optimum interface bonding, and analytical and experimental tools for evaluating the long-term durability and structural adequacy of encapsulated modules. Field testing, accelerated stress testing, and design studies have demonstrated that encapsulation materials, processes, and configurations are available that will meet the FSA cost and performance goals. Thirty-year module life expectancies are anticipated based on accelerated stress testing results and on extrapolation of real-time field exposures in excess of 9 years.

Foreword

Throughout U.S. history, the Nation's main source of energy has changed from wood to coal to petroleum. It is inevitable that changes will continue as fossil fuels are depleted. Within a lifetime, it is expected that most U.S. energy will come from a variety of sources, including renewable energy sources, instead of from a single type of fuel. More than 30% of the energy consumed in the United States is used for the generation of electricity. The consumption of electricity is increasing at a faster rate than the use of other energy forms and this trend is expected to continue.

Photovoltaics, a promising way to generate electricity, is expected to provide significant amounts of power in years to come. It uses solar cells to generate electricity directly from sunlight, cleanly and reliably, without moving parts. Photovoltaic (PV) power systems are simple, flexible, modular, and adaptable to many different applications in an almost infinite number of sizes and in diverse environments. Although photovoltaics is a proven technology that is cost-effective for hundreds of small applications, it is not yet cost-effective for large-scale utility use in the United States. For widespread economical use, the cost of generating power with photovoltaics must continue to be decreased by reducing the initial PV system cost, by increasing efficiency (reduction of land requirements), and by increasing the operational lifetime of the PV systems.

In the early 1970s, the pressures of the increasing demand for electrical power, combined with the uncertainty of fuel sources and ever-increasing prices for petroleum, led the U.S. Government to initiate a terrestrial PV research and development (R&D) project. The objective was to reduce the cost of manufacturing solar cells and modules. This effort, assigned to the Jet Propulsion Laboratory, evolved from more than a decade-and-a-half of spacecraft PV power-system experience and from recommendations of a conference on Solar Photovoltaic Energy held in 1973 at Cherry Hill, New Jersey.

This Project, originally called the Low-Cost Solar Array Project, but later known as the Flat-Plate Solar Array (FSA) Project, was based upon crystalline-silicon technology as developed for the space program. During the 1960s and 1970s, it had been demonstrated that photovoltaics was a dependable electrical power source for spacecraft. In this time interval, solar-cell quality and performance improved while the costs decreased. However, in 1975 the costs were still much too high for widespread use on Earth. It was necessary to reduce the manufacturing costs of solar cells by a factor of approximately 100 if they were to be a practical, widely used terrestrial power source.

The FSA Project was initiated to meet specific cost, efficiency, production capacity, and lifetime goals by R&D in all phases of flat-plate module (non-concentrating) technology, from solar-cell silicon material purification through verification of module reliability and performance.

The FSA Project was phased out at the end of September 1986.

Acknowledgments

Authorities in the field were used throughout this program as consultants to provide critiques, participate in critical technology reviews, and address specific technical problems. Otto Vogl of the University of Massachusetts, and James Guillet of the University of Toronto were consultants in photodegradation and its control. Jack Koenig of Case Western Reserve University, James Boerio of the University of Cincinnati, Edwin Plueddemann of Dow Corning in Midland, Michigan, and Wolfgang Knauss of the California Institute of Technology consulted in the area of interfacial bonding.

The Jet Propulsion Laboratory staff members were involved in laboratory research, materials technology development, process and design analyses, and the technical management of contracts. The following engineers contributed to the encapsulation technology program: Clifford Coulbert (Task Manager), Andre Amy, Ed Cuddihy, Ami Gupta, John Repar, Ranty Liang, Dan Coulter, Jovan Moacanin, Peter Frickland, Keri Oda, William Carroll (deceased), Frank Bouquet, Robert Holtze, Hugh Maxwell, Mohammad Sarbolouki, John Garba, and Harold Marsh.

This document reports on work done under NASA Task RE-152, Amendment 419, DOE/NASA IAA No. DE-A101-85CE89008.

FSA Project Summary

The Flat-Plate Solar Array (FSA) Project, a Government-sponsored photovoltaic (PV) project, was initiated in January 1975 with the intent to stimulate the development of PV systems for economically competitive, large-scale terrestrial use. The Project's goal was to develop, by 1985, the technology needed to produce PV modules with 10% energy conversion efficiency, a 20-year lifetime, and a selling price of $\$0.50/W_p$ (in 1975 dollars). The key achievement needed was cost reduction in the manufacture of solar cells and modules.

As manager, the Jet Propulsion Laboratory organized the Project to meet the stated goals through research and development (R&D) in all phases of flat-plate module technology, ranging from silicon-material refinement through verification of module reliability and performance. The Project sponsored parallel technology efforts with periodic progress reviews. Module manufacturing cost analyses were developed that permitted cost-goal allocations to be made for each technology. Economic analyses, performed periodically, permitted assessment of each technical option's potential for meeting the Project goal and of the Project's progress toward the National goal. Only the most promising options were continued. Most funds were used to sponsor R&D in private organizations and universities, and led to an effective Federal Government-University-Industry Team that cooperated to achieve rapid advancement in PV technology.

Excellent technical progress led to a growing participation by the private sector. By 1981, effective energy conservation, a leveling of energy prices, and decreased Government emphasis had altered the economic perspective for photovoltaics. The U.S. Department of Energy's (DOE's) National Photovoltaics Program was redirected to longer-range research efforts that the private sector avoided because of higher risk and longer payoff time. Thus, FSA concentrated its efforts on overcoming specific critical technological barriers to high efficiency, long life, reliability, and low-cost manufacturing.

To be competitive for use in utility central-station generation plants in the 1990s, it is estimated that the price of PV-generated power will need to be $0.17/kWh (1985 dollars). This price is the basis for a DOE Five-Year Photovoltaics Research Plan involving both increased cell efficiency and module lifetime. Area-related costs for PV utility plants are significant enough that flat-plate module efficiencies must be raised to between 13 and 17%, and module life extended to 30 years. Crystalline silicon, research solar cells (non-concentrating) have been fabricated with more than 20% efficiency. A full-size experimental 15% efficient module also has been fabricated. It is calculated that a multimegawatt PV power plant using large-volume production modules that incorporate the latest crystalline silicon technology could produce power for about $0.27/kWh (1985 dollars). It is believed that $0.17/kWh (1985 dollars) is achievable, but only with a renewed and dedicated effort.

Government-sponsored efforts, plus private investments, have resulted in a small, but growing terrestrial PV industry with economically competitive products for stand-alone PV power systems. A few megawatt-sized, utility-connected, PV installations, made possible by Government sponsorship and tax incentives, have demonstrated the technical feasibility and excellent reliability of large, multimegawatt PV power-generation plants using crystalline silicon solar cells.

Major FSA Project Accomplishments

- Established basic technologies for all aspects of the manufacture of nonconcentrating, crystalline-silicon PV modules and arrays for terrestrial use. Module durability also has been evaluated. These resulted in:
  - Reducing PV module prices by a factor of 15 from $\$75/W_p$ (1985 dollars) to $\$5/W_p$ (1985 dollars).
  - Increasing module efficiencies from 5 to 6% in 1975 to more than 15% in 1985.
  - Stimulating industry to establish 10-year warranties on production modules. There were no warranties in 1975.
  - Establishing a new, low-cost high-purity silicon feedstock-material refinement process.
  - Establishing knowledge and capabilities for PV module/array engineering/design and evaluation.
  - Establishing long-life PV module encapsulation systems.
  - Devising manufacturing and life-cycle cost economic analyses.
- Transferred technologies to the private sector by interactive activities in research, development, and field demonstrations. These included 256 R&D contracts, comprehensive module development and evaluation efforts, 26 Project Integration Meetings, 10 research forums, presentations at hundreds of technical meetings, and advisory efforts to industry on specific technical problems.
- Stimulated the establishment of a viable commercial PV industry in the United States.

Module Encapsulation Summary

The Flat-Plate Solar Array (FSA) Encapsulation Task had two major objectives during its 11-year activity span. The first was the identification, development, evaluation, and qualification of photovoltaic (PV) module encapsulation systems and fabrication processes that would meet the FSA Project cost, performance, and durability goals. The second was the achievement of an understanding and quantification of encapsulation degradation mechanisms and the development of techniques for eliminating or controlling degradation in order to attain a 30-year module lifetime.

The FSA Project, in its analysis of requirements for the achievement of cost-effective PV module designs, developed specific performance goals and cost allocations for each of the module technologies. The following goals were defined for the encapsulation task:

- Module life of 30 years (increased in 1983 from the original 20 years).
- Cost of encapsulation materials, including substrate and/or superstrate, not exceeding $\$1.30/ft^2$ (1980 dollars).
- Initial optical transmission of 90%, and loss of less than 5% after 30 years of use.
- Capability to withstand an electrical breakdown voltage of 3000 V DC.
- Structural integrity and durability in the operational environment.
- Cost-effective processing in an automated factory.

Following initial definition of the performance and cost requirements and identification of expected environmental hazards, an extensive survey of many possible candidate material systems and processes was conducted. It was concluded that new or modified low-cost materials (especially polymers) and improved processing techniques would be required to meet the Project goals. The available polymer materials considered weatherable (such as silicones, fluorocarbons, and acrylics) were either too expensive or not available in a suitable form for pottant or outer cover application.

Early module encapsulation material systems experienced several typical failure modes that required both new materials and revised design configurations. The more significant problems included: delamination, water penetration, surface soiling, substrate deterioration, short circuits, cracked cells, and interconnect fatigue failures. This report reviews how these problems were resolved.

The resolution of these problems required research and development (R&D) in the areas of polymer synthesis, photodegradation mechanisms, ultraviolet stabilizer synthesis, accelerated testing techniques, primer and adhesive technology, unique processing concepts, and anti-soiling surface treatments. Analytical modeling studies (including the development of new computer programs) were undertaken to understand and predict thermal, structural, optical, electrical, and photodegradation effects as a function of materials, module configuration, and time. This report reviews the development of these models and how they were used in the design of PV module encapsulation systems.

Working relationships and technical exchange interfaces were established with the PV-module and material-supply industries as well as with the academic and Government R&D organizations. A number of subcontracts were established to support these efforts. Cooperative exchanges of requirements and capabilities information that occurred with major material suppliers aided in the development by industry of new material products and in the transfer of technology to module manufacturers.

Significant accomplishments resulting from the FSA Encapsulation Task include:

- Development of several new polymeric pottant materials with high light-transmission, including an improved ethylene vinyl acetate (EVA) with processing characteristics suitable for mass production of modules. Optical transmission of solar radiation to solar cells for modules made with these materials exceeds 90%.
- Identification and evaluation of suitable candidate materials and manufacturing processes for each element of a complete module encapsulation system, including front-cover superstrates, pottants, adhesives, back covers, substrates, and edge seals with projected costs less than $\$1.30/ft^2$ (1980 dollars).

- Development of anti-soiling treatments for module covers that have reduced light transmission losses to less than 2% from more than 8% without treatment.

- Development and test verification of module design procedures and design tools for PV modules that meet the Project cost and performance goals.

- Development and verification of accelerated testing equipment and techniques for encapsulation materials subjected to photodegradation and long-term environmental stresses.

- Establishment of technical interfaces with the major U.S. materials suppliers (e.g., Dow Corning, Du Pont, 3M, General Electric, and Gulf Oil), resulting in commercialization of the more promising encapsulant candidates such as EVA.

- Effective transfer of encapsulation technology to industry and the PV module manufacturers' response in adopting it for their new product lines.

- Development of encapsulation systems with electrical breakdown voltages greater than 5000 V DC.

- Verification by accelerated tests of the probability of 30-year PV module lifetimes. Several PV module manufacturers are now granting 10-year warranties.

Contents

Figures

Tables

SECTION I

Introduction

In 1975, the encapsulation requirements for photovoltaic (PV) cells in terrestrial use had not been comprehensively assessed, needs had not been defined, nor potential low-cost encapsulation materials investigated. Therefore, the Flat-Plate Solar Array (FSA) Project set out to assess the needs to identify, and/or develop new materials and new material technologies that were inexpensive and could reliably protect and support the fragile solar cells for years. The assessment led to the establishment of encapsulation needs, goals, and detail requirements and a plan on how to meet the goals.

The four basic functions of a PV module encapsulation system are to:

(1) Provide structural support and positioning for the solar cell circuit assembly during fabrication, handling, storage, transportation, installation, and operation in the terrestrial environment.

(2) Achieve and maintain maximum optical coupling between the silicon solar cell and the incident solar irradiation in a prescribed spectral region.

(3) Achieve and maintain reliable electrical isolation of the solar cell circuit elements from both the operational and safety viewpoints during the useful life of the module. Voltage potentials above ground may exceed 1000 V.

(4) Provide and maintain physical isolation of the silicon solar cells and circuit components from exposure to hazardous or degrading environmental factors (e.g., hail, salt spray, and birds).

A. TASK OBJECTIVES

To fulfill these functions most economically and reliably, the objectives of the FSA Encapsulation Task were to define, develop, demonstrate, and qualify encapsulation systems and materials and processes that meet the FSA Project module life, cost, and performance goals; and to develop and validate an encapsulation system life-prediction methodology based on modeling life-limiting failure modes and on conducting and analyzing aging tests.

B. TASK GOALS

The goals of the FSA Encapsulation Task were to develop encapsulation system technology adequate for:

(1) Module life of 30 years (increased from 20 years).

(2) Encapsulation materials costs, including substrate and/or superstrate not exceeding $\$1.30/ft^2$ (1980 dollars).

(3) Initial optical transmission of 90% and a loss of less than 5% after 20 years of use.

(4) Capability to withstand an electrical breakdown voltage of 3000 V DC.

(5) Structural integrity and durability to withstand handling and weather.

(6) Cost-effective processing in an automated factory with high yields.

C. BACKGROUND

The FSA Project goal established in 1975 was to develop the technology for manufacturing solar cell modules at a manufactured price of $0.50 per watt, or $\$5/ft^2$ (in 1975 dollars), assuming a 10% module efficiency at an insolation level of 100 W/ft^2. The module was to have the necessary design features, sufficient strength, and the appropriate materials of construction to ensure outdoor operating performance for at least 20 years.

Out of this $\$5/ft^2$ cost goal, the initial allocation for all of the encapsulation construction materials was $\$0.25/ft^2$ (in May 1976), including structural support. The allocation was increased in 1979 to $\$14/m^2$, or about $\$1.30/ft^2$, to include also any required frame and edge seals[1]. The durability goal was increased in 1983 to 30 years.

Encapsulation material systems are defined as all construction materials required in a PV module to provide mechanical support, electrical insulation, and environmental isolation for the solar cells and their ancillary electrical circuitry. Figure 1 illustrates early 1970 encapsulation systems employed by the emerging PV industry. In general, the encapsulation approaches were an extension of the technology for conformally coated electronic circuit boards used for spacecraft and aircraft. The circuit board panels were either a Nema-G10 fiber reinforced epoxy board or a glass fiber reinforced polyester panel, on one surface of which were mounted the various electronic components which were then encapsulated in a conformal coating of a curable silicone elastomer. Early PV module designs also included the use

[1] Conversion factors: 1 m^2 = 10.76 ft^2; 1 ft^2 = 0.0929 m^2.

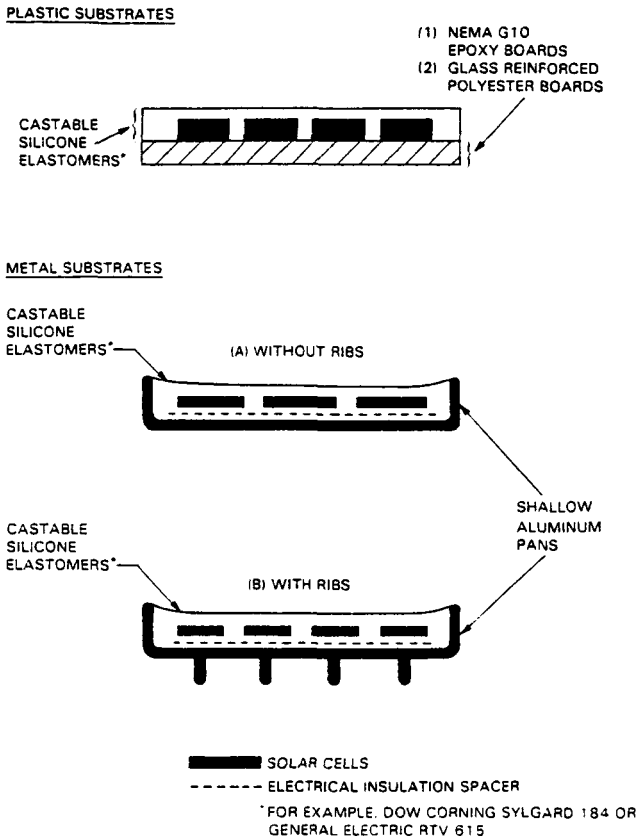

Figure 1. Early Substrate Design Encapsulation Packaging Schemes (1970 to 1975)

of aluminum pan substrates as an alternative to the plastic panels. Glass sheet covers were also used, but were initially considered too brittle to be practical.

In 1975, silicon elastomers cost approximately \$9/lb, which was equivalent to about \$0.05/ft^2/mil of thickness. Thus, 5 mils of silicone elastomer alone equalled the total initial cost allocation of \$.0.25 for encapsulation materials. Aluminum as a structural panel approached \$1.24/ft^2, reinforced plastic substrate panels exceeded \$0.55/ft^2, and polyvinyl butyral (PVB) was approximately \$0.026/ft^2/mil of thickness. Thus, a major challenge to the Encapsulation Task was the identification, development, and qualification of materials systems and configurations of greatly reduced cost.

In addition to the challenge of reducing costs, experience with early module designs revealed technology limitations. When these early PV module encapsulation packages with silicone pottants were deployed outdoors in sunlight, several characteristic degradation modes developed. Some of the more significant problems included:

(1) Delamination of the silicone elastomer from the solar cells and substrate panels.

(2) Liquid water penetration to both the cells and metallization, causing visible corrosion.

(3) Heavy surface soiling on the soft silicone surfaces with attendant light obscuration and power loss.

(4) Weathering and physical degradation of the substrate panels.

(5) Short circuits and arcing, particularly with the aluminum panels.

(6) Cracked solar cells, for both plastic and aluminum substrate designs, attributed to differential thermal expansion stresses.

(7) Cell interconnect failure due to thermal cycling fatigue.

(8) Overheated cells resulting in charring and solder melting.

Most of these degradation and failure modes have been solved in modern PV module designs by the development of new material systems and optimized circuit configurations. This report presents a summary of the development of these improved encapsulation material systems and a description of their properties with guidelines for the design of efficient, durable, and cost-effective PV modules.

References 1 to 64 (listed chronologically) refer to research covering 11 years of Task activities, but may not be individually referred to in the report. References 65 to 86 were not generated by the Task and are referenced in the report.

SECTION II

Encapsulation Research and Development Task

A. BACKGROUND

In assessing for material options and material developmental needs having the likelihood of meeting the encapsulation cost goal, it was expedient to identify and recognize, from existing and conceptual module designs, construction elements basic to all designs, and which would have a high promise of being incorporated in various combinations in future modules. From examination (see Figures 1 and 2) of the industrial trends, it was observed that these designs could be separated into two basic classes (Figure 3). These are designated as substrate-bonded and superstrate-bonded designs, referring to the method by which the solar cells are mechanically supported. In the substrate design, the cells are encapsulated in an elastomeric media on a structural substrate panel, whereas in the superstrate design the cells are encapsulated behind a transparent structural superstrate. From industrial experience, the solar cells were not to be bonded directly to the structural panel, to avoid cell breakage from expansion mismatches, and the encapsulation process itself would include at least liquid casting or dry film lamination.

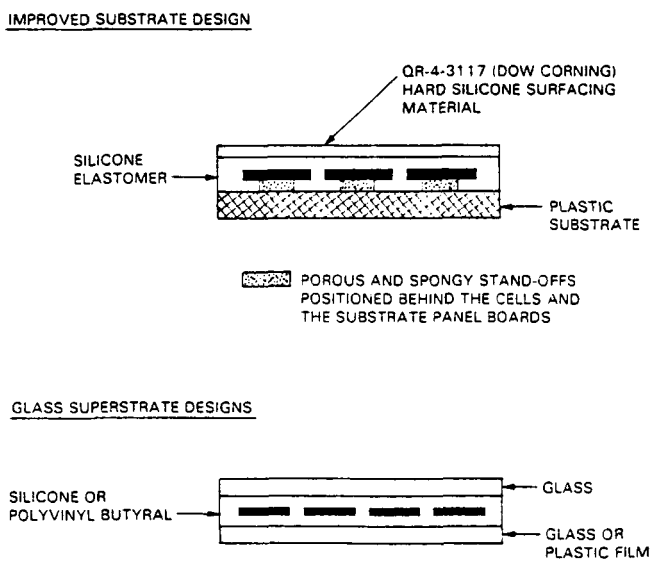

Figure 2. Second Generation Encapsulation Design Concepts (1976 to 1980)

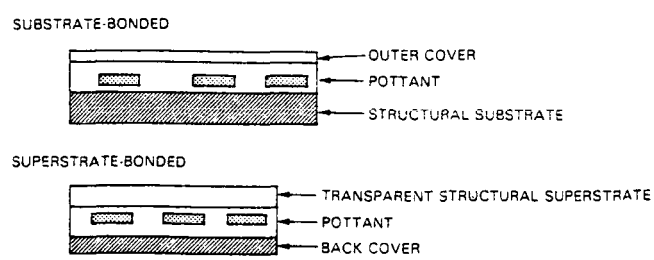

Figure 3. Flat-Plate Module Design Classifications

From these two basic design classes, up to seven construction elements, which could be incorporated into a PV encapsulation system, ultimately became identified; these construction elements and their functions are shown in Figure 4.

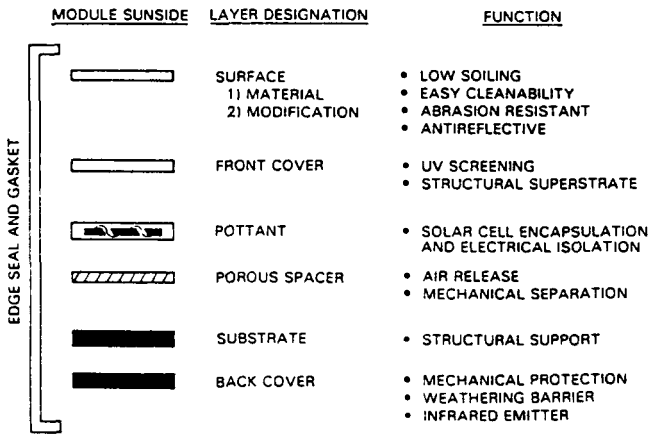

Figure 4. Construction Elements of PV Encapsulation Systems

For each construction element, a uniform costing basis was established for comparative analysis. Extensive surveys were conducted of existing commercial materials that could be used. These surveys generated an appreciation of the minimum costs that must be paid for the materials of each construction element, and a better awareness of the likelihood of fabricating a $\$0.25/ft^2$ encapsulation system. The essential results from these early surveys are herein briefly presented.

B. ENCAPSULATION MATERIAL DEVELOPMENT

1. Superstrates/Substrates

Structural panel materials surveyed included paper products, wood, glass, metal, opaque plastics for substrates, and transparent plastics and glass for superstrates. For comparative cost analysis, the panel was assumed to be 45 in. long by 15 in. wide, and was to be of a minimum thickness with a center-point deflection no greater than 0.1 in. when pressurized at 50 lb/ft^2 by winds at 100 mph. This deflection assumed that the solar cells which were bonded to the panel would tolerate this level of bending without cracking. From structural equations published in Roark (see Reference 65), a minimum thickness t could be calculated for each panel material, and from knowledge of the

volume cost ($/ft^3) of each material, a comparative cost per ft^2 of panel area was generated. The minimum cost in 1976 dollars for each of the above panel classifications, and associated material whether practical or not, is shown in Table 1.

Note that only wood and paper panel products cost less than $0.25/ft^2, thus, suggesting that only a substrate design would meet the cost goals. For a superstrate design, glass as a transparent structural material was significantly lower costing than any commercially available transparent structural plastics. For reasons of cost as well as a well-established history of outdoor weatherability, glass was clearly selected for the superstrate designs, and transparent plastics for this use were not investigated under the JPL program.

For the investigation of substrate designs, both mild steel and fiberboard (also called hardboard) were selected for investigation. It was recognized, however, that some development would be needed to achieve long-term and low-costing weatherproofing techniques for the wood panel, and to achieve low-costing methods of corrosion protection for the mild steel.

2. Pottants

The central core of an encapsulation system is the pottant: an elastomeric, transparent, polymeric material that is the actual encapsulation medium in a module. There is a significant difference between the thermal-expansion coefficients of polymeric materials and the silicon cells and metallic interconnects. Stresses developed from the daily thermal cycles can result in fractured cells, broken interconnects, or cracks and separations in the pottant material. To avoid these problems, the pottant material must accommodate the differential expansions of the different module materials without overstressing the cell and interconnects, and must itself be resistant to fracture. To achieve this, the pottant must be a low-modulus, elastomeric material (e.g., less than 3000 psi). A list of Specifications and Requirements for pottant materials is given in Table 2.

For expected temperature levels in operating modules (see References 66 and 67), ≈ 55°C in a rack-mounted array and possibly up to 80°C on a rooftop, there are three transparent polymers that are generally resistant to the weathering actions of ultraviolet (UV) photooxidation, thermal oxidation, and hydrolysis. They are silicones as a general class of elastomeric materials, and two specific plastics, polymethyl methacrylate (PMMA), and TEFLON FEP (Du Pont), a fluorocarbon (see References 17, 68, and 69). Only silicones, which were expensive, had been available as low-modulus elastomers suitable for pottant application.

All other transparent, low-modulus elastomers are, in general, sensitive to some degree of weathering degradation. However, less weatherable and lower-cost materials can be considered for pottant application if the module design can provide the necessary degree of environmental protection. For example, a hermetic design, such as a glass superstrate with a metal foil back cover and appropriate edge sealing, will essentially isolate the interior pottant from exposure to oxygen and water vapor, with the glass itself providing a level of UV shielding.

The situation is different for a substrate module that could employ a weatherable plastic-film front cover, or a superstrate module with a plastic-film back cover. Because all plastic films are permeable (see Reference 70) to oxygen and water vapor (permeation rates vary for different plastics), the pottant is exposed to oxygen and water vapor, and also to UV if the plastic-film front cover is non-UV screening. In these design options, because isolation of the pottant from oxygen and water vapor is not a practical possibility, it became a requirement that the pottant be intrinsically resistant to hydrolysis and thermal oxidation, but sensitivity to UV was allowed if the weatherable front-cover plastic film of a substrate design could provide UV shielding.

Therefore, surveys were carried out to generate a master list of all commercially known transparent polymers. This list was then sorted to yield a cost/

Table 1. Comparative Cost of Structural Panels[a] (in 1976 Dollars)

Material Classification	Minimum Costing Material	Area Cost, $/ft^2
Paper	Kraft paper honeycomb	0.10
Wood	Fiberboard[b]	0.14
Glass	Soda lime window glass	0.31
Metal	Mild steel	0.45
Plastic (substrate)	Reinforced polypropylene	0.53
Plastic (superstrate)	Polymethyl methacrylate	1.90

[a] For high-volume purchases.

[b] Also referred to as hardboard.

Table 2. Specifications and Requirements for Compounded Pottant Materials

Characteristic	Specification or Requirement
Glass transition temperature (T_g)	$< -40°C$
Total hemispherical light transmission through 20-mil-thick film integrated over the wavelength range from 0.4 μm to 1.1 μm	>90% of incident
Hydrolysis	None at 80°C, 100% RH
Water absorption	<0.5 wt % at 20°C/100% RH
Resistance to thermal oxidation	Stable up to 85°C
Mechanical creep	None at 90°C
Tensile modulus as measured by initial slope of stress-strain curve	<3000 lb/in.^{2} at 25°C
Fabrication temperature	≤170°C for either lamination or liquid pottant systems
Fabrication pressure for lamination potants	≤1 atm
Chemical inertness	No reaction with embedded copper coupons at 90°C
UV absorption degradation	None at wavelength >0.35 μm
Hazing or clouding	None at 80°C, 100% RH
Minimum thickness on either side of solar cells in fabricated modules	6 mils
Odor, human hazards (toxicity)	None

weathering relationship as summarized in Table 3. In general, materials costing less than $0.55/lb were sensitive to all three forms of the weathering actions. Materials above $1.50/lb could be found, such as the silicones that were generally weatherable, but, for other practical reasons, were not suitable for pottant application.

Table 3. Transparent Polymeric Pottants

Modes of outdoor weathering degradation
Thermal oxidation
Hydrolysis
UV photooxidation
Cost[a]/weathering relationship
>$1.50/lb: generally weatherable
$0.55 to $1.50/lb: UV sensitive, resistant to thermal oxidation/hydrolysis
<$0.55/lb: generally unweatherable

[a]Cost in 1976 dollars; the lowest costing transparent polymer averaged around $0.23/lb.

In the price range between $0.55 to $1.50/lb, several transparent materials were found that were resistant to thermal oxidation and hydrolysis up to 80°C, but that were UV sensitive. None of the materials were liquid casting systems. Out of this subset of materials, one polymer, ethylene vinyl acetate (EVA) at $0.65/lb stood out as the most viable pottant candidate, on the basis of weatherability considerations, elastomeric properties, and module processing by dry-film lamination techniques.

Consequently, from these initial surveys, four pottant materials emerged as most viable and are currently in various stages of development or industrial use. The four pottants are based on EVA, ethylene methyl acrylate (EMA), poly-n-butyl acrylate (P-n-BA), and aliphatic polyether urethane (PU). EVA and EMA are dry films designed for vacuum-bag lamination at temperatures up to 150°C. Above 120°C during the lamination process, EVA and EMA undergo peroxide crosslinking to tough, rubbery thermosets. P-n-BA and PU are liquid casting systems. P-n-BA, a polymer/monomer syrup, was developed jointly by JPL and Springborn Laboratories, and was formulated to cure within 15 min at 60°C. The most promising PU for PV module application is a urethane designated Z-2591, marketed by Development Associates, North Kingston, Rhode Island.

a. *Ethylene Vinyl Acetate.* EVA is a copolymer of ethylene and vinyl acetate typically sold in pellet form by Du Pont and U.S. Industrial Chemicals, Inc. (USI). The Du Pont name is Elvax; the USI trade name is Vynathane. The cost of EVA typically ranged between $0.60 to $0.70/lb. in 1980 dollars. All commercially available grades of EVA were examined and the list reduced to four candidates based on maximum transparency: Elvax 150, Elvax 250, Elvax 4320, and Elvax 4355. Because EVA is thermoplastic, processing into a module is best accomplished by vacuum-bag lamination with a film of EVA. Therefore, based on film extrudability and transparency, the best choice became Elvax 150.

As sold, Elvax 150 softens to a viscous melt above 70°C and, therefore, must be cured (cross-linked) for service temperatures above 70°C. A cure system was developed for Elvax 150 that results in a temperature-stable elastomer. Elvax 150 was also compounded with an antioxidant and UV stabilizers, which improved its weather stability, but did not affect its transparency. The formulation of the first-generation encapsulation-grade EVA is given in Table 4, which carries the Springborn Labs designation A-9918. These ingredients are compounded into Elvax 150 pellets, followed by extrusion at 85°C to form a continuous film. The thickness of the clear film was nominally 18 mils. The peroxide curing system is inactive below 100°C, so that film extruded at 85°C undergoes no curing reaction. The extruded film retains the basic thermoplasticity of the Elvax 150. Therefore, during vacuum-bag lamination, the material will soften and process as a conventional laminating resin. Properties of Elvax 150 and cured A-9918 EVA are given in Table 5.

This EVA pottant (A-9918) was well received by manufacturers of PV modules who reported certain advantages of EVA when compared to PVB, a laminating film material developed for manufacturing automobile safety glass and in common use within the PV module industry. The reported advantages of EVA were:

(1) Lower cost.

(2) Better appearance.

(3) Better clarity.

(4) Elimination of cold storage (required for PVB).

(5) Dimensional stability.

(6) No need to use a pressure autoclave.

(7) Good flow properties and volumetric fill.

Although this first generation encapsulation-grade EVA was favorably received by the industry, its status was still considered to be experimental. With increasing industrial experience, as well as observations noted during accelerated aging tests of this EVA formulation, several limitations involving the A-9918 compounding ingredients became evident, as follows:

Compounding Ingredients	Problem
Peroxide Curing Agent	
Lupersol 101	EVA immiscibility
	Rapid physical loss
	Limited storage life
	EVA cure problems
Weathering Stabilizers	
Tinuvin 770	Low molecular weight
	Rapid physical depletion
Cyasorb UV-531	Gradual loss of EVA weathering protection

Table 4. Formulation of the First Generation EVA Encapsulation Film, Designated A-9918

Component	Composition (Part by Weight)
EVA (Elvax 150, DuPont)	100.0
Lupersol 101 (peroxide)	1.5
Naugard-P (antioxidant)	0.2
Tinuvin 770 (UV stabilizer)	0.1
Cyasorb UV-531 (UV stabilizer)	0.3

To correct these problems, a new curing agent designated Lupersol-TBEC was identified by Springborn Laboratories. This curing agent is completely miscible with Elvax 150, and virtually eliminated problems associated with storage life and cure. In fact, TBEC was found to cure EVA faster, and at lower temperatures, as compared to Lupersol-101. The cure characteristics of those two peroxide curing agents are compared in Table 6, using the gel content of the cured EVA as one measure of the level of cure. EVA is considered adequately cured if its gel content exceeds 65%.

In addition, the low molecular weight UV screening agent Cyasorb UV-531 has been replaced with a chemically attachable UV screening agent UV-2098, and a polymeric (UV-3346) hindered amine light stabilizer (HALS) has replaced Tinuvin 770. HALS are essentially antioxidants effective against UV photooxidation. This second-generation EVA is an advanced EVA formulation designated 18170, and is detailed in Table 7. Note that Naugard-P (see Table 4), an antioxidant effective against thermal oxidation has been eliminated, since experimental testing has indicated that UV-3346 also fulfills the same function.

Initial experience with fabrication and module performance testing with the EVA 18170 pottant has indicated a significant improvement over EVA A-9918.

Table 5. Properties of Elvax 150 and Cured A-9918 EVA[a]

Property	Condition	Elvax 150	Cured A-9918 EVA	Remarks
Optical transmission		90.5%	91.0%	ASTM E-424 (Springborn)
Glass transition temperature, T_g		−43°C	−43°C	JPL measurement
Young's modulus[b]	23°C	850 lb/in.^{2}	890 lb/in.^{2}	ASTM D-638 (Springborn)
	23°C	700 lb/in.^{2}	—	ASTM D-1708 (Du Pont)
Secant modulus	1% elongation, 23°C	—	1120–1330 lb/in.^{2}	ASTM D-882 (Du Pont)
Tensile strength at break	23°C	850 lb/in.^{2}	1890 lb/in.^{2}	ASTM D-638 (Springborn)
	23°C	700–900 lb/in.^{2}, [c]	1160–1490 lb/in.^{2}, [c]	ASTM D-638[d]/D-882[e] (Du Pont)
	23°C	850 lb/in.^{2}	—	ASTM D-1708 (Du Pont)
	−20°C	2700 lb/in.^{2}	—	ASTM D-638 (Du Pont)
Elongation at break	23°C	1050%	510%	ASTM D-638 (Springborn)
	23°C	900–950%[c]	580–740%[c]	ASTM D-638[d]/D-882[e] (Du Pont)
	23°C	1050%	—	ASTM D-1708 (Du Pont)
	−20°C	300%	—	ASTM D-638 (Du Pont)
Flexural modulus	23°C	1000 lb/in.^{2}	—	ASTM D-790 (Du Pont)
Compression modulus	10 days at 25°C	65%	—	ASTM D-395 (Du Pont)
	22 h at 70°C	91%	—	ASTM D-395 (Du Pont)
Stiffness	23°C	800 lb/in.^{2}	—	ASTM D-747 (Du Pont)
	−20°C	4300 lb/in.^{2}	—	ASTM D-747 (Du Pont)
Hardness	Shore A, 10s	65-73	76-79	ASTM D-2240 (Du Pont, Springborn)
	Shore D, 10s	24	—	ASTM D-2240 (Du Pont)
Vinyl acetate content		33 wt %	33 wt %	Du Pont technical bulletins
Density, g/cm^3	23°C	0.957[c]	0.920[c]	Du Pont[d]/JPL[e] measurements
Refractive index, n_d	25°C	1.482[c]	1.482[c]	Du Pont[d]/Springborn[e] measurements
Dielectric strength, V/mil	25°C	—	620	Spectroblab measurement
	25°C	—	580	Springborn measurement
Water absorption	23°C, 24 h water immersion	0.13 wt %	—	ASTM D-570 (Du Pont)
	18-mil film, 55°C, 100% RH	—	0.70 wt %	16-h exposure (JPL)
Specific heat, W-s/g-°C		—	2.09	Spectrolab measurement
Thermal conductivity, W-mil/ft^2-°C		—	9×10^2	Spectrolab measurement
Infrared emissivity	25°C	—	0.88	JPL measurement
Thermal expansion	Below T_g (−43°C)	1.0×10^{-4} °C^{-1}	0.9×10^{-4} °C^{-1}	JPL measurement
	−43°C to +10°C	—	2.0×10^{-4} °C^{-1}	JPL measurement
	Above +10°C	—	4.0×10^{-4} °C^{-1}	JPL measurement

[a] Sources: Property measurements made at Springborn Laboratories under FSA Contract 954527.
Property measurements made at Spectrolab, Inc., under FSA Contract 955567.
Property measurements made at the JPL's analytical test facilities
Various Du Pont Technical Bulletins on Elvax resins.
Du Pont Technical Bulletin, "Elvax 150 Resin as a Solar Photovoltaic Module Pottant, Technical Guide," Polymer Products Department, Technical Services Laboratory, Wilmington, Delaware (June 1982).

[b] Initial slope of stress-strain curve.

[c] Refer to the Remarks column.

[d] Made by Du Pont.

[e] Made by JPL.

Table 6. Cure of Elvax 150 EVA at Various Times and Temperatures with Lupersol-101 and Lupersol-TBEC as Monitored by Gel Content in wt %

Cure Time, min	Degree of Cure, % Gel								
	Lupersol 101					Lupersol TBEC			
	130°C	140°C	150°C	160°C	170°C	120°C	130°C	140°C	150°C
1			0	2.1	28.8				
2		1.0	4.1	29.5	74.2	0	0	73.4	81.5
5		11.8	21.1	73.0	81.2	0	60.3	83.7	88.6
10	1.0	23.5	63.2	82.6	92.7	0	75.0	88.2	91.6
15	2.3	59.3	88.3			0	85.0	90.2	93.5
20						60.0	78.3	92.7	93.0
30	3.4	68.2					82.7	92.2	92.6
60	32.1	80.6							

Table 7. Advanced EVA Formulation (Experimental) (Springborn 18170)

Component	Function	Composition (Parts by Weight)	Remarks
Elvax 150	EVA resin	100.0	Same as A-9918
TBEC	Curing agent	3.0	Faster, lower temperature curing, improved storage life
UV-2098	UV screening agent	0.3	Chemically attachable, non-fugitive
UV-3346	Hindered amine light stabilizer	0.1	Polymeric, non-fugitive

Furthermore, individual module manufacturers have also incorporated additional EVA modifications tailored to their specific module design and fabrication requirements.

b. *Ethylene Methyl Acrylate.* EMA, a copolymer of ethylene and methyl acrylate, was identified by Springborn Laboratories as having potential as a solar-cell lamination pottant. There are three suppliers of EMA resins; two are domestic, Du Pont and Gulf Oil Chemicals. The Du Pont EMA resin, designated "VAMAC N-123," cannot be used because of its lack of transparency. The third supplier is foreign.

Gulf markets three highly transparent EMA resins that are designated 2205, 2255, and TD-938. Grade 2255 is the same base resin as 2205, except that it contains lubricant and antiblocking additives. Gulf literature for these resins indicate the following features:

(1) Low-extrusion temperatures.

(2) Good heat sealability.

(3) Thermal stability to 315°C (600°F) for short periods of time (manufacturer's claim).

(4) Stress-crack resistance.

(5) Low melt viscosities.

(6) Good adhesion to a variety of substrates.

The three Gulf EMA resins were experimentally evaluated and TD-938 was selected on the basis of film transparency, extrudability, and ease of module fabrication by lamination. The TD-938 base resin sold for about $0.60/lb in April 1981. A trial formulation is shown in Table 8. Modules have been fabricated with this EMA by the vacuum-bag lamination process, and have successfully passed module engineering qualification tests.

Unlike EVA, EMA does not soften to a viscous melt above 70°C and, therefore, may not need curing as does EVA to achieve high-temperature creep resistance. This may be a potential advantage of EMA over EVA.

c. *Poly-n-Butyl-Acrylate.* Compared to silicones, no lower-costing commercially available liquid casting system could be found. Because acrylics were low in cost, an all-acrylic liquid-casting and curable-elastomeric system was developed as part of the Jet Propulsion Laboratory (JPL) PV program. A requirement

Table 8. Formulation of EMA Encapsulation Film

Component	Composition (Part by Weight)
EMA (TD 938, Gulf Oil Co.)	100.0
Lupersol 231 (peroxide)	3.0
Naugard-P (antioxidant)	0.2
Tinuvin 770 (UV stabilizer)	0.1
Cyasorb UV-531 (UV stabilizer)	0.3

of encapsulation-grade pottants is retention of elastomeric properties over the temperature range from −40 to +90°C. This requirement is met by PnBA, which has a glass-transition temperature of −54°C (Reference 71).

PnBA is not commercially available in a form suitable for use as an encapsulation pottant, but the n-butyl acrylate monomer was readily available at a bulk cost of about $0.45/lb, in 1980 dollars. As a result of the developmental program, a 100% pure PnBA liquid was developed that could be cast as a conventional liquid-casting resin, and that subsequently cures to a tough, temperature-stable elastomer. Modules fabricated with the PnBA elastomer have successfully passed module engineering tests.

In general, the process for producing the prototype liquid PnBA consisted of first polymerizing a batch of n-butyl acrylate to achieve a high-molecular-weight elastomer, then dissolving the elastomer in a n-butyl acrylate monomer to obtain a solution of acceptable viscosity. Following this process, a crosslinker, curing agent, UV stabilizers, and an antioxidant are added. The current formulation is given in Table 9. This formulation will cure in 20 min at 60°C. The projected high-volume cost for this material was estimated at about $0.85 to $0.90/lb (1980 dollars).

An industrial evaluation of this acrylic pottant resulted in mixed reviews that were primarily negative, as the uncured liquid had a strong and unpleasant odor. This generally created a problem in the module manufacturing area that was difficult to resolve, and industrial interest therefore quickly diminished. All developmental work was subsequently stopped.

d. *Aliphatic Polyether Urethane.* Almost all commercially available polyurethanes are of the aromatic, polyester type, which are not favorable because of their tendency toward hydrolysis of the ester groups, and UV degradation because of UV absorption by the aromatic structure. Only a few aliphatic polyether urethanes have been identified, and one of the more promising for PV module application is a urethane designated Z-2591, marketed by Development Associates, North Kingston, Rhode Island. This material is being used industrially, and is available for further evaluation by module manufacturers for module designs requiring a casting rather than a laminating process.

Table 9. Formulation of P-n-BA Casting Liquid

Component	Composition (Part by Weight)
n-Butyl acrylate (monomer)	60.00
P-n-BA (polymer)	35.00
1, 6-hexanediol diacrylate (crosslinker)	5.00
Alperox-F (curing agent)	0.50
Tinuvin P (UV stabilizer)	0.25
Tinuvin 770 (UV stabilizer and antioxidant)	0.05

3. Ultraviolet Screening Plastic Films

The concept of employing the lowest costing transparent elastomers as pottants, by permitting UV sensitivity, requires in turn the need for an outer cover material that is both UV screening and naturally weatherable. For a superstrate design, this is provided by glass, which is also the module structural panel.

For a substrate design, however, the outer cover material may be a transparent plastic film that will be in direct contact with all of the weathering elements: UV, humidity, dew, rain, oxygen, dust, etc.; therefore, the selected cover materials must be weatherable. Only three classes of transparent materials are known to be weatherable: silicones, PMMA, and the fluorocarbon film, FEP TEFLON (Du Pont) (see References 17, 68, and 69).

In addition to weatherability, the front cover must also function as a UV screen to protect underlying pottants that are sensitive to degradation by UV photo-oxidation. The outer surface of the front cover should also be easily cleanable and resistant to atmospheric soiling, be abrasion-resistant, and antireflective to increase module light transmission. If any of these outer-surface characteristics are absent in the front-cover material, additional surfacing materials may have to be applied.

Excluding glass, the only commercially available transparent, UV-screening plastic films that have been identified are polyvinyl fluoride (PVF) films, Tedlar (Du Pont), and PMMA films, Acrylar (3M Co.).

a. *Tedlar.* Du Pont markets three 1-mil-thick, clear, Tedlar fluorocarbon UV-screening films. The designation of these three films are:

(1) Tedlar 100 AG 30 UT.

(2) Tedlar 100 BG 15 UT.

(3) Tedlar 100 BG 30 UT.

An initial difficulty with Tedlar was poor adhesion to EVA and EMA. This was corrected by the use of an all-acrylic contact adhesive that could be coated directly onto one surface of Tedlar films. The adhesive coating, a Du Pont product designated 68040, is dry and non-tacky at ambient conditions; thus, coated Tedlar can be readily unwound from supply rolls. Experimental testing indicates that when the adhesive is heated during the EVA and EMA lamination cycle, strong adhesive bonding develops between the pottants and the Tedlar films. The thickness of the adhesive coating ranged between 0.3 and 0.4 mil. An additional concern with Tedlar is a potential toward shrinkage during outdoor service on a module, which can lead to cracks. Experimental studies suggest that the Tedlar film should be thermally annealed before being fabricated into a module, to reduce this shrinkage concern.

b. *Acrylar.* 3M Co. markets UV screening, oriented PMMA films under the tradename "Acrylar." The films are available in two thicknesses: a 2-mil version, designated X-22416; and a 3-mil version, designated X-22417. An initial concern with these films is their tendency for thermal shrinkage when heated above 105 °C, the glass transition temperature of PMMA. Although true for a free-standing film, this has not been a problem when uniformly pressed at 150 °C in a module assembly by one atmosphere of lamination pressure.

4. Back Covers

Back covers are back-surface material layers that should be weatherable, hard, and mechanically durable and tough. The color of the back-surface material layer should be white, to aid module cooling. Back covers function to provide necessary back side protection for structural substrates, such as for example corrosion protection for low-cost mild steel panels, or humidity barriers for moisture sensitive panels such as hardboard. For superstrate designs, the back covers provide a tough overlay on the back surface of the soft, elastomeric pottant. Candidate back-cover films are listed in Table 10.

Table 10. Back Covers[a] (White-Pigmented Plastic Films)

Tedlar 150 BL 30 WH, 1.5 mils (DuPont)
Tedlar 400 BS 20 WH, 4.0 mils (DuPont)
Scotchpar 10 CP white, 1.0 mils (3M Co.)
Scotchpar 20 CP white, 2.0 mils (3M Co.)
Korad 63000 white, 3.0 mils (Xcel Corp.)

[a]Approximate cost per mil of thickness:
(1) Tedlar PVF films, $\approx$ \$0.07/ft^2.
(2) Scotchpar polyester films, $\approx$ \$0.02/ft^2.
(3) Korad acrylic film, $\approx$ \$0.02/ft^2.

5. Edge Seals and Gaskets

Trends based on technical and economical analysis suggest that compounds containing butyl groups should be considered for edge seals, and ethylene propylene (diene monomer) rubber (EPDM) elastomers should be considered for gaskets. Several materials for each application are under investigation. One of the most promising edge seal materials is a butyl edge sealing tape designated "5354" (3M Co.), and one of the most promising EPDM gasket materials is designated "E-633" (Pauling Rubber Co.).

6. Porous Spacer

As modules became bigger, the complete removal of air under vacuum from the interfaces between the various material layers became increasingly difficult. This removal difficulty resulted in entrapped air bubbles in finished modules. To solve this problem, non-woven glass mats were included in the module assembly to facilitate complete air removal during vacuum pumpdown. Generally, the non-woven glass mats were used as separating layers between the cells and the adjacent films of EVA, as most of the air that could be trapped was associated with the spaces between solar cells.

A great variety of candidate spacer materials were investigated by Springborn Laboratories, and the best materials identified to date, in terms of handling, fabrication, and cost, are non-woven glass mats manufactured by the Crane Company, Dalton, Massachusetts. The materials are sold under the trade Name "Craneglas," and are distributed by Electrolock, Inc., Chagrin Falls, Ohio. The specific mat being used is Type 200, 5 mils thick, at a cost of less than \$0.01/ft^2 in 1980 dollars.

SECTION III

Primers and Adhesives (Chemical Bonding)

One of the first encapsulation problems experienced with PV modules fabricated in the early 1970s was delamination of the silicone elastomers. At that time, PV manufacturers were not employing adhesion promoters, and therefore, module interfaces in common with the silicone materials were only in physical contact, and easily prone to separation if, for example, liquid water were to penetrate to the interfaces. Delamination with silicone materials virtually vanished when adhesion promoters, recommended by silicone manufacturers, were used.

With the decrease in use of silicone encapsulants, and the increase in use of hydrocarbon encapsulants such as EVA, the need arose for adhesion promoters specifically developed for these new materials. The adhesion promoters developed for EVA-type materials are based on organosilane chemistry, called silane coupling agents. These coupling agents generate primary chemical bonds across an interface, i.e., chemical bonding (see References 16, 46, and 62). A solution of an organosilane coupling agent in a solvent is called a primer solution, or just simply a primer.

The organosilane coupling agents are chemically bifunctional molecules, and using glass and EVA as an example, one of the chemical groups on a silane coupling agent is reactive with glass, while the other is reactive with EVA. Thus, the interfacial bonding between EVA and glass is accomplished by actual primary chemical bonds bridging across their interface.

In general, for glass, silane coupling agents have the chemical form $X\text{-}(CH_2)_3\text{-}Si\text{-}(OR)_3$, where the functional group X is reactive with a polymer matrix, and can be varied depending on the polymer chemistry. The (OR) groups are short chain ethers that hydrolyze in slightly acidic water to produce alcohols that are reactive with the surfaces of glass. The general scheme for chemically bonding polymers to glass with silane coupling agents is shown in Figure 5, and specifically for EVA, the X-group is a methacrylate. From studies of the interfacial chemistry, there is growing evidence that coupling to a polymer involves not only chemical bonding, but also the formation of what is referred to as an "interpenetrating network" (IPN). An IPN is an interphase that can be viewed as an interlocking of two three-dimensional meshes. The current concept of a chemically bonded interface between EVA and glass is shown in Figure 6.

A. ADHESION PROMOTERS

Table 11 lists primers and adhesives that have been developed or identified for bonding EVA to glass, Acrylar, Tedlar, and polyester plastic films. Experimental quantities of the EVA/glass primer are available from Springborn Laboratories, under the designation A-11861. For bonding EVA to Tedlar, Du Pont identified an adhesive designated "68040" that is normally pre-coated as a dry film on the Tedlar. Limited experimental testing suggests that these same adhesion promoters work equally well with EMA.

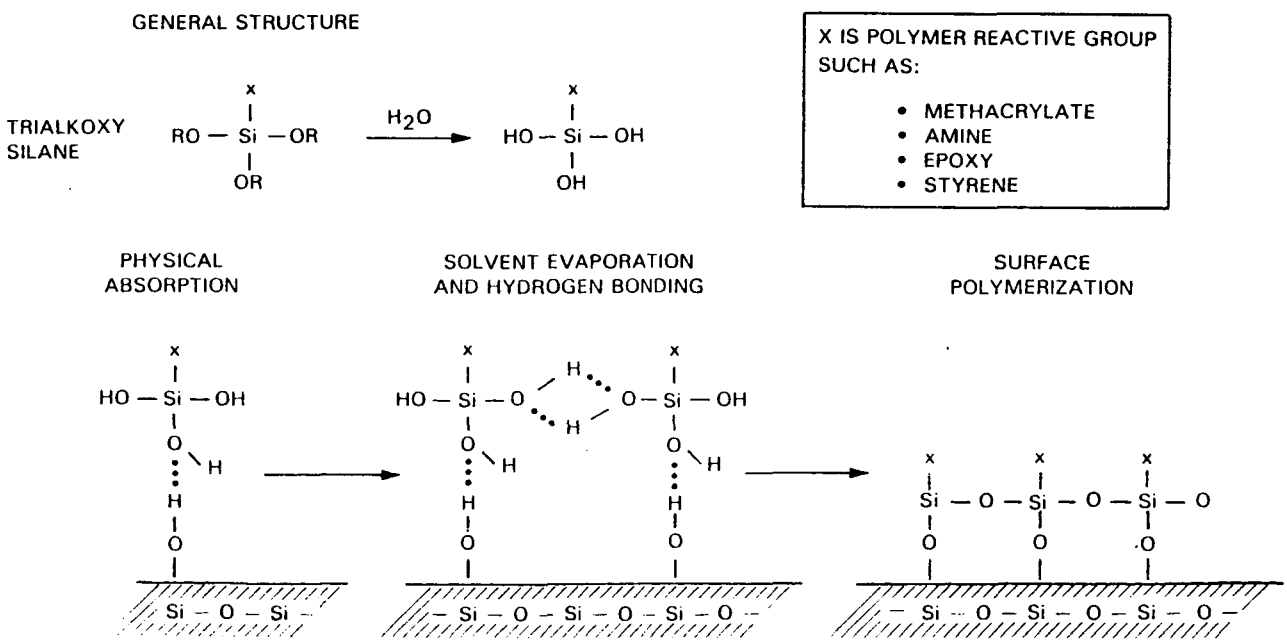

Figure 5. Bonding of Silane Coupling Agents to Glass

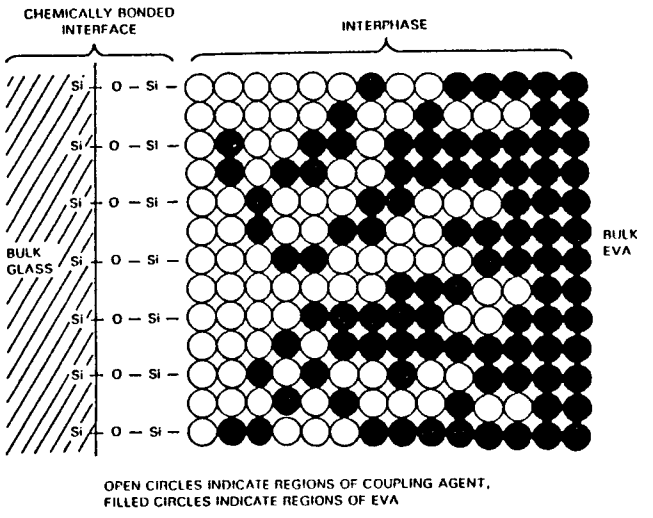

Figure 6. Interdiffusion Model for a Silane-Primed EVA/Glass Joint

Table 11. Primer and Adhesives for Bonding EVA[a] to Various Materials

Component	Composition, wt %
Primer[b] for Bonding EVA to Glass	
Z-6030 silane (Dow Corning)	9.0
Benzyl dimethyl amine	1.0
Lupersol 101	0.1
Methanol	89.9
Primer for Bonding Ethylene Vinyl Acetate to Polyester Films	
Z-6040 silane (Dow Corning)	1.25
Resimene 740 (Monsanto)[c]	23.75
Isopropanol	75.0
Primer for Bonding Ethylene Vinyl Acetate to Acrylar	
Z-6020 (Dow Corning)	1.95
Z-6030 (Dow Corning)	0.05
Acroloid AT-51 (Rohm and Hass)	36.0
Toluene	62.0
Adhesive for Bonding EVA to Tedlar	
68040 Acrylic Contact Adhesive (Du Pont)	

[a] Experimental testing indicates these adhesion promoters also work for EMA.

[b] Experimental quantities available from Springborn Laboratories, under the designation A-11861.

[c] Resimene 714 may be used as a substitute for Resimene 740.

With the exception of Tedlar, Table 12 lists adhesion promoters for the Z-2591 polyurethane liquid system that are available as commercial products from Development Associates, North Kingston, Rhode Island, the polyurethane manufacturer. An experimental primer for bonding Z-2591 to Tedlar, developed by Dow Corning, is also given in Table 12.

Table 12. Primer and Adhesives for Bonding Z-2591 to Various Materials

Material	Primer/Adhesive Designation[a]
Glass/metals	Z-3012
Acrylar/Korad	Z-2881
Mild steel[b]	I-1022
Experiment[c] Primer Formulations for Bonding Z-2591 Polyurethane to Tedlar Fluorocarbon Films	
Component	Composition, wt %
Formulation 1	
Z-6020 silane (Dow Corning)	9.5
Water	0.5
Methanol	90.0
Formulation 2	
Z-6020 silane (Dow Corning)	2.5
Z-6082 silane (Dow Corning)	2.5
Methanol	95.0

[a] These adhesion promoters are marketed by Development Associates, North Kingston, Rhode Island, for their polyurethane product Z-2591.

[b] Specially developed for mild steel; for other metals, use Z-3012.

[c] Both primers yield acceptable bond strengths on freshly made test specimens, but long-term outdoor aging stability not known at this time, therefore, these are still to be considered as experimental primer systems.

B. ADHESION TESTING

EVA that has been laminated and cured on a flat glass will have a reasonable bond strength in a dry environment, but will readily delaminate when exposed to a wet environment. Bond strength is normally measured as the load in pounds to sustain a steady-state

peeling of a 1-in. strip of EVA from the flat glass surface, and is expressed in units of pounds/(inch-of-width). The dry strength with unprimed glass is typically 5 to 8 lb/in., but will drop to zero when wet.

Bond strengths measured with primed glass are shown in Table 13, using the A-11861 EVA/glass primer (see Table 11), for both Sunadex and window glass. An experiment was also carried out with Sunadex glass substituting the Lupersol-TBEC peroxide for Lupersol-101, in the A-11861 EVA formulation. Lastly, the primer was compounded into the EVA film to produce a self-priming EVA formulation. The results from this experiment with window glass are also shown in Table 13.

In general, the dry bond strengths with L-101 ranged from 35 to 39 lb/in. for all experimental conditions, and was 51.3 lb/in. when using Lupersol-TBEC in place of L-101. These values can be compared with 5 to 8 lb/in. for unprimed glass.

The significant benefit of chemical bonding with the organosilane coupling agents is observed in the wet strengths, both after 2 weeks immersion in 25°C water, and after 2 h in boiling water. Essentially the bond strengths are virtually unchanged. Without primer, EVA would have readily delaminated from the glass.

There is industrial interest in having a commercially available self-priming EVA to eliminate a separate priming step currently used. Another observation with important industrial ramifications is the indication that the bond strength of the self-priming EVA formulation improves with water exposure, reaching a level of strength where, in mechanical peel testing, the EVA fails rather than the bond (cohesive failure).

C. HYDROTHERMAL AGING

In general, the silanes employed for these coupling agents are typically resistant to deterioration by UV light, therefore, the main weathering concern is from the potential of hydrothermal deterioration over a long exposure time outdoors. Almost nothing is known about the chemical reactions, mechanisms, and kinetics of the chemistry of a chemically bonded interface undergoing hydrothermal aging. Therefore, a study was initiated at Case Western Reserve University, to directly interrogate a chemically bonded interface for chemical information, using an infrared (IR) technique based on diffuse reflectance (DRIFT) from glass surfaces.

Using glass and EVA with primer A-11861 (see Table 11), the concept was to monitor the IR spectra of the interface of test specimens undergoing hydrothermal aging. The initial specimens consisted of EVA laminated onto flat glass that did not yield sufficient interfacial surface area for IR detection. Therefore, it was decided to disperse glass beads into EVA to increase the surface-to-volume ratio. Experimentally, a loading of 30 vol % glass beads provided sufficient surface for IR detection of the interfacial chemistry. Both chemical interrogation and mechanical property testing of hydrothermally aged test specimens were carried out.

Mechanical properties measured for primed and unprimed EVA/glass specimens that were hydrothermally aged at 40, 60, and 80°C for times up to 2000 h are given in Table 14. Because it was noted during trial testing that these specimens tended to absorb large quantities of water, it was also decided to measure and record the absorbed water content of the specimens, as given in Table 14. For comparison, unfilled EVA under the same hydrothermal aging conditions absorbs less than 1 wt % water, therefore, the enormous uptake of water associated with the filled EVA was initially believed to be locally clustered at the glass/EVA interface. This was subsequently verified by IR.

For the unprimed EVA/glass specimens, the general pattern was to absorb copious quantities of water, such as over 2000 wt % after 2000 h at 60°C, and to also undergo a reduction in mechanical properties, at a rate that seems to increase with increasing temperature.

For the primed samples, there was a dramatic decrease in the quantities of absorbed water, as compared to the unprimed specimens, and overall, mechanical properties were more generally preserved, even after 500 and 1000 h at 80°C. For the primed sample aged 2000 h at 60°C, its absorbed water content was only

Table 13. Adhesive Bond Strengths for EVA Bonded to Flat Glass

Materials	Peroxide	Bond Strengths, lb/in. of Width		
		Control	After 2 wk Immersion in 25°C Water	After 2 h in Boiling Water
Sunadex glass	L-101	34.8	30.0	32.3
Window glass	L-101	39.6	37.9	27.1
Window glass (self-priming EVA)	L-101	35.4	41.9	Cohesive
Sunadex glass	L-TBEC	51.3	32.9	33.3

Table 14. Effect[a] of Hydrothermal Aging in Water at 40, 60, and 80°C on TBEC-Cured EVA With 30 vol % Glass Beads, With and Without Primer

Characteristics	Control	At 40°C			At 60°C				At 80°C			
		100 h	500 h	2000 h	100 h	250 h	500 h	2000 h	100 h	250 h	500 h	1000 h
Unprimed												
Modulus, psi	2830	1600	1700	830	1800	1600	380	30	1700	930	1100	b
Ultimate strength, psi	1380	1295	1230	1210	1240	960	530	50	460	285	310	b
Ultimate elongation, %	600	600	570	510	570	515	300	60	365	120	100	b
Δ absorbed water, %[c]	—	0.15	18.9	51.0	0.92	29.3	410	2015	17.4	568	503	b
Primed												
Modulus, psi	2500	1600	1800	2400	2000	2500	2000	1600	2200	2300	3000	1700
Ultimate strength, psi	905	1070	900	1150	935	930	990	830	987	1010	910	725
Ultimate elongation, %	350	385	190	390	445	285	315	120	275	245	220	140
Δ absorbed water, %[c]	—	0.19	2.0	3.5	0.36	4.0	6.3	34.7	1.0	12.9	16.9	61.7

[a]Properties measured in air at nominal conditions of 25°C (77°F) and 40% RH.
[b]Samples deteriorated.
[c]Values quoted are the percent grain in absorbed water compared to initial weight equilibrated at nominal room conditions of 25°C (77°F) and 40% RH.

34.7 wt %, as compared to its unprimed counterpart with over 2000 wt %. These data in Table 14 clearly reveal the positive influence of the organosilane coupling agents in both minimization of interfacial water absorbtion, and preservation of mechanical properties. Duplicates of the specimens, whose properties are reported in Table 14, were dried for 72 h in an air-circulated oven at 105°C, to dry out the specimens. The intent was to measure the mechanical properties after dry-out to assess reversibility and recovery behavior of the mechanical properties. These data are reported in Table 15. In general, for all hydrothermal aging conditions, the dried out primed specimens virtually recovered their initial properties.

D. CORROSION PREVENTION

Metallic corrosion usually requires the presence of liquid water, as one necessary requirement. The adhesion studies with primed EVA/glass specimens clearly demonstrated that organosilane coupling agents are enormously effective in reducing the accumulation of interfacial water. This suggests that organosilanes chemically reacted onto metallic surfaces may function as anti-corrosion agents, through the action of reducing or excluding liquid water at the metallic surface.

Several solar cell manufacturers deposit an aluminum layer on the back surface of their solar cells, for reasons related to enhanced performance. In the natural environment, the surface of aluminum will oxidize, and then in a moist condition, this oxidized aluminum layer will form a hydrate called pseudoboehmite (see Reference 72). This aluminum salt is friable, crumbly, and very weak cohesively. In adhesively bonding polymers to aluminum, it is this aluminum salt, when formed, that leads to low strength bonding failures. It was, therefore, of interest to determine if the EVA/glass coupling agent, Z-6030 (see Table 11), would also couple to aluminum, and stop the formation of pseudoboehmite in moist environments.

Table 15. Effect of Drying[a] the Hydrothermally Aged Test Specimens Reported in Table 14 to Assess the Reversible Recovery of Properties

Characteristics	Control	At 40°C			At 60°C				At 80°C			
		100 h	500 h	2000 h	100 h	250 h	500 h	2000 h	100 h	250 h	500 h	1000 h
Unprimed												
Modulus, psi	2830	2400	3400	2200	2500	3000	2700	1100	2700	1800	b	b
Ultimate strength, psi	1380	1205	1280	1210	1270	1340	960	480	1175	560	b	b
Ultimate elongation, %	600	590	565	570	590	575	500	280	545	290	b	b
Primed												
Modulus, psi	2500	2200	3000	2600	2600	3100	3100	2800	2600	2600	2800	2600
Ultimate strength, psi	905	965	990	860	955	890	980	850	905	920	1020	880
Ultimate elongation, %	350	325	315	260	290	240	240	240	240	310	405	260

[a]Dried in circulating air oven for 72 h at 105°C.
[b]Samples unusable.

This work, carried out at the University of Cincinnati, first observed that pseudoboehmite will generate a characteristic IR band at 1080 cm^{-1}, which can be detected on the aluminum surface using an IR technique based on surface reflection. Figure 7 consists of plots of the IR spectra of an aluminized back surface of a commercial solar cell, when new (spectrum A), and after 20 min (spectrum B), and 50 min (spectrum C) immersion in boiling water. At 50 min, there was clear IR evidence for the formation of pseudoboehmite. Fortunately, EVA does not have any IR absorbance at this wavenumber, and thus this IR band originating from an aluminum surface can be observed through an overcoating of an EVA film.

The aluminized back surface of the same commercial solar cell was next primed with A-11861 primer, followed by overcoating with a laminated and cured layer of EVA. This work is current, but initial results show that no pseudoboehmite has formed after 1-week immersion in boiling water. The aging is continuing, but already the evidence is accumulating that a self-priming EVA with Z-6030 coupling agent accomplishes both structural bonding to glass, and also corrosion protection for the solar cell's aluminized back surface.

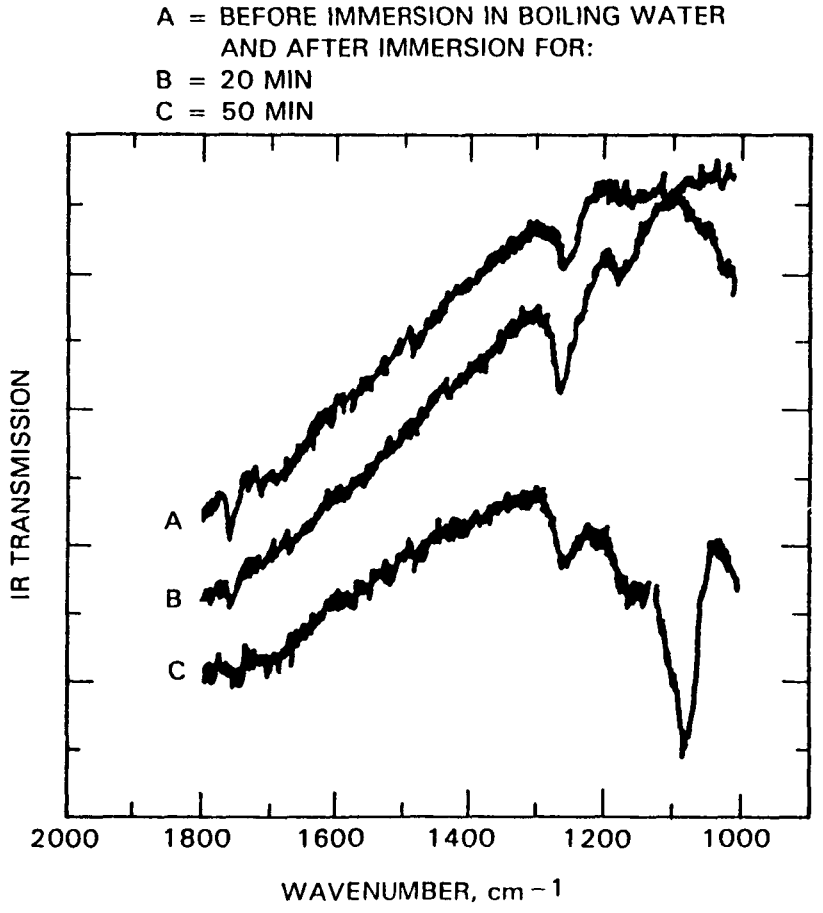

Figure 7. Reflection Infrared Spectra Obtained from the Aluminized Back Side of a Silicon Cell that has been Coated with a Thin Film of EVA

SECTION IV

Anti-Soiling Coatings

Soil accumulating on the front surfaces of PV modules reduces light transmission to the solar cells and, therefore, reduces power output. A study was carried out to investigate experimentally the details of natural soil accumulation, and derive a basic understanding of the surface requirements to reduce soil accumulation. The studies resulted in the development of effective low-soiling surface treatments for glass and plastic films. A summary of the experimental studies, and performance of the low-soiling coatings are described in the following paragraphs.

A. NATURAL SOILING BEHAVIOR

The behavior of natural soiling on different material surfaces was monitored at seven different climatic locations by measuring the reduction in the short circuit current (I_{SC}) of solar cells positioned behind seven transparent materials, that ranged from soft silicone elastomers to semi-hard plastic films, and hard glasses (see References 73 and 74). In general, the soiling accumulation behaved as illustrated in Figure 8 by the solid oscillating line, indicating that some soil accumulating during dry periods was removed during rain periods. It was noted that the minimums of the oscillations could be connected by a dotted line, suggesting the formation of a rain-resistant base layer of soil deposited on the surface. On top of this rain-resistant soil layer resided a loose layer that could be removed by rain. It was further observed that the rain-resistant base layer formed in about 30 to 60 days.

Closer examination of the base layer revealed that it, in turn, consisted of two layers (see Reference 55). Thus, including the top rain-removable layer, a total of three soil layers, labeled A, B, and C from the module surface out, could be identified. The three soiling layers are described in Figure 9. Layer C is the rain-removable top layer. Layer B is the soiling removable by washing. Layer A soil involves strong chemical attachment or chemisoption and if formed on the module cover, it can only be removed by abrasive scrubbing. Accepting the soiling layer concept, the soiling curves for each of the seven transparent materials could be separated into light obscuration caused by the base layers (A + B), and by the rain-removable Layer C. This was done by connecting the data minimums in the asymptotic region of the soiling curves, and assigning the magnitude of the dotted line to the layers "A + B" (they cannot be resolved by this data technique). For layer C, the difference between the dotted line and the maximum observed peak was calculated as the light obscuration caused by layer C. The light obscuration values assigned to the layer "A + B", and layer C are given in Table 16, for the seven locations and seven materials.

The data indicate that the largest quantity of rain-resistant soil (Column A + B) was found on the soft silicone, followed next by the semihard silicone and, least,

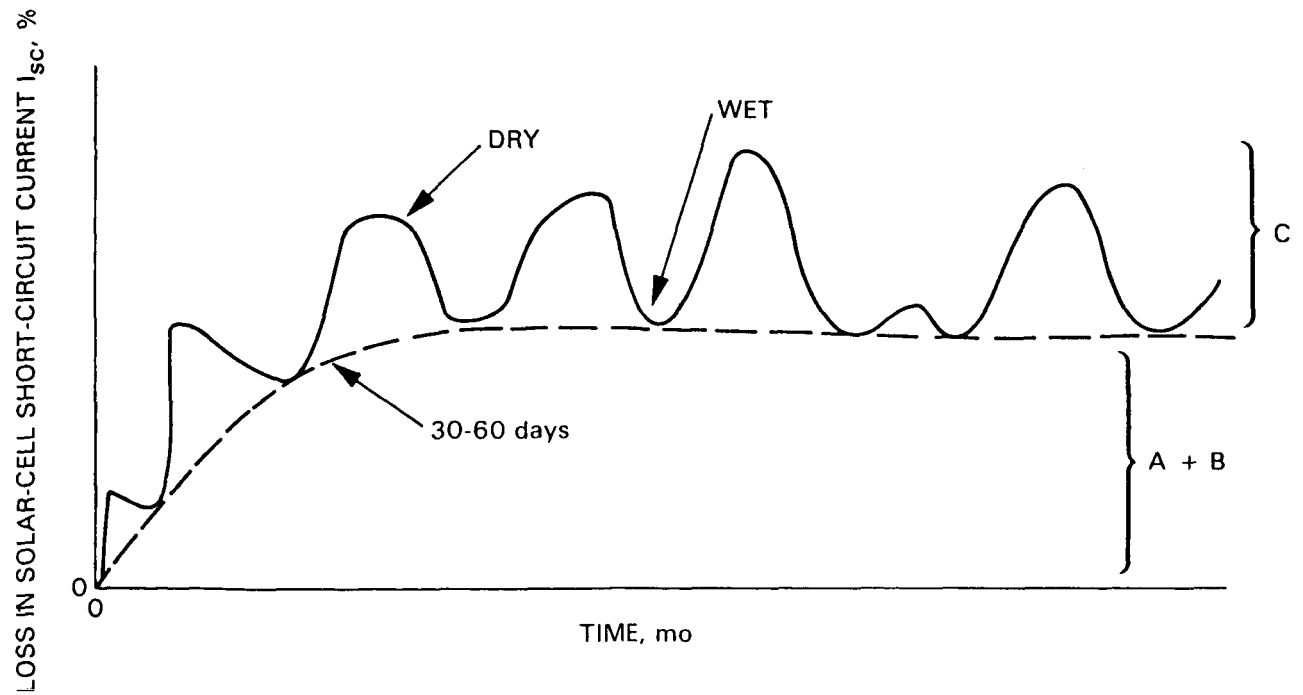

Figure 8. Behavior of Natural Outdoor Soiling

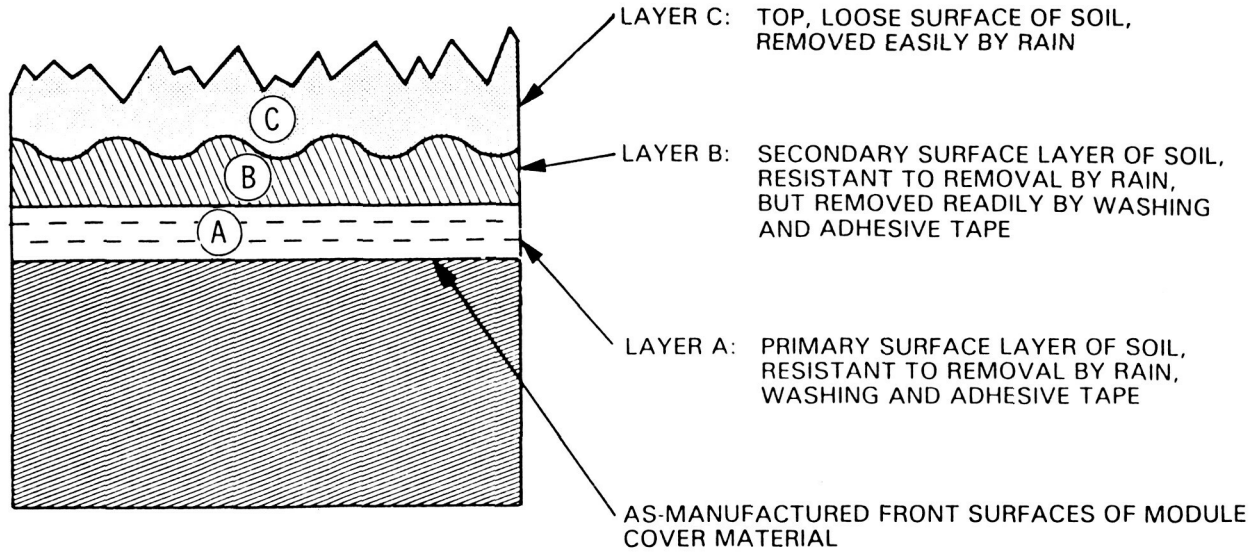

Figure 9. The Three Soiling Layers

by the remaining five harder materials. Although the numbers for these five materials are small, there is an indicated ranking. Comparing the plastic films, the fluorocarbon (Tedlar) is slightly better than the acrylic (Korad). Comparing the glasses, the ranking (in improving order) is soda-lime, aluminosilicate, and borosilicate. Note, that for some combinations of sites and materials, that neither layer A nor layer B has formed (the minima of the soiling curves were zero). The data suggest that the formation of the rain-resistant soil layers are both material- and site-dependent, but that module cover material dependency dominates.

Table 16. JPL Soiling Data: Reduction Percentages in PV Cell Short-Circuit Current from Soiling Layers on Cell Cover[a]

Site	Torrance		Point Vicente		Goldstone		Table Mountain		Pasadena[b]		JPL 34-deg Site[c]		JPL 45-deg Site[c]	
Cover Materials	A+B	C	A+B	C	A+B	C	A+B	C	A+B	C	A+B	C	A+B	C
Soft silicone RTV 615	20	10	NA	NA	NA	NA	NA	NA	25	8	24	6	24	7
Semihard silicone, Q1-2577	14	8	5	2	6	2	1	3	17	15	16	12	15	8
Acrylic film, Korad 212	3	8	0	8	1	2	2	1	5	14	3	13	3	11
Fluorocarbon film, Tedlar	1	8	0	5	0	2	0	2	3	13	1	16	2	12
Soda-lime glass	2	6	1	4	2	2	0	2	3	9	4	12	3	9
Aluminosilicate glass	1	12	1	5	0	2	0	2	2	12	2	13	2	11
Borosilicate glass	0	7	0	5	0	2	0	2	1	11	1	15	1	13
Average for layer C		4.8		4.8		2.0		2.0		12.3		13.5		10.6

[a] Data from Reference 74.
[b] Pasadena station of South Coast Air Quality Management District.
[c] 34- and 45-deg tilt angles from ground.

The site dependency of layer C relates to the atmospheric concentrations of soiling materials, their types, and rain cycles. The average of the six or seven values of light obscuration by layer C is also included in Table 16. If the average value for layer C is treated as a measure of the soiling characteristics of an environment, then (of the sites listed in Table 16) JPL and Pasadena are the dirtiest, and Goldstone and Table Mountain are the cleanest.

The soiling data from two JPL sites designated as 34 and 45 deg, differing only in the module tilt angles, show a reduction in layer C soil accumulation with increasing tilt toward the vertical. Figure 10 is a plot of tilt-angle data for layer C. A linear extrapolation based on two points would suggest no layer C deposition at a near-vertical alignment.

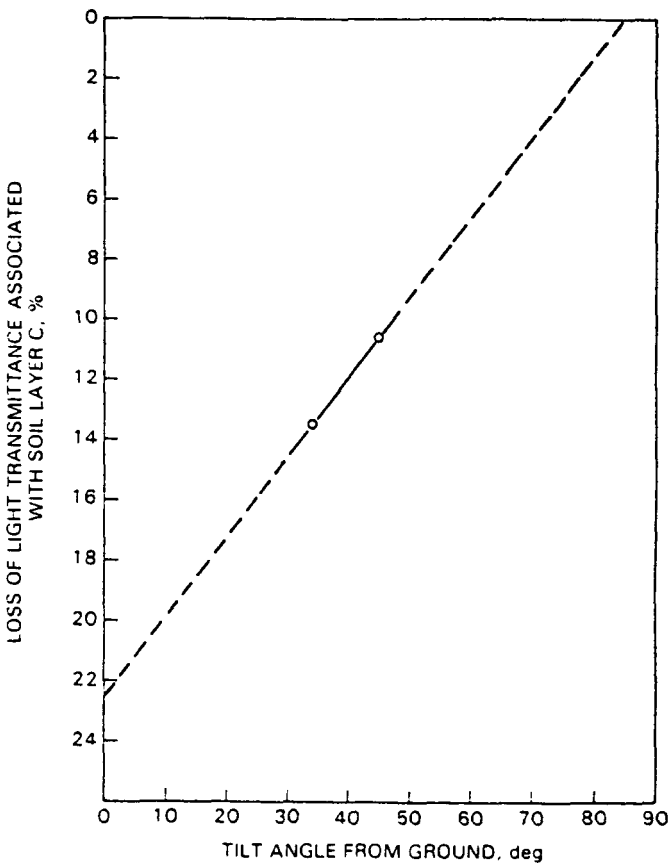

Figure 10. Effect of Tilt Angle on Accumulation of Soil Layer C

B. LOW-SOILING COATINGS

Both field soiling observation and experimental soiling data indicate that there are two distinct soiling problems to be dealt with to achieve low soiling. The first is to have top surfaces that resist the formation of the rain-resistant soil layers; the second is related to the rain-removable layer.

From the soiling data, it is possible to theoretically (see References 22 and 55) derive seven characteristics required to have low-soiling surfaces, as follows:

(1) Hardness.

(2) Smoothness.

(3) Hydrophobicity.

(4) Low-surface energy.

(5) Nonstickiness (chemically clean of sticky materials, surface, and bulk).

(6) Cleanliness (chemically clean of water-soluble salts and first-period elements, surface, and bulk).

(7) Weatherability (resistance to UV photo-oxidation and/or hydrolysis).

These seven postulates relate to surface requirements for resisting the formation of rain-resistant soil layers and, taken in total, lead to the conclusion that the top surface must be a hard, smooth, fluorocarbon material, or a very thin (micrometers) coating of a fluorocarbon on a hard, smooth backing (i.e., glass). These requirements were guidelines for the development of durable fluorocarbon coatings to be applied to solar-module surfaces to achieve low maintenance costs and to preserve high transparency.

Candidate materials for the outer surfaces of PV modules currently consist of low-iron glass, Tedlar fluorocarbon film (Du Pont Co., 100BG3OUT), and a biaxially oriented acrylic film, Acrylar (3M Corp., X-22417). These materials are all relatively hard, smooth, and free of water-soluble residues. Experiments were conducted to determine if an improvement in soiling resistance could be obtained by the application of low surface-energy treatments. A survey of coating materials showed that very few commercial materials exist that could be useful for this purpose. Nevertheless, two candidate fluorocarbon coating materials were identified:

(1) L-1668, an experimental fluorochemical silane produced by 3M Corp. that is used to impart water and oil repellency to glass surfaces. This material will bond chemically to glass surfaces.

(2) Dow Corning Corp., E-3820-103B, an experimental treatment consisting of perfluorodecanoic acid chemically reacted with a Dow Corning silane, Z-6020. This compound, which is not commercially available, will bond chemically to glass surfaces.

In a trial test at Springborn Laboratories, each of these two fluorocarbon coatings, which are supplied in solvent solutions, were brushed onto the surfaces of the

three outer-surface candidate materials, and allowed to dry in air and react chemically for 24 h. The treated materials were then soaked in water, simulating rain, to determine if they were adequately attached chemically. The criterion for judging this attachment was whether water would bead, or spread on the surfaces when the materials were periodically removed from the water bath. By this criterion, both coatings were judged to have become permanently attached to glass, the E-3820 to have become attached only to the Tedlar, and the L-1668 to have become attached only to the Acrylar.

To promote chemical attachment of the L-1668 on Tedlar, and the E-3820 on Acrylar, the surfaces of both of these films were then activated by exposure to ozone, to generate surface polar groups that would react chemically with the silanes, followed by brushing on the fluorocarbon coating solutions. This technique worked well. Therefore, as an additional experiment effort, E-3820 was also applied to an ozone-treated Tedlar surface, and L-1668 was also applied to an ozone-treated Acrylar surface. The concept was that the ozone treatment may also enhance the adhesion of these fluorocarbon coatings to the plastic films. Glass and plastic films coated with the fluorocarbon coatings were then mounted on outdoor racks on the roof of Springborn Laboratories' facilities in Enfield, Connecticut. Evaluation was performed monthly and a record of rainfall was kept to correlate soiling effects with precipitation. The surfaces of these test specimens were not washed or touched with the hands.

C. PERFORMANCE OF LOW-SOILING COATINGS

The degree of soiling on the test specimens was monitored by measurement of the percentage of decrease in the I_{SC} output of a standard silicon solar cell positioned behind the soiled test specimens. For Tedlar, the best coating is found to be E-3820, and Figure 11 compares the soiling behavior of uncoated Tedlar (control) and E-3820-coated Tedlar. For Acrylar, the best coating is found to be E-3820 in combination with ozone, and Figure 12 compares the soiling behavior of uncoated Acrylar (control) and the E-3820 ozone-coated Acrylar specimen. For glass, little difference is noted in comparing E-3820 and L-1668, but E-3820 might be slightly better (Figure 13).

Comparing the uncoated controls, glass has the least tendency to retain natural soil, followed by Tedlar and then Acrylar. However, with the fluorocarbon anti-soiling coatings, the soiling behavior and optical losses for all three materials become essentially the same.

The soiling data were averaged over the 28-month period, and the summary of time-averaged values are given in Table 17. The untreated glass control sample realized an average optical loss of about 2.65% over the 28-month period; the Tedlar control realized an average loss of about 5.38%; and the Acrylar control specimen realized an average loss of about 7.20%.

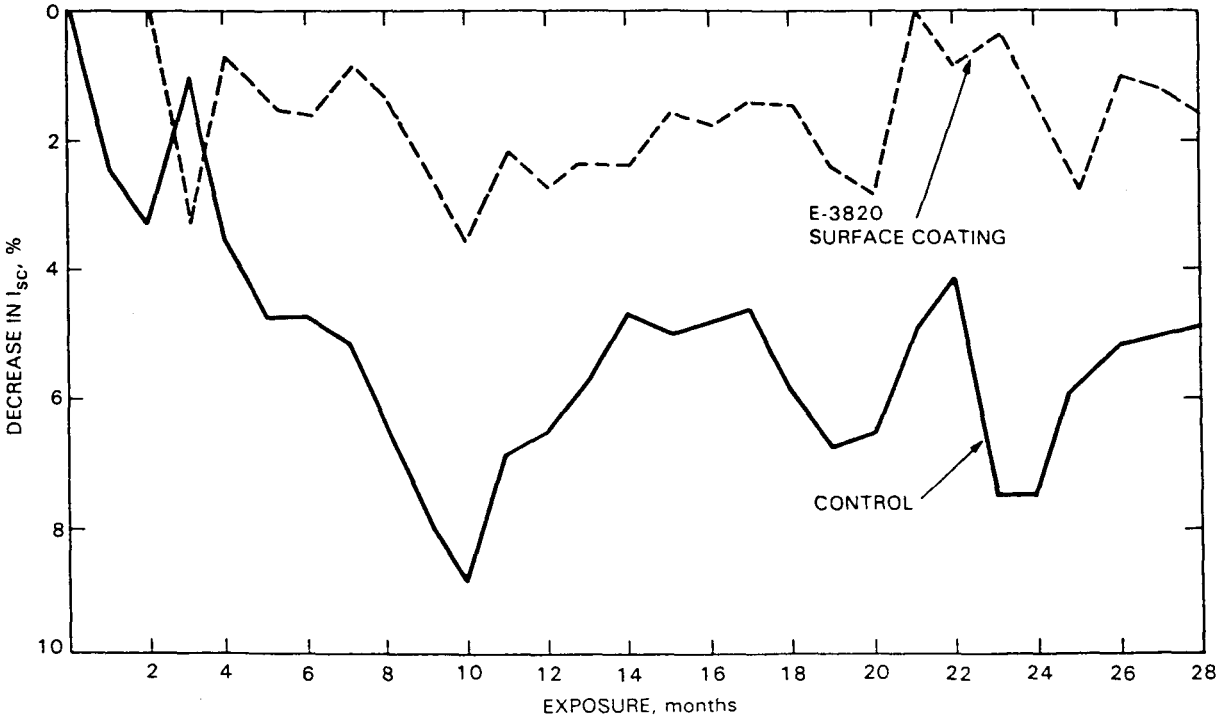

Figure 11. Outdoor Soiling Behavior of Tedlar 100BG3OUT Plastic Film, With and Without a Fluorocarbon Anti-soiling Coating

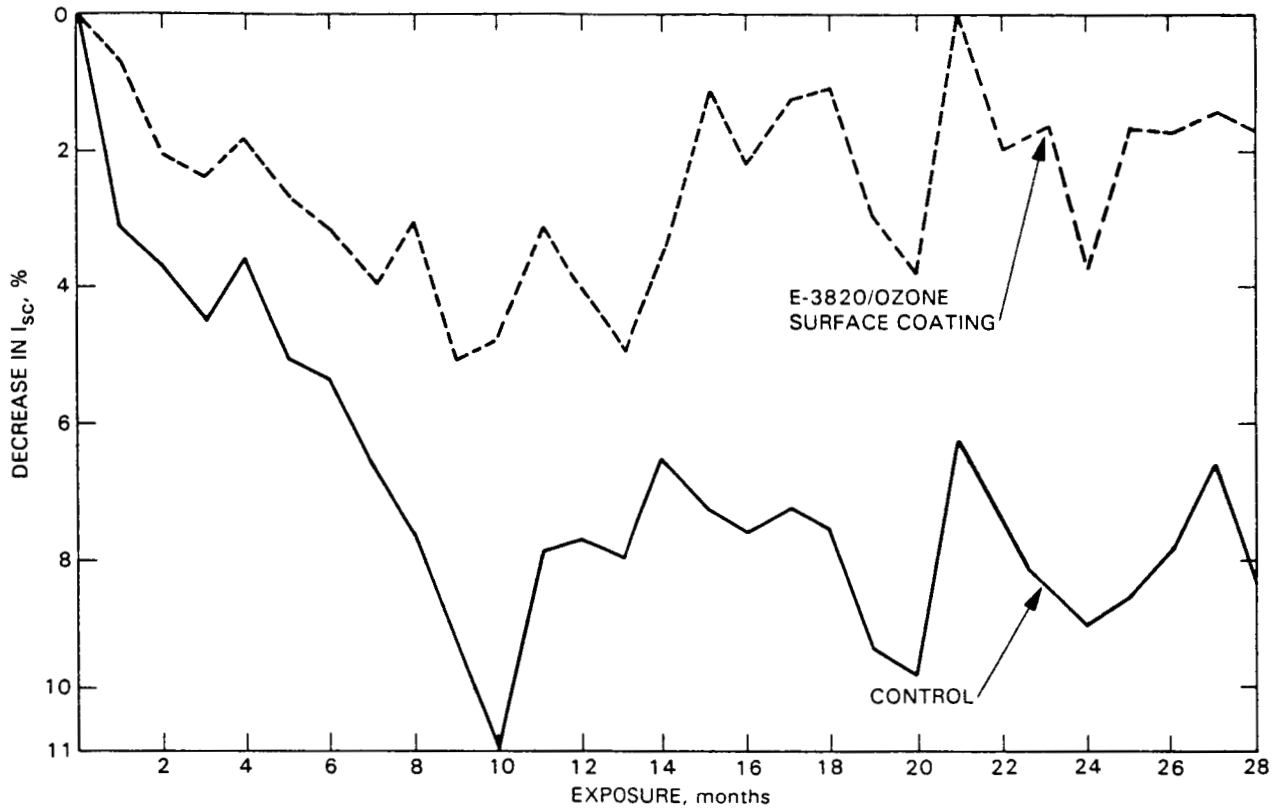

Figure 12. Outdoor Soiling Behavior of Acrylar X-22417 Plastic Film, With and Without a Fluorocarbon Anti-soiling Coating

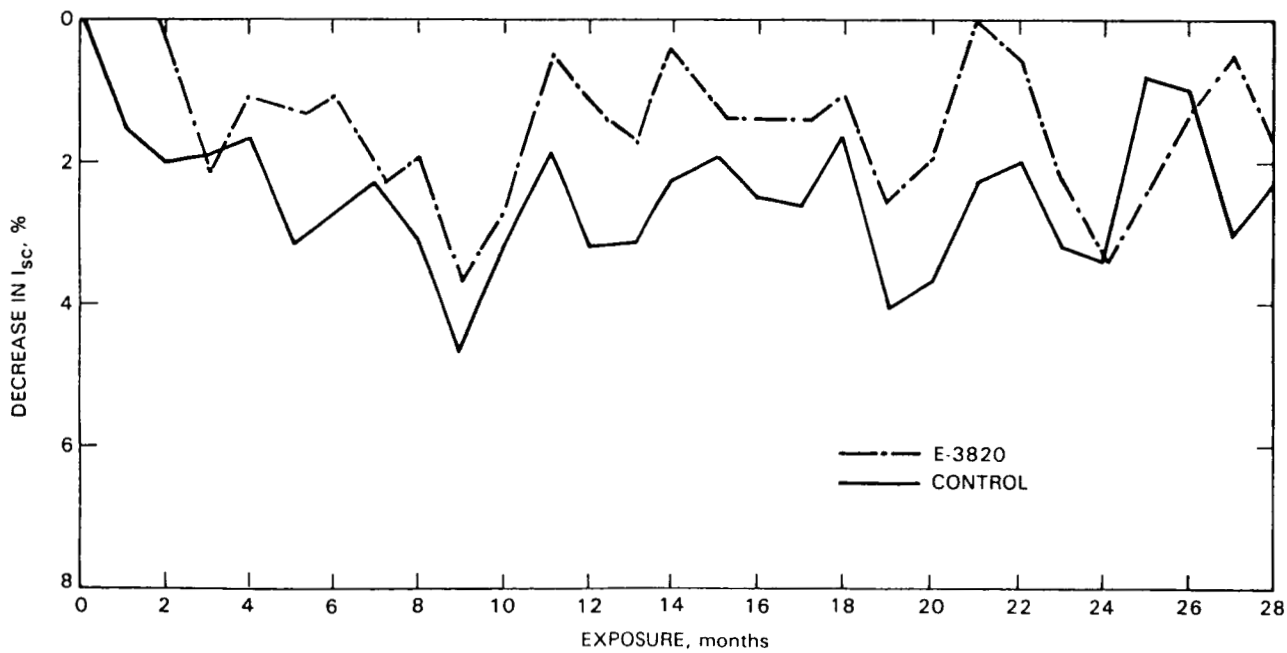

Figure 13. Outdoor Soiling Behavior of Glass With and Without a Fluorocarbon Anti-soiling Coating

The data in Table 17 also indicate clearly that E-3820 is the better-performing fluorocarbon coating for all three materials. On glass, the E-3820 coating resulted in a reduction of soiling-related optical losses from 2.65% for untreated glass, to 1.55% for treated. Similarly, on Tedlar, the E-3820 optical losses were reduced from 5.38 to 1.70%. Acrylar realized an average reduction in soiling loss from 7.20% down to

Table 17. Time-Averaged Values of the 28-Month Soiling Data

Materials	Time-Averaged Optical Losses, %
Glass	
Control	2.65
With E-3820	1.55
With L-1668	1.59
Tedlar	
Control	5.38
With E-3820	1.70
With L-1668/ozone	4.28
With L-1668	4.43
With E-3820/ozone	4.68
Acrylar	
Control	7.20
With E-3820/ozone	2.59
With L-1668	4.21
With E-3820	4.44
With L-1668/ozone	5.15

2.59%, or a performance gain of nearly 4.61%. These performance gains can be economically important to the electrical power output of a PV module.

Figure 14 is a plot of the rainfall pattern in Enfield, Connecticut, over the soiling exposure period. The data are plotted as monthly rainfall totals in inches versus the month in which the rainfall occurred. The highs and lows in the rainfall totals generally correlate with the soiling highs and lows shown in Figures 11, 12, and 13. A sustained dry period with little rain occurred during the fourth to the tenth month, with no rain at all in the eighth and ninth months. This resulted in the maximum accumulation of surface soiling observed from all test specimens over the entire outdoor exposure period. After the ninth and tenth months, rainfall began to increase and the surfaces became cleaner.

During this exposure period, the monthly rainfall totals were accumulated from a fair number of rainstorms distributed throughout the month. In the twenty-first month, however, an especially intense and heavy rainstorm of several days duration accounted for almost all of the monthly total. As shown in Figures 11, 12, and 13, this intense rainstorm removed virtually all of the measurable soil from the fluorocarbon-coated surfaces.

With respect to Layer C behavior, if it can be assumed that no rain-resistant layers (A or B) formed on the E-3820 coated glass specimen, then the time-average value of 1.55% (see Table 17) can be considered as the time-average optical loss associated with the cyclical deposition and rain removal of layer C soil, in Enfield, Connecticut. The higher minimums observed for Tedlar and Acrylar, respectively 1.70 and 2.59%, may indicate the formation of layers that resist removal by gentle rainfall, but not by intense rainfall. This suggests possibilities for further performance gains from the use of improved fluorocarbon coating materials.

This work suggests that maintenance-cleaning techniques for hard surfaces should be developed for layer C, perhaps a low-pressure water spray (rain simulation) during dry cycles.

In conclusion, low-surface energy treatments based on fluorosilane chemistry seem to be effective in retard-

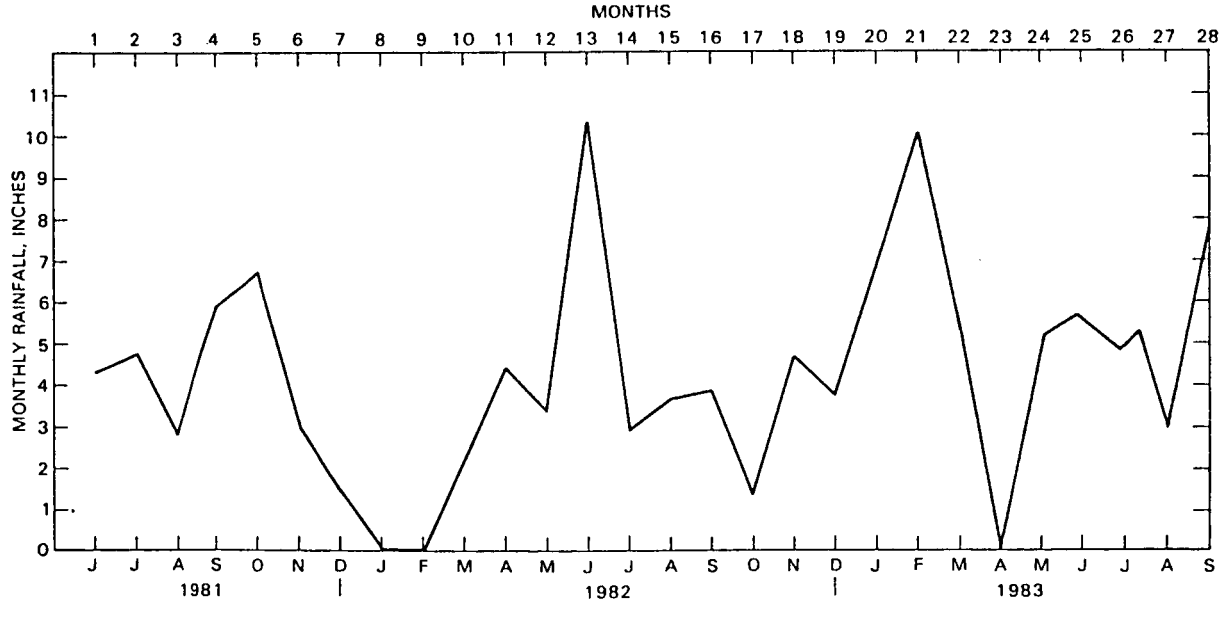

Figure 14. Rainfall in Enfield, Connecticut, Over a 28-Month Period

ing the accumulation of dirt on the candidate outer surfaces of interest. The most effective soil retardant treatments identified to date are: for Sunadex glass, E-3820; for Acrylar, ozone activation followed by E-3820; and for Tedlar, treatment with E-3820.

After 28 months of outdoor exposure, the E-3820, anti-soiling treatments resulted in potential performance gains from nearly 1% for glass to 4% for Acrylar in light transmission measured with a standard cell and light source. The removal of accumulated soil correlated well with rainfall, but not with precipitation such as snowfall. These 28 months of experimental effort provided support for the theoretically derived considerations for low-soiling coatings, and a rationale for future activities for improvements in fluorocarbon coating chemistry. Experimental evidence suggests that layer C is site-dependent, rain-frequency dependent, and possibly tilt-dependent.

SECTION V

Encapsulation Engineering

An engineering analysis of encapsulation systems was conducted to understand the requirements to achieve a reliable and practical engineering design involving the following engineering features:

(1) Structural adequacy.

(2) Electrical isolation (safety).

(3) Maximum optical transmission.

(4) Minimum module operating temperature.

The engineering analyses contributed to achieving the following objectives:

(1) Development and verification of general analytical methods and techniques, employing material costs and physical properties as data inputs, to generate for any combination of materials an optimized module design involving the following:

   (a) Minimum thickness of the structural panel satisfying Project load requirements.

   (b) Solar cells not to be stressed greater than mechanical stress limits.

   (c) Minimum material thicknesses required for electrical isolation (safety).

   (d) Maximum module power output as a function of module operating temperature and optical transmission to solar cells.

(2) Generation of encapsulation design general principles and design guidelines.

This activity was carried out by Spectrolab and was divided into two technical phases. Phase I involved computer analysis and simulation modeling with limited experimental work where necessary to measure critical material properties. Phase II was an experimental activity that measured the properties and performance of fabricated modules, for which properties and performance were predicted analytically during Phase I. Necessary refinements and modifications to the computer programs and/or analytical models were then made, depending on the deviations encountered between prediction and measurement.

A major effort of Phase I was to identify the relevant physical properties of encapsulation materials needed to complete the various technical analyses, such as thermal conductivities, tensile modulus, and strength. The sensitivity of system response to variations in a relevant property was assessed, and predictions of the performance of specific encapsulation designs were made.

Phase I was generally done by specifying encapsulation materials in terms of the magnitude of relevant properties, rather than by chemical name (e.g., EVA). As a result the impact, if any, of the interchangeability of encapsulation materials can be assessed, because the properties required for comparison are known, and the system sensitivity to such properties has been determined. Also, this approach identified optimum magnitudes of relevant properties, material thicknesses, and configurations.

The major findings and key results from the encapsulation engineering activity are summarized for thermo-optical modeling, structural characterization, and electrical isolation (safety). For electrical isolation, this work resulted in a method for identification of the intrinsic dielectric strength of electrical insulation materials, which, if valid, would stand as a significant accomplishment of this task. The concept is described in this document, and as of this writing, is undergoing review by engineering and scientific personnel.

A. THERMAL-OPTICAL MODELING

The purpose of thermal-optical modeling was to arrive at an assessment of those thermal and optical properties of an encapsulation system that are important for minimizing the module operating temperature and maximizing optical transmission to the solar cells, both of which are keys to achieving higher module power output.

Although thermal and optical analytical models can, and could be, independently developed, of necessity they were combined because incident solar insolation is partitioned between that which is converted to electrical energy and that which is converted to heat.

Results from the thermal-optical modeling can be summarized as follows:

1. Maximum Optical Transmission

   Analysis has shown that:

   (1) Incident solar flux at wavelengths on either side (UV, IR) of the spectral-response range of silicon solar cells (0.4 μm to 1.1 μm), that is not reflected at the surface, is essentially absorbed by the module and converted to heat. This is because the transparent front materials are designed to be UV-absorbing, and they also have inherently strong IR absorption bands. In addition to this, the silicon solar cell absorbs strongly in the infrared.

(2) Incident solar flux in the wavelength region of 0.4 μm to 1.1 μm should be transmitted maximally to the solar cells. The optical properties and features affecting this transmission are surface reflection ($\approx$ 4%), anti-reflective (AR) coating on the solar cell, absorption bands in the encapsulation materials, and index-of-refraction mismatch at the interfaces.

(3) Front-side transparent encapsulation materials should have virtually flat transmission (no absorption bands) in the wavelengths from 0.4 μm to 1.1 μm, and an integrated transmittance $\geq$98%, after correcting for surface reflection losses of about 8%. Low-cost pottant candidates described in this document have these optical properties. Computer predictions of power output of modules with 10 to 25 mils of EVA indicated no penalty because of EVA thickness. High-iron (Fe^{+++}) glass does have undesirable absorption in the wavelength region from 0.4 μm to 1.1 μm.

(4) AR coatings on silicon solar cells are a necessity. The AR coating should be optically matched with the pottant, but being optically matched with air is acceptable, resulting in only a small power loss when encapsulated. However, significant power loss occur in cells without any AR coating.

(5) AR coatings on the module top cover surface may be beneficial, if application cost performance and durability can provide a cost-benefit advantage. AR coatings on the second surface of glass, that is, at the pottant interface, tend to reduce transmission. Glass superstrates with AR coatings on both sides are not recommended.

(6) Computer analysis and experimental exposures to normal-incident light on stippled glass superstrates, either stipple-up or stipple-down, found no optical effects, either beneficial or detrimental.

(7) Matching indexes of refraction of adjacent material layers are desirable, but if not done, back-reflection losses for the combinations of glass, plastic-film front covers, and pottant materials being considered are small because the index-of-refraction differences for these various materials are small. The best situation for mismatched index-of-refraction is to have them increased in each layer from the surface layer inward toward the cells. The reverse, decreasing index-of-refraction toward the cells, can result in power losses.

2. Minimizing Module Temperature

Analysis has shown that:

(1) The relevant thermal properties of encapsulation materials regulating module operating temperature are IR emissivity of the front and back surface, solar absorption of the back surface, and thermal conductivity. Figure 15 illustrates the strong sensitivity of the solar cell temperature on back-side emissivity, for a glass-superstrate design.

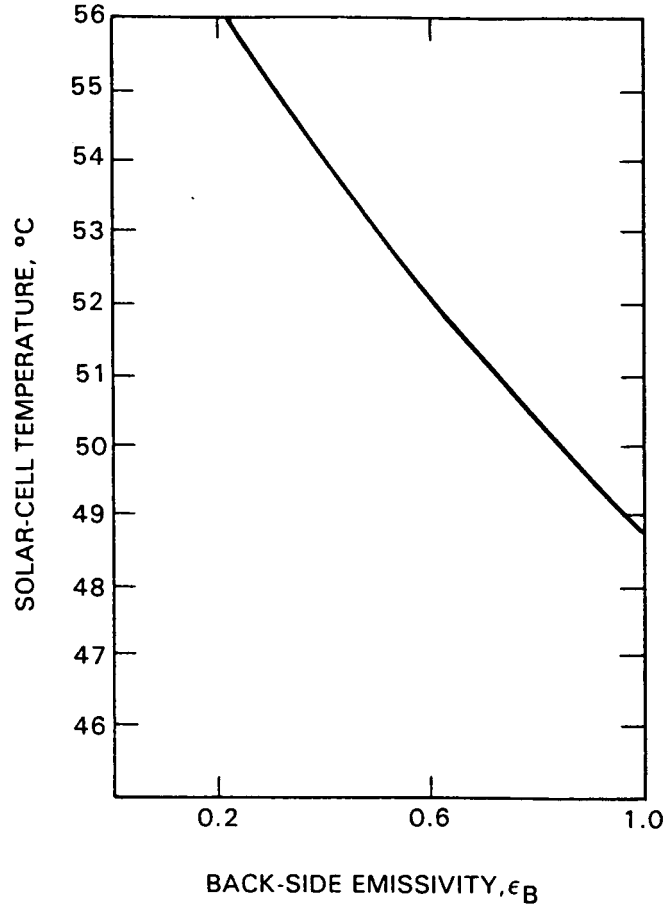

Figure 15. Solar-Cell Temperature Versus Back-Side Emissivity for a Glass-Superstrate Design

(2) In terms of these thermal properties, module operating temperature is primarily regulated by the IR emissivity of the front and back surfaces, and to a lesser extent by thermal conductivity. This leads to the finding that a glass superstrate design and wood substrate design may have nominally the same solar cell operating temperatures.

(3) The dominant control on module operating temperature, which can be exercised

through selection of encapsulation materials, involves the use of front- and back-cover materials with maximum IR emissivity (ϵ). Transparent glass and plastic-film front covers have ϵ values ranging between 0.85 to 0.90. Back-cover materials should also have very low solar absorptivity. The two requirements for the back cover are best satisfied using a white organic (non-metallic) material. Values of ϵ for white organic materials can be >0.90.

(4) Lower module operating temperature is aided by the use of fins on the substrates (no horizontal cross fins) which also function as stiffening ribs. The mounting design should provide maximum accessibility of front and back surfaces to circulating air.

3. Estimating Module Temperatures

A key finding from thermo-optical modeling is that those features of PV modules that are involved in the absorption of solar insolation and conversion to heat can be mathematically treated independently of those features of a PV module that relate to heat dissipation, with negligible error. Accordingly, a PV module can be viewed as a thick slab of material layers having as a core a simple heat generator. This heat-dissipation model is illustrated schematically in an outdoor environment in Figure 16. Heat, Q_C, generated by the core (solar cell assembly), is conducted thermally through the sun-side and back-side material layers to the front and back surfaces, and then is dissipated from the surfaces by radiation, free convection, and wind convection. For fixed environmental conditions and thermal properties of the material layers and surfaces, an equilibrium relationship between Q_C and the core temperature T_C can be found.

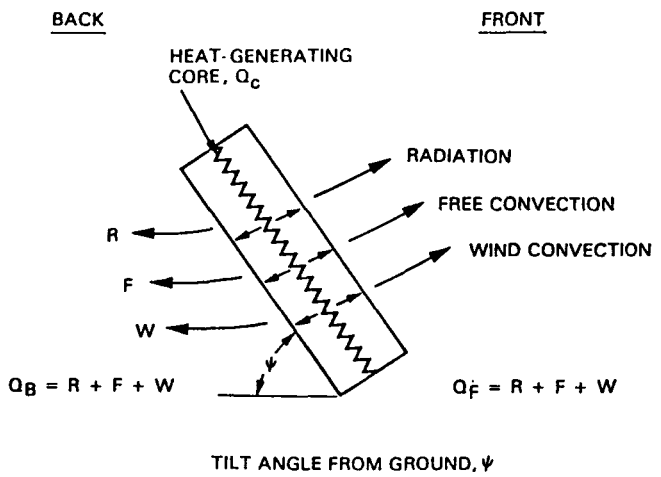

Figure 16. Heat Dissipation Model

The thermal model for back-side and front-side material layers is shown in Figure 17. The encapsulation material layers can be described by the sum of

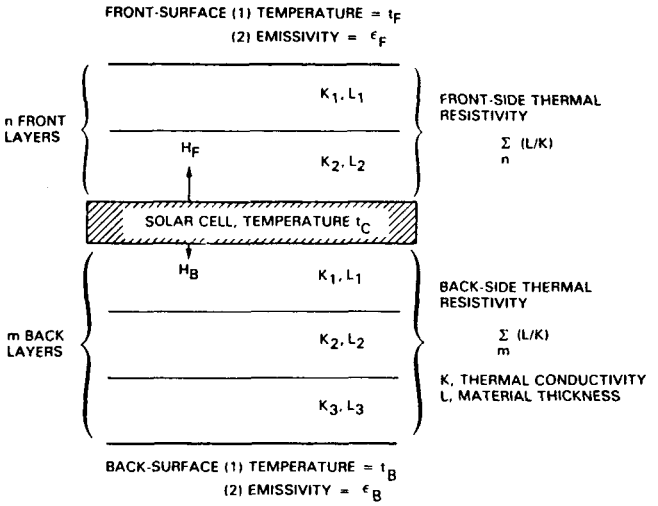

Figure 17. Thermal Conduction Model

their individual thermal resistivities, which is the thickness L of the layer, divided by the thermal conductivity K of the material in the layer. Representative thermal-resistivity values for encapsulation materials are given in Table 18. The sum of front and back thermal resistivities of encapsulation layers for a glass-superstrate design and a wooden (hardboard)-substrate design are given in Table 19. For these examples, the thickness of the glass and the wood is 1/8 in. (125 mils), and each is the dominant contributor to the thermal resistivity on their respective side of the module. A mild-steel substrate design would have a back-side thermal-resistivity sum less than that of the wooden-substrate design. The surfaces of the thermal model are described by the magnitude of the IR emissivity that is involved in regulating the dissipation of heat from the surface by radiation.

Another related aspect of the thermal-optical model was also investigated. The detailed computer program may not be readily available to PV module designers for analysis of their systems or design options. It therefore, was of interest to determine if a simple set of expressions for thermal radiation, conduction, and free convection and wind convection could be derived for the heat dissipation model, with negligible error. A JPL publication (see Reference 75) set forth heat-transfer equations for radiation and convection reproduced from References 76 and 77. These equations are given in Table 20. With fixed environmental conditions, and thermal resistivity values such as those shown in Tables 18 and 19, the equations in Table 20 can be solved simultaneously for the equilibrium relationship between Q_C and T_C, with negligible error. For this analysis, a value of 0.8 was used for the ground emissivity ϵ_g.

Using the equations in Table 20 and the thermal resistivity values in Table 18, the equilibrium relationship between Q_C and T_C for a 1/8-in-thick glass-superstrate module was found, and is plotted in Figure 18. Two cases are shown: a field-array installation in which heat

Table 18. Thermal Resistivities

Material	(K), $\frac{\text{Watts-mils}}{\text{ft}^2-°\text{C}}$	L, mils	Thermal Resistance, L/K
Acrylic film	3	7×10^2	4.3×10^{-3}
Glass	125	3×10^3	41.6×10^{-3}
EVA	10	9×10^2	11.1×10^{-3}
Steel	28	2×10^5	0.14×10^{-3}
Wood (hardboard)	125	7×10^2	178×10^{-3}
Mylar	3	6×10^2	5×10^{-3}
Aluminum foil	2	7×10^5	0.003×10^{-3}
Stainless-steel foil	2	2×10^5	0.01×10^{-3}

Table 19. Thermal-Resistivity Sums for Glass-Superstrate and Wooden-Substrate Module Designs

Module Design	Thermal Resistivity, $\frac{\text{ft}^2-°\text{C}}{\text{Watts}}$
Glass, EVA,[a] Mylar,	$\Sigma\,(L/K)_{front} = 52.7 \times 10^{-3}$
	$\Sigma\,(L/K)_{back} = 16.1 \times 10^{-3}$
Acrylic, EVA,[a] Wood, Mylar	$\Sigma\,(L/K)_{front} = 15.4 \times 10^{-3}$
	$\Sigma\,(L/K)_{back} = 194.1 \times 10^{-3}$

[a]This example assumes that the EVA layer in front of the cells and the EVA layer behind the cells are each 10 mils thick.

dissipation can occur from both the front and back surfaces, and a rooftop installation where heat dissipation can occur from the front side only (i.e., $Q_B = 0$).

The relationship between T_c and Q_c is nearly linear over the range from 30 to 100 mW/cm^2. For the example shown in Figure 18, if the glass-superstrate module mounted on an array installation were required to dissipate 70 mW/cm^2 of heat, its equilibrium temperature would be near 47°C. Mounted on a rooftop with no back-side heat dissipation ($Q_B = 0$), its equilibrium temperature to dissipate 70 mW/cm^2 would be near 67°C.

The effect of air temperature on the operating temperature of a glass-superstrate module is shown in Figure 19 for air temperatures of 10, 20, and 30°C.

Figure 20 compares the heat-dissipation behavior of three module designs: a glass-superstrate module, a wooden-substrate module, and a mild-steel substrate module.

The absorption and conversion to heat of incident sunlight that must be dissipated from a module, Q_c, can be estimated from simple considerations when modules are classified into three distinct absorption types (Figure 21). Simplifying assumptions for all three module types are that incident sunlight is normal to the module surfaces, and that surface back-reflection losses are 4%.

Module Type A in Figure 21 has 100% solar cell area coverage. Hence, Q_c is simply entering insolation minus any electric power output: mathematically,

$$Q_c = (0.96)\,(S) - \text{electric power} \qquad (1)$$

For normal operating cell temperature (NOCT) estimates, electric power is zero; therefore, $Q_c = (0.96)\,(S)$.

Module Type B in Figure 21 has partial solar-cell coverage (less than 100%), with transparent intercell spaces. Denoting the fraction of solar-cell area coverage as A, then Q_c is estimated by

$$Q_c = (0.96)\,(A)\,(S) - \text{electrical power} \qquad (2)$$

For this case, it is assumed that all insolation entering the transparent intercell area, 1 − A, passes out of the module with no heat contribution. Again, for NOCT estimates, electric power is zero, and, therefore, $Q_c = (0.96)\,(A)\,(S)$.

Module Type C, in Figure 21, has partial solar cell coverage, with a white background in the intercell spaces. Therefore, Q_c is estimated:

$$Q_c = (0.96)\,(A)\,(S) + (0.96)\,(1 - A)\,(S)/3 - \text{electrical power} \qquad (3a)$$

The assumption is made that one third of the sunlight incident on the white background is absorbed by the

Table 20. Heat Transfer Equations for Heat-Dissipation Modeling

Module Sun Side

$$Q_{FF} = Q_{\text{free convection}} = (1.52)(\cos\psi)^{1/3}(t_F - t_A)^{4/3}\ (W)/(m^2)\ (°C)$$

$$Q_{WF} = Q_{\text{wind convection}} = H(t_F - t_A)$$

$$Q_{RF} = Q_{\text{radiation}} = \epsilon_F \alpha (T_F^4 - T_{sky}^4)$$

$$Q_{\text{front}} = Q_{\text{conduction}} = (t_C - t_F)/\Sigma(L/K)_{\text{front}} = Q_{FF} + Q_{WF} + Q_{RF}$$

Module Back Side

$$Q_{FB} = Q_{\text{free convection}} = (1.31)(\cos\psi)^{1/3}(t_B - t_A)^{4/3}\ (W)/(m^2)\ (°C)$$

$$Q_{WB} = Q_{\text{wind convection}} = H(t_B - t_A)$$

$$Q_{RB} = Q_{\text{radiation}} = \epsilon_B \epsilon_g \alpha (T_B^4 - T_A^4)$$

$$Q_{\text{back}} = Q_{\text{conduction}} = (t_C - t_B)/\Sigma(L/K)_{\text{back}} = Q_{FB} + Q_{WB} + Q_{RB}$$

Total Heat Dissipation (Q_c)

$$Q_c = Q_{\text{front}} + Q_{\text{back}}$$

Terms and Constants

H = wind convection coefficient, $W/(m^2)$ (°C)

(a) $H = 3.8\ V$, $V \leq 5$ m/s

(b) $H = 7.17\ V^{0.78} - 6.0$, $V > 5$ m/s

T_A = ambient air temperature, K

T_B = front-surface temperature, K

T_F = front-surface temperature, K

T_{sky} = $0.914\ T_A$ (Reference 86)

t_A = ambient air temperature, °C

t_B = back-surface temperature, °C

t_C = core temperature, °C

t_F = front-surface temperature, °C

V = wind velocity, m/s

α = Stefan-Boltzmann constant, $0.56699 \cdot 10^{-8}$ $mW/cm^2(K^4)$

ϵ_B = back-surface emissivity

ϵ_F = front-surface emissivity

ϵ_g = ground emissivity

ψ = module tilt angle from horizontal, deg

$\Sigma(L/K)_{\text{front}}$ = thermal resistance of back-side encapsulation layers

$\Sigma(L/K)_{\text{back}}$ = thermal resistance of sun-side encapsulation layers

solar cells. Again, for NOCT estimates, electric power is zero, and, therefore

$$Q_c = (0.96)(A)(S) + (0.96)(1 - A)(S)/3. \qquad (3b)$$

NOCT values have been measured experimentally and reported (see Reference 66) for a Block II Spectrolab, Inc., module in an array installation and for a Block II Solar Power Corp. module in both array and rooftop installations. The Spectrolab Block II module had a glass superstrate with transparent intercell area (Module Type A); the Solar Power Block II module had a structural-plastic substrate with a white background in the intercell area (Module Type C). Both module designs had a solar-cell area coverage A of about 0.7. The experimentally measured NOTC values are given in Table 21.

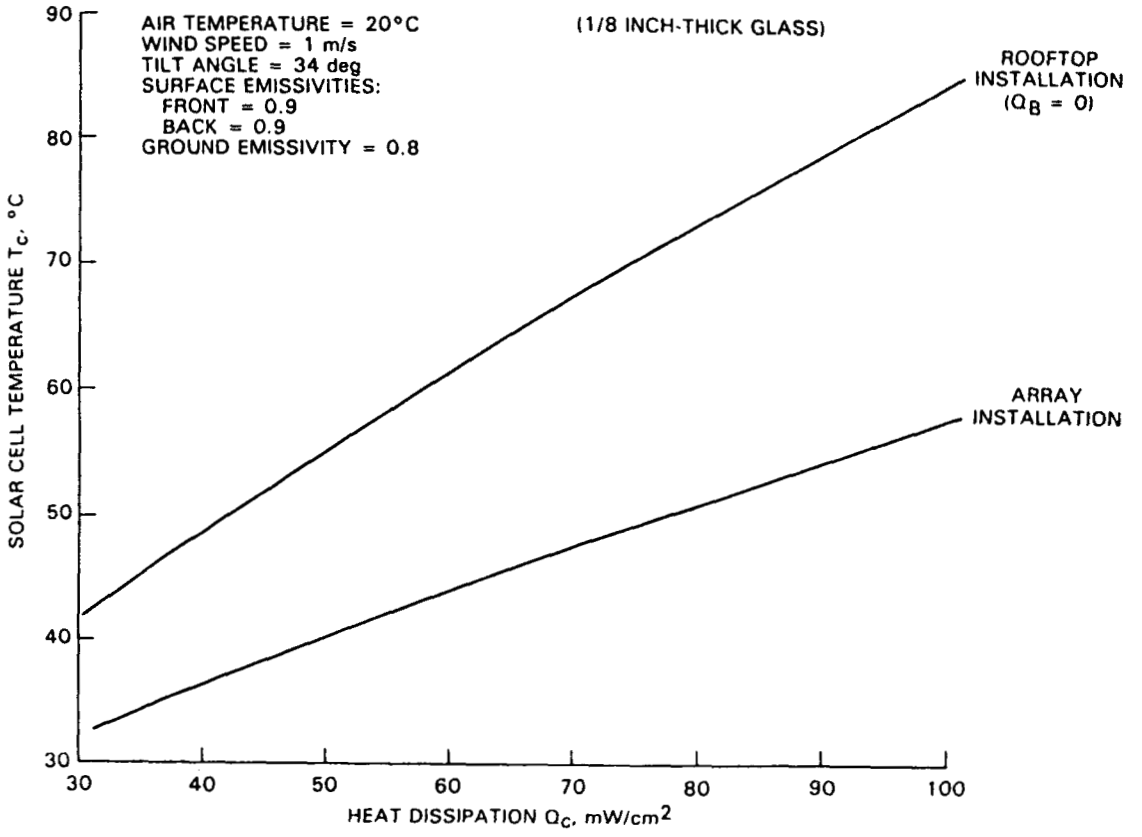

Figure 18. Heat-Dissipation Behavior of a Glass-Superstrate Module

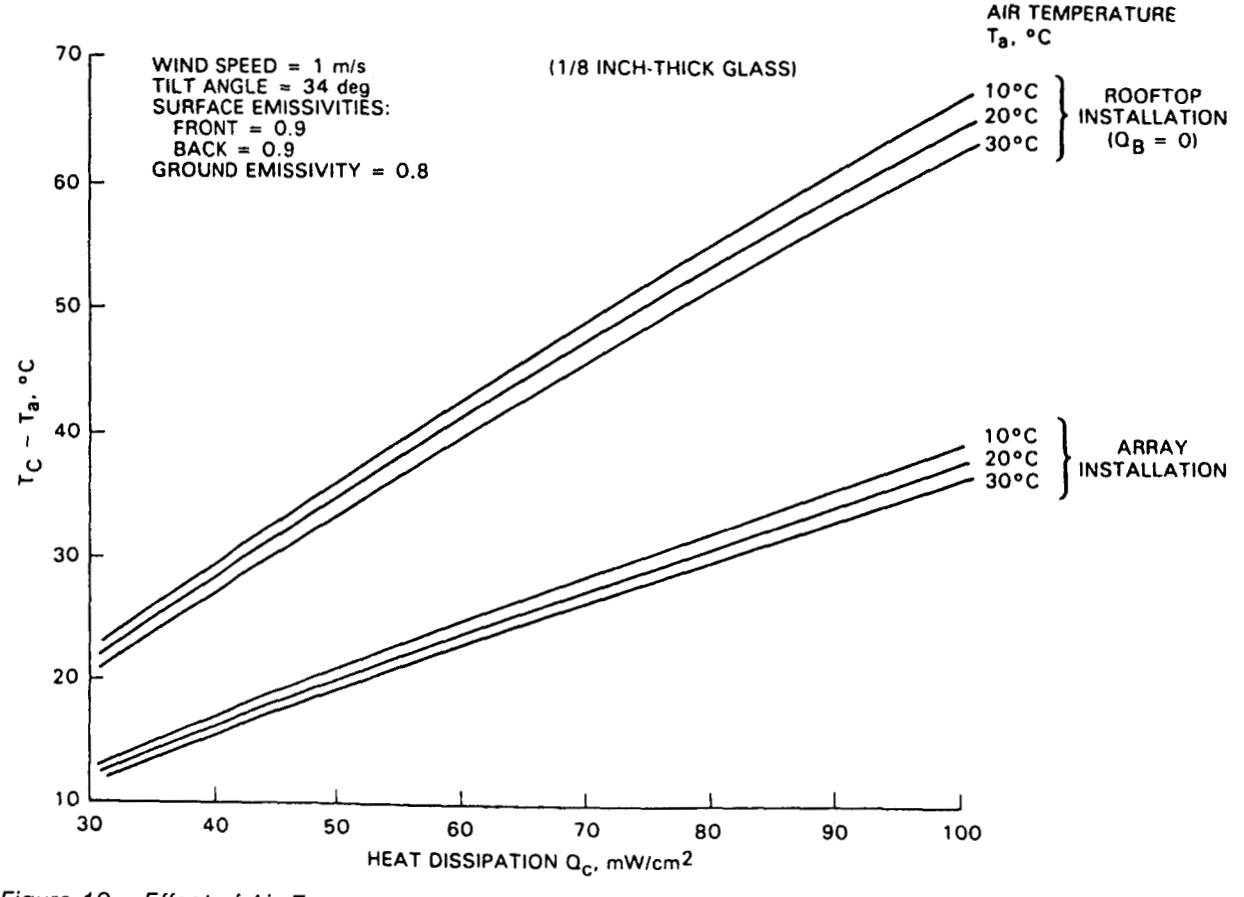

Figure 19. Effect of Air Temperatures (T_A) on the Heat-Dissipation Behavior of a Glass-Superstrate Module

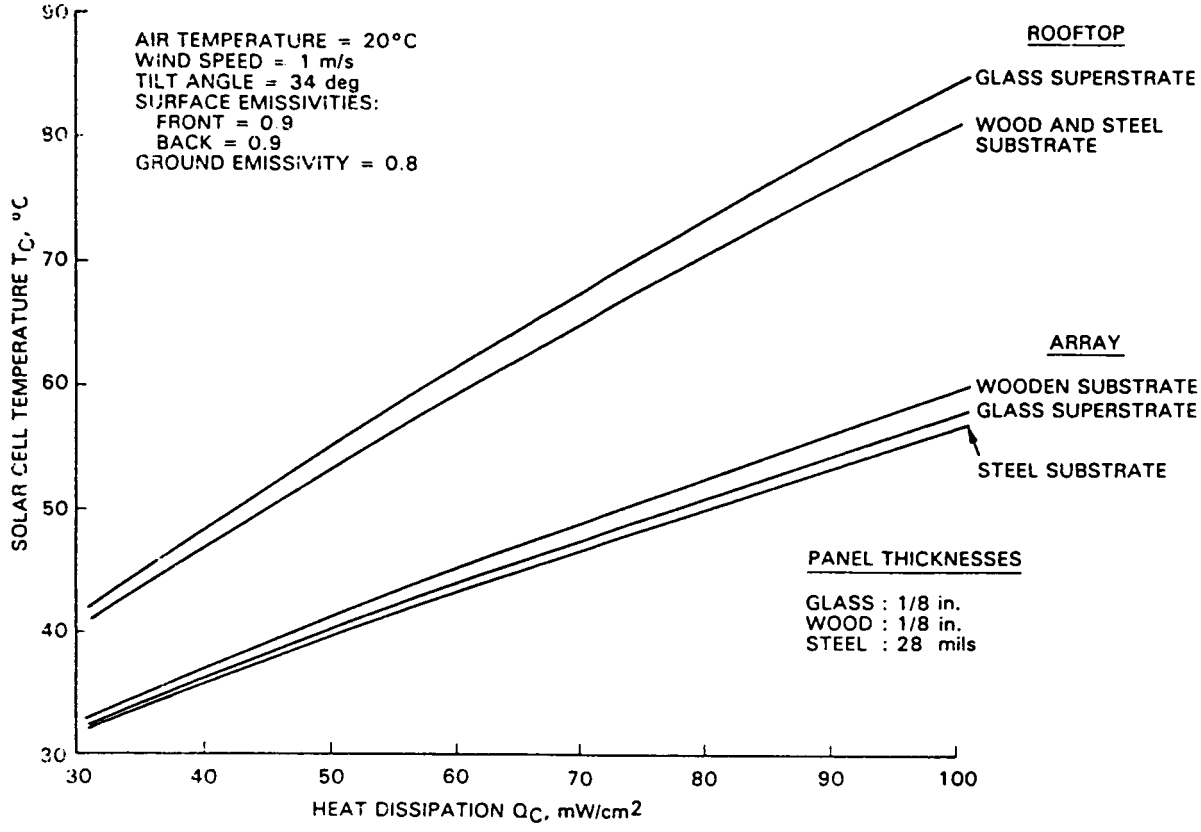

Figure 20. Comparative Heat-Dissipation Behavior of a Glass-Superstrate Module and of a Wood-and-Steel Substrate Module

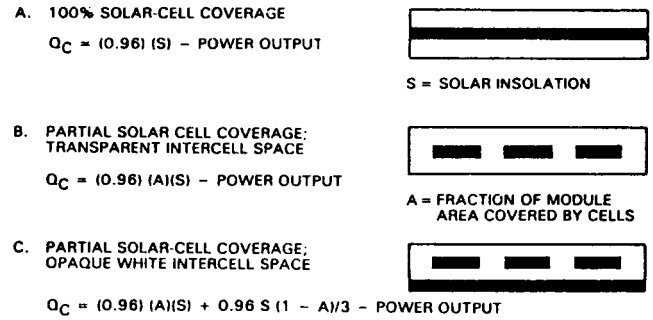

Figure 21. Module Models for Q_C Calculations

The NOTC solar insolation level S is 80 mW/cm^2. Therefore, for the Spectrolab Block II module, Q_C is estimated as

$$Q_C = (0.96)\,(80)\,(0.7) = 53.7 \text{ mW/cm}^2 \qquad (4)$$

Using this value of Q_C and the heat dissipation line for a glass-superstrate module in Figure 20, NOCT is estimated at 42 °C, which can be compared with the measured value of 41 °C. The more extensive thermal-optical model used in the Spectrolab computer program also yields a NOCT in the range of 42 °C to 43 °C.

Table 21. Experimental[a] and Predicted NOCT Values for Spectrolab, Inc., and Solar Power Corp. Block II Modules

Installation	Measured Value	Predicted Value
Spectrolab	41 °C	42 °C
Solar Power Array Installation	45 to 46 °C	45 °C
Solar Power Rooftop Installation	61.5 °C	60 °C

[a]Reference 66.

For the Solar Power Block II module, Q_C is estimated as

$$Q_C = (0.96)\,(80)\,(0.7) + (0.96)\,(80)\,(0.3)/3 = 61.4 \text{ mW/cm}^2 \qquad (5)$$

Using the above value of Q_C, and the wooden-substrate heat-dissipation line of Figure 20, an array installation NOCT value of 45 °C is estimated, which can be compared with the measured value of 45 to

46 °C. The rooftop NOCT value is estimated to be near 60 °C, using the same value of Q_C and the wooden-substrate and steel-substrate rooftop heat-dissipation line in Figure 20.

The method described herein for estimating module operating temperatures is intended to be a convenient desktop approach for PV module designers assessing their specific encapsulation systems, or encapsulation design options. The heat dissipation curves shown in Figures 18, 19, and 20 were generated with the equations in Table 20. Interestingly, these computer-generated curves are virtually linear.

Figures 22 through 25 are reproduced from Reference 77, and are plots of $T_{cell} - T_{air}$ (°C) versus

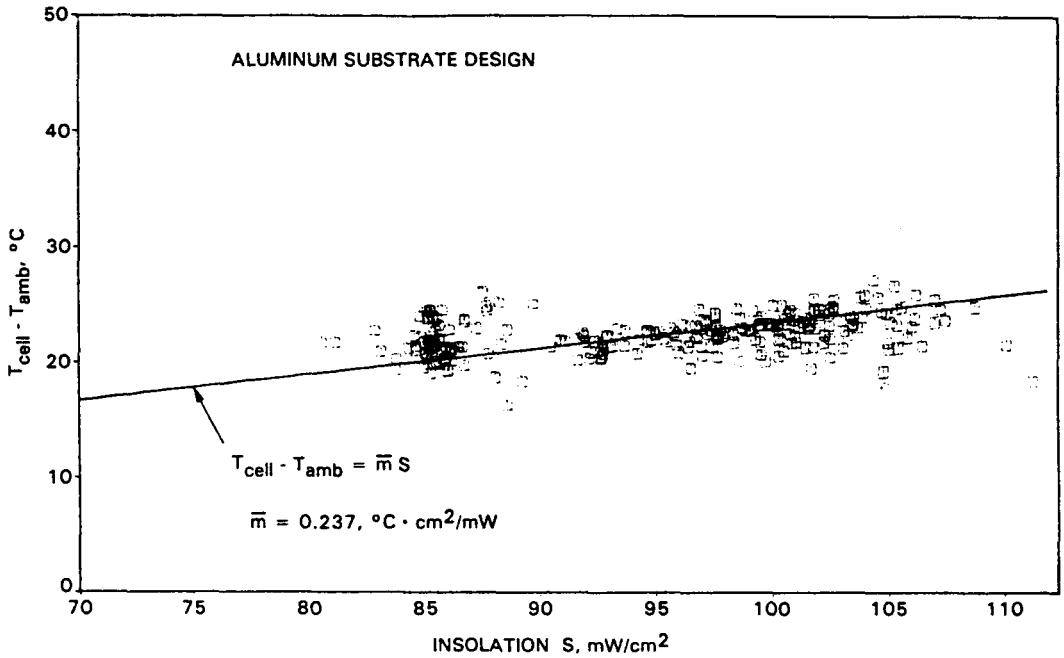

Figure 22. ΔT Versus Insolation for Sensor Technology, Inc. (Photowatt International, Inc.) Block I Module

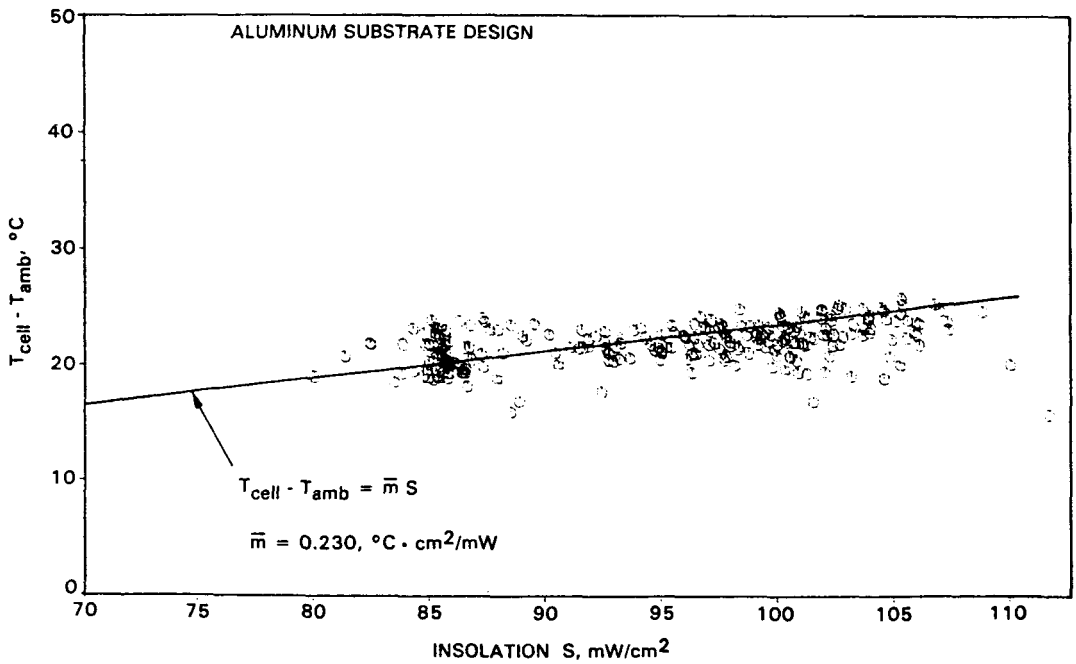

Figure 23. ΔT Versus Insolation for Spectrolab, Inc., Block I Module

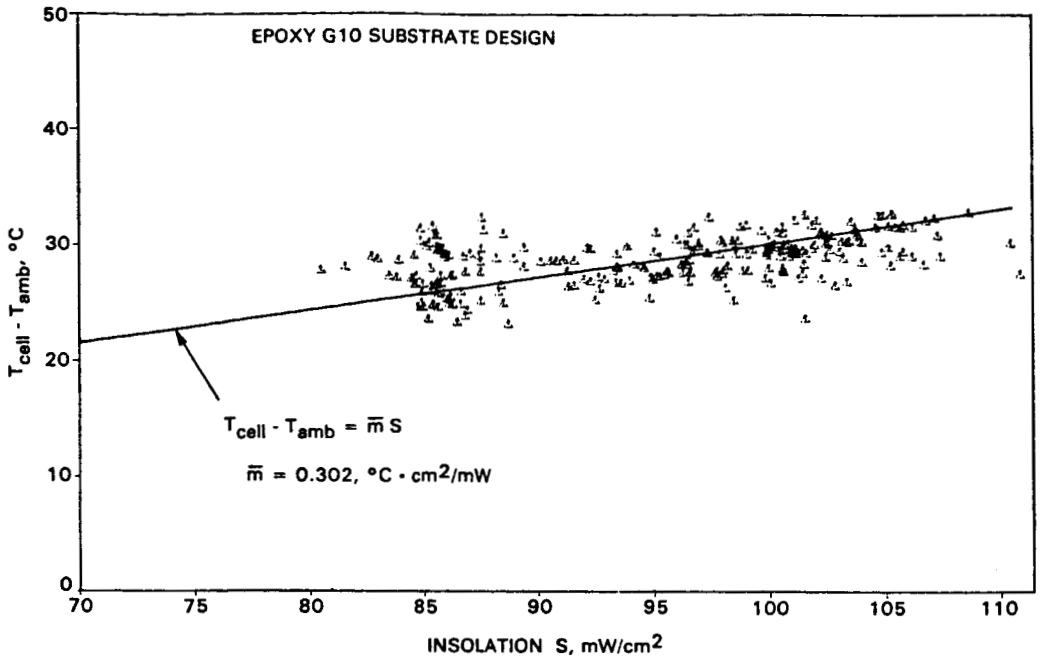

Figure 24. ΔT Versus Insolation for Solarex Corp., Block I Module

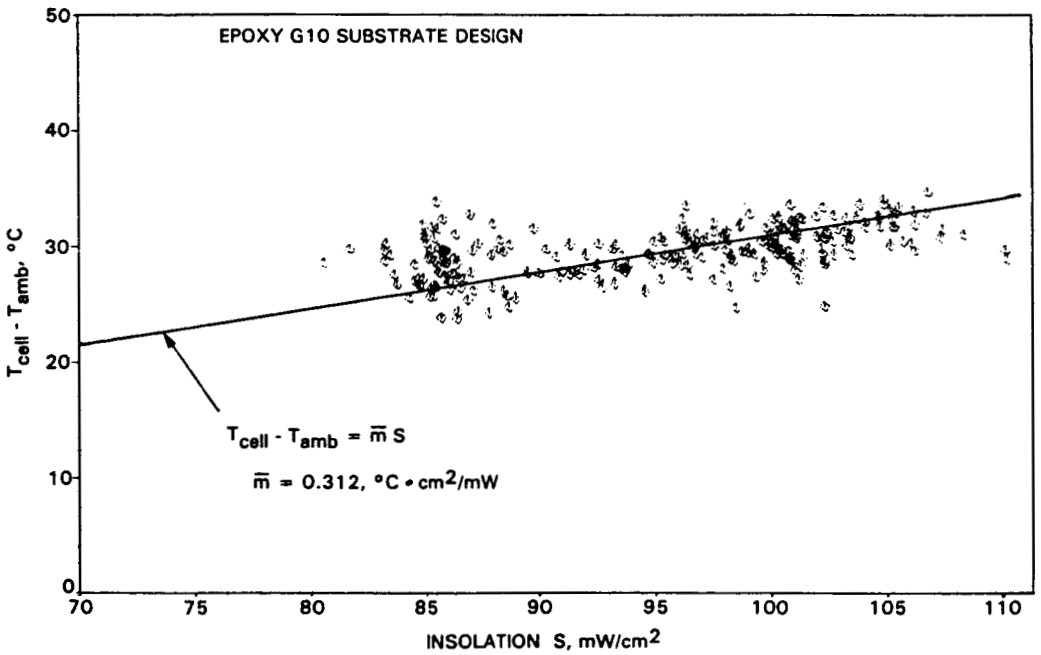

Figure 25. ΔT Versus Insolation for Solar Power Corp., Block I Module

insolation in mW/cm^2 for four early 1970 substrate design modules mounted outdoors at JPL in Pasadena, California. Experimental observations revealed that the temperature difference between the solar cell and ambient air was essentially linearly proportional to the solar insolation level S. Thus, the computer-generated curves are in agreement with these experimental observations. What appears as data scatter around the straight lines in Figures 22 through 25, was related to local fluctuations in ground wind velocities around the modules (see Reference 75).

B. STRUCTURAL MODELING

Outdoors, a PV module is subjected to daily cycles of thermal expansion and contraction associated with the diurnal temperature swings, and to out-of-plane deflections when subjected to wind. The stresses set up throughout a PV module from differential expansions and/or deflections must be limited to levels that would not cause the solar cells to fracture or crack over the outdoor service lifetime. The purpose of the structural analysis was to understand the relation between encapsulation designs, that is, the mechanical and thermal properties of the encapsulation materials, and the level of stresses established in the solar cells when the module is subjected to deflection, and to thermal expansion and contraction.

The structural analysis consisted of two parts: prediction of stress distribution throughout a module when deflected by a 100-mi/h wind (50-lb/ft^2 loading pressure), and prediction of stress distribution throughout a module because of thermal-expansion differences when a module is heated or cooled over a temperature range of 100°C. These represented extreme conditions. For both cases, a zero-stress state was assumed to exist throughout the module before deflection or thermal stressing.

Details of the module construction that were analyzed are:

(1) Module dimension: 1.2 m^2 (4 × 4 ft^2).

(2) Solar cells: 10 × 10 cm^2 (4 × 4 in. × 0.015-in.-thick).

(3) Spacing between solar cells: 1.3 mm (0.050 in.).

For the deflection analysis, the perimeter of the module was assumed to be constrained and restricted from being twisted or deflected out of planarity.

Structural analysis was done on three encapsulation systems: glass-superstrate, and wooden and mild-steel substrate design. The structural properties (Table 22) of the glass, wood, and mild steel were fixed-input data. The pottant was treated as a variable, expressed in terms of its Young's modulus. Output data consisted of the stress distribution throughout the module (especially solar cell stresses), calculated as a function of pottant modulus, and pottant thickness between the cells and the structural panel. The structural analysis model is summarized in Figure 26.

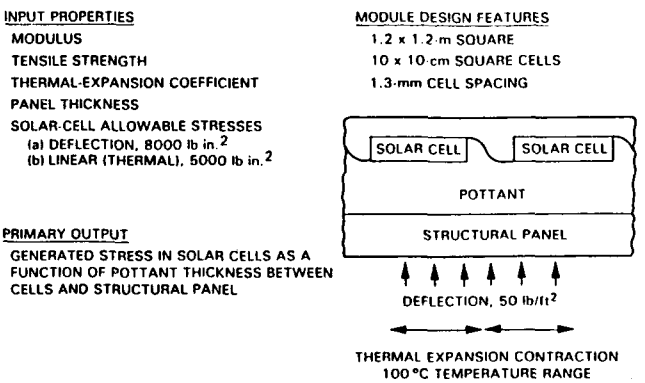

Figure 26. Structural Analysis, Deflection, and Thermal Stress

The allowable design limit for 4-in.^{2}, single-crystal, silicon solar cells has been estimated to be 8000 lb/in.^{2} in bending, and 5000 lb/in.^{2} in tension (in-plane thermal stressing). Part of the basis for establishing these estimates was derived from a JPL report on the strength of single-crystal, silicon solar cells (see Reference 78).

1. Glass Superstrate Design

For a glass superstrate design, using 1/8-in.-thick tempered glass, Figures 27 and 28 are plots of solar cell stresses versus the thickness of pottant between the cells and the glass, for parametric levels of the pottant's Young's modulus. Figure 27 shows data for bending deflection at a loading of 50 lb/ft^2, and Figure 28 shows data for thermal expansion over

Table 22. Structural Analysis: Material Properties

Material	Modulus, lb/in.^{2}	Thermal-Expansion Coefficient, in./in./°C	Allowable Stress, klb/in.^{2}
Glass			
Tempered	10×10^6	9.2×10^{-6}	13
Annealed	10×10^6	9.2×10^{-6}	1 to 3.6
Wood	0.8 to 1.2 $\times 10^6$	7.2×10^{-6}	2.5
Silicon (PV cell)	17×10^6	4.4×10^{-6}	5 to 8
Steel	30×10^6	10.8×10^{-6}	28

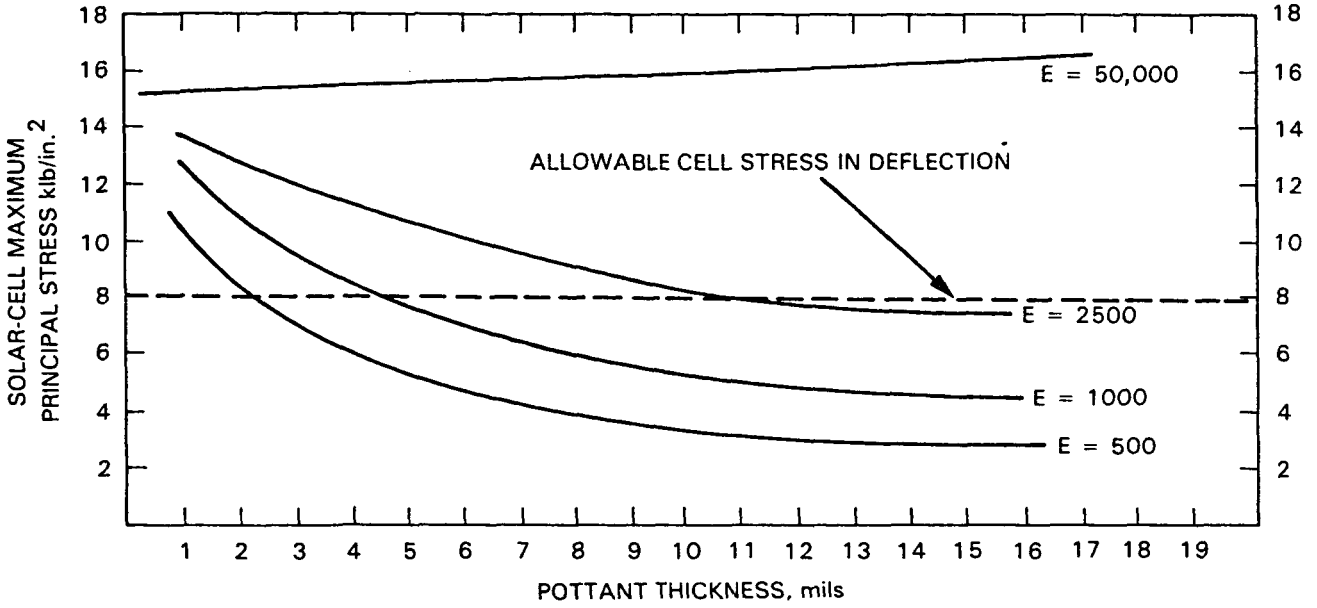

Figure 27. Deflection Analysis: Glass-Superstrate Design

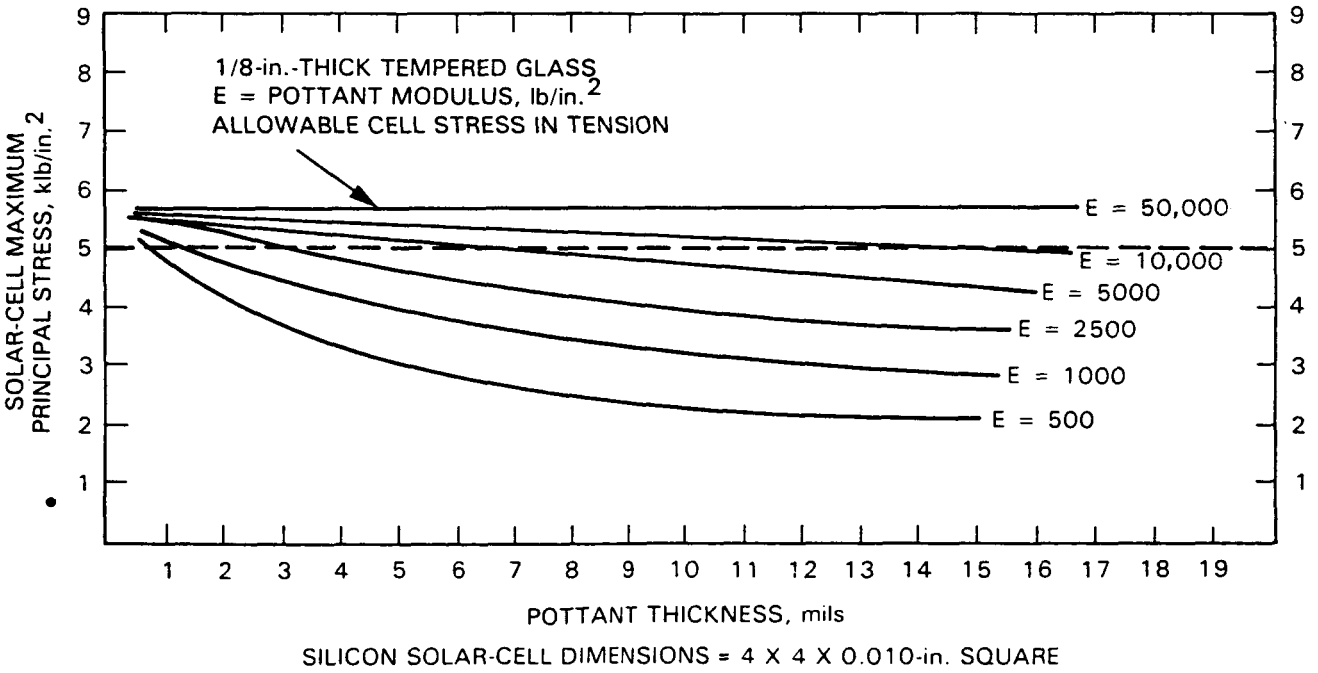

Figure 28. Thermal Stress Analysis (ΔT = 100°C): Glass-Superstrate Design

a temperature range of 100°C. For deflection, assuming that 8000 lb/in.^{2} is the allowable solar-cell stress in deflection, the calculated stress curves indicate that the solar cells must be separated from the glass by a pottant thickness of at least 2 to 3 mils for a pottant material having a Young's modulus of 500 lb/in.^{2}, which is typical of room-temperature vulcanized (RTV) silicones. For pottant modulus of 1000 lb/in.^{2}, (i.e., EVA), the solar-cell separation distance or pottant thickness must be >4 to 5 mils, and the thickness must be about 11 mils for a pottant modulus of 2500 lb/in.^{2}. Using a pottant with a modulus 50,000 lb/in.^{2}, the tensile stress in the solar cell will exceed 8000 lb/in.^{2} for any thickness.

For thermal-expansion stressing, (see Figure 28), the calculated relationship between solar-cell tensile stress, pottant thickness, and modulus behave similarly as observed for the bending deflection analysis. Comparing Figure 28 for thermal stressing with Figure 27 for deflection stressing reveals that the deflection stressing of the glass-superstrate module determines the minimum pottant thickness required, assuming that the allowable cell stress in tension is 5000 lb/in.^{2}.

For this glass superstrate analysis, the level of stresses developed in the glass were significantly less than the stress-design limit for tempered glass.

2. Mild Steel Substrate Design

In thermal stressing over a 100°C-temperature range, analysis indicated that the tensile stresses developed in the solar cells are independent of the thickness of the mild-steel panel. As in the glass-superstrate design, the tensile stresses in the cells are a function of the pottant thickness and modulus.

The calculated relationship between solar-cell tensile stress and pottant thickness resulting from thermal stressing is shown in Figure 29, for a single case of pottant with a Young's modulus equal to 1000 lb/in.^{2} (i.e., EVA). Assuming an allowable cell stress in tension of 5000 lb/in.^{2}, the minimum pottant thickness required between the cells and the steel plate is about 4 mils.

The deflection analysis for 50-lb/ft^2 wind loading on an unribbed steel panel has been analyzed for a single pottant with a modulus of 1000 lb/in.^{2}, and for three different thicknesses of a steel plate: 0.168, 0.087, and 0.028 in. The peak bending stress developed in a 4-ft^2 steel plate of these thicknesses during wind loading of 50 lb/ft^2 are 5000 lb/in.^{2} for 0.168 in., 15,000 lb/in.^{2} for 0.087 in., and 28,000 lb/in.^{2} for 0.028 in. A steel-plate of less than 0.028 in. thickness will experience a peak bending stress exceeding its allowable stress limit of 28,000 lb/in.^{2}.

For a 1000-lb/in.^{2} pottant modulus, the calculated relationship between solar-cell tensile stress and pottant thickness for each of the three steel-plate thicknesses are plotted in Figure 30. Because the level of the out-of-plane deflection at constant pressure loading increases with decreasing plate thickness, the bending stresses imposed on the solar cells increase with decreasing plate thickness. For a steel plate thickness of 0.028 in., approximately 12 mils of pottant are required between the cells and the steel plate to have the deflection stress in the cells less than 8,000 lb/in.^{2}, the allowable cell-stress estimate in deflection.

Increasing the plate thickness to about 0.087 in. reduces the pottant thickness required to about 4 mils, which coincidentally matches the pottant thickness requirement for thermal stressing (see Figure 29). A plate thickness of 0.168 in. is sufficiently stiff against a 50 lb/ft^2 wind load that the bending stresses imposed on the solar cells are below the allowable cell stress, down to a pottant thickness of 1 mil.

3. Wood-Hardboard Substrate Designs

Hardboards are typically sold in thicknesses that incrementally increase by 1/8 in., such as 1/8, 1/4, 3/8-in., etc. As with mild steel, stresses developed in solar cells from thermal expansion differences are virtually independent of the thickness of the wood panel. The results of the thermal stress analysis for hardboard is shown in Figure 31. There is virtually little effect from the pottant as the thermal expansion coefficients of hardboard and solar cells are very close. For deflection (Figure 32), the minimum panel thickness allowable for a 4-ft^2 module is 1/4 in., but 1/8 in. may be allowable if structurally reinforced with stiffening ribs.

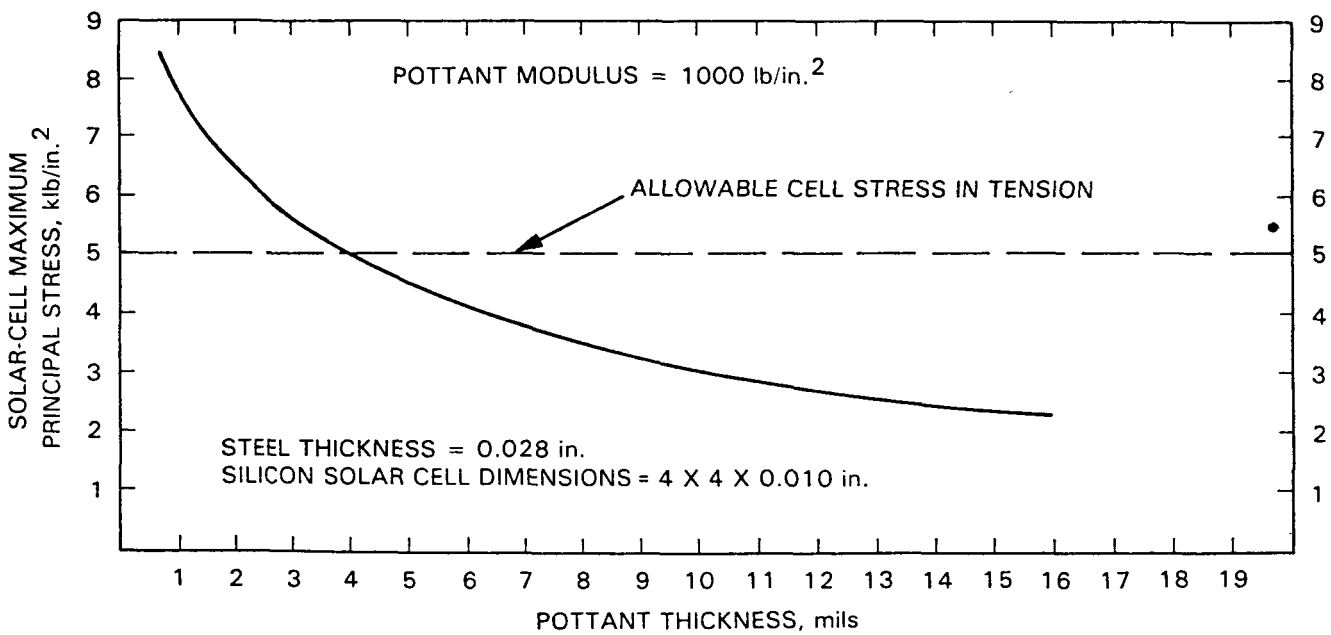

Figure 29. Thermal Stress Analysis (ΔT = 100°C: Steel-Substrate Design

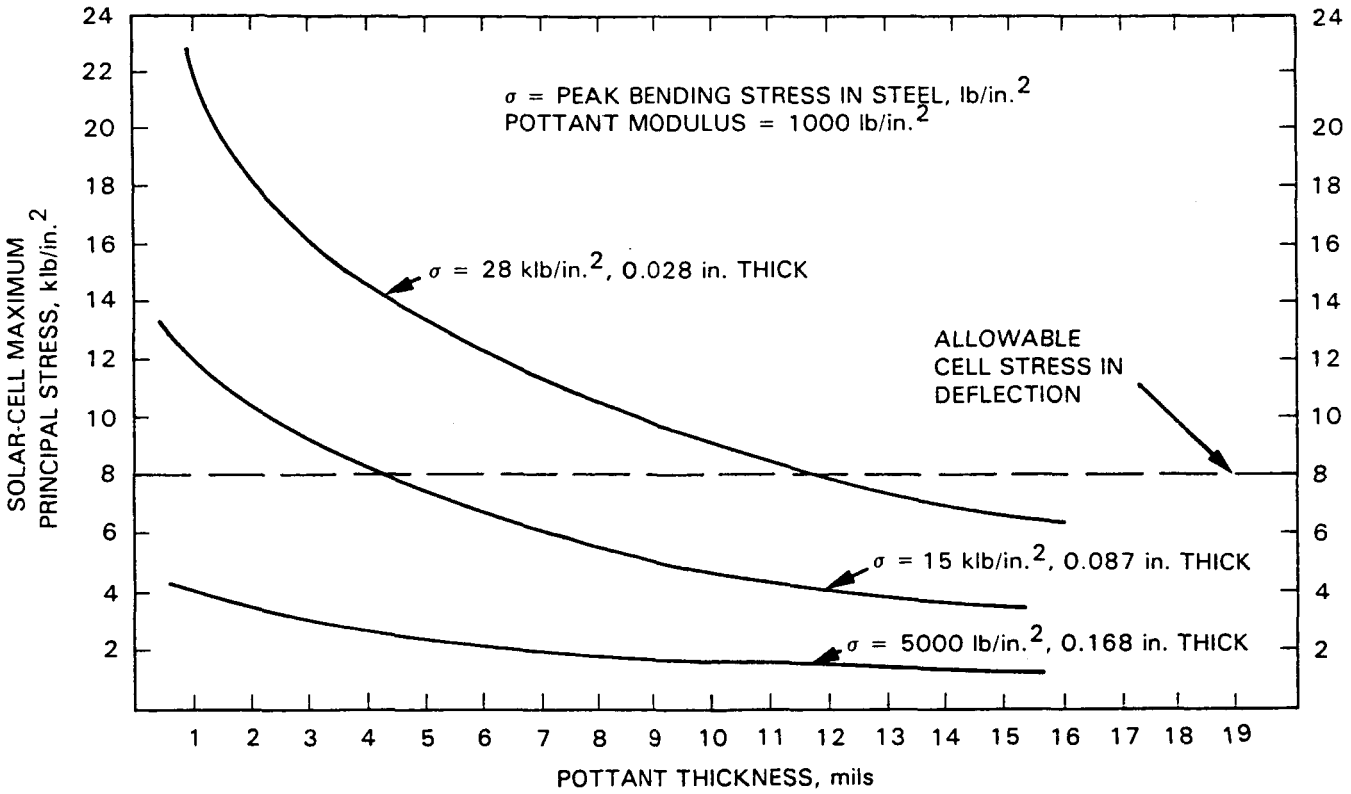

Figure 30. Deflection Analysis: Steel-Substrate Design

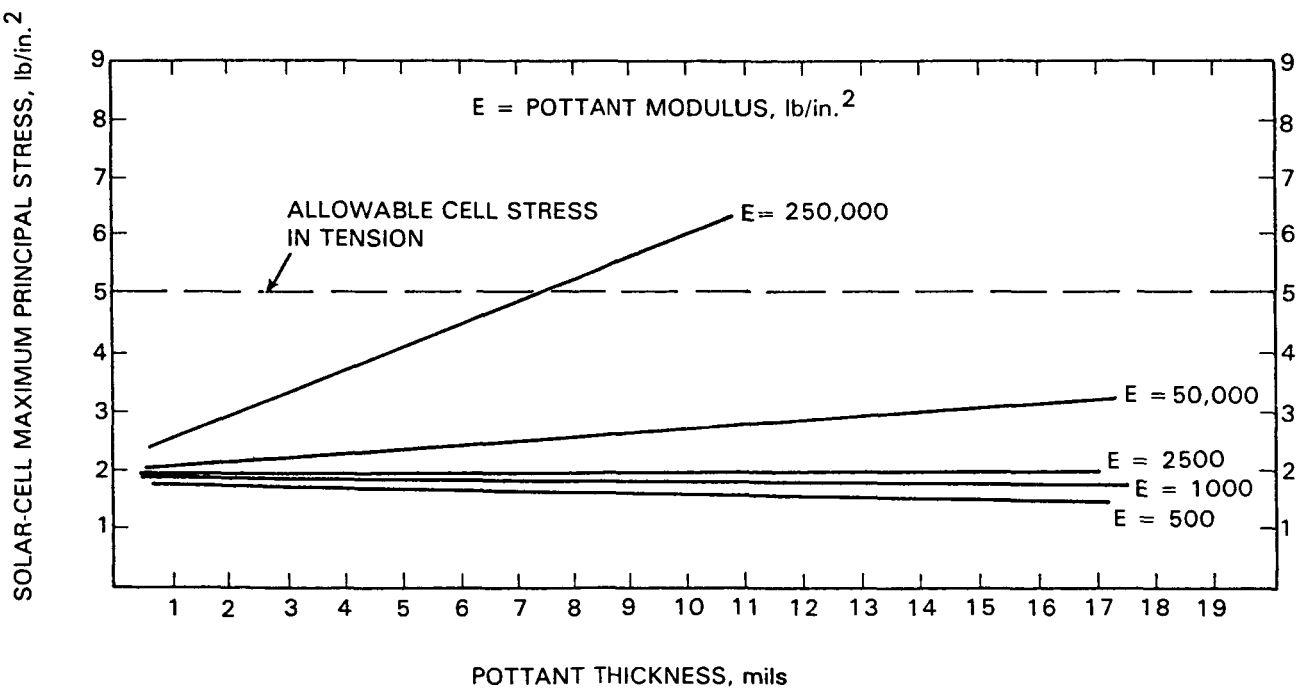

Figure 31. Thermal Stress Analysis (ΔT = 100°C): Wooden-Substrate Design

4. Master Curves For Structural Analysis

The thermal stress results given in Figure 28 for the glass-superstrate design were generated for six parametric levels of Young's modulus for the pottant material, as a function of pottant thickness. In efforts to derive crossplots of this same data as solar cell stress versus pottant modulus, for parametric levels of thickness, an intermediate log-log plotting format was generated as shown in Figure 33. In this format, it was observed that the data traces could be shifted horizontally to yield a master curve as shown in Figure 34, using a reduced

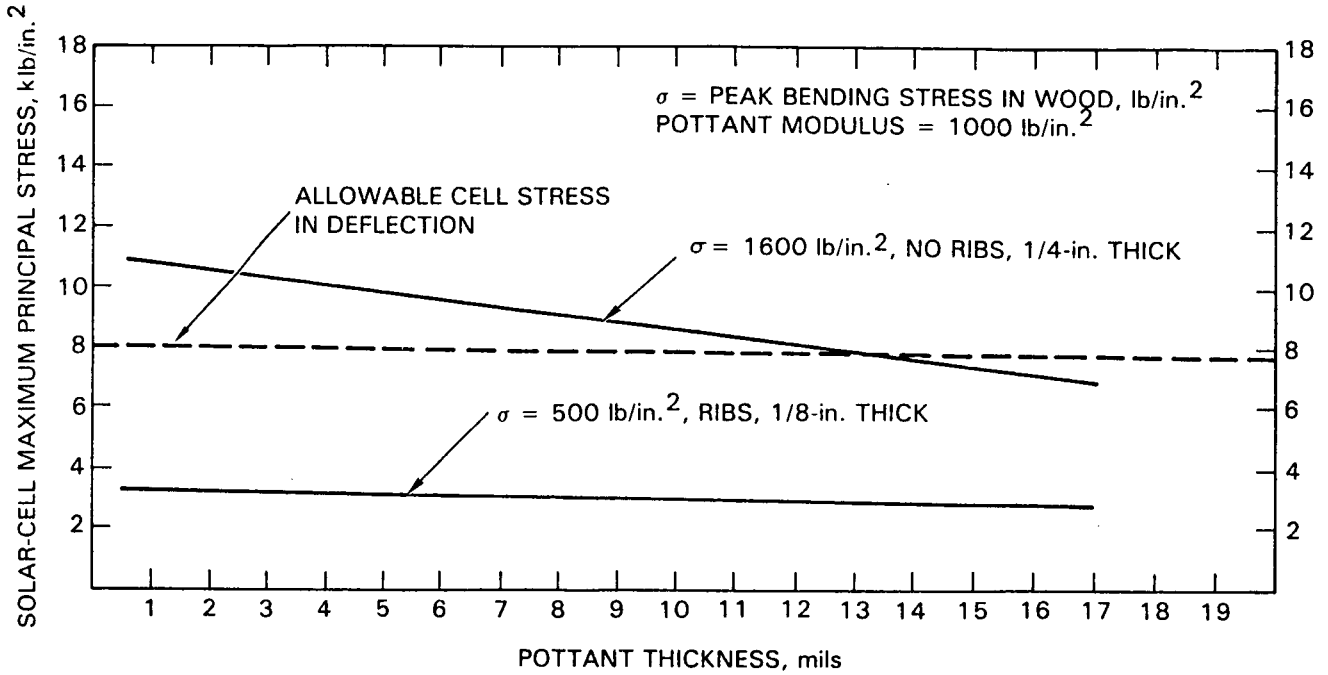

Figure 32. Deflection Analysis: Wooden-Substrate Design

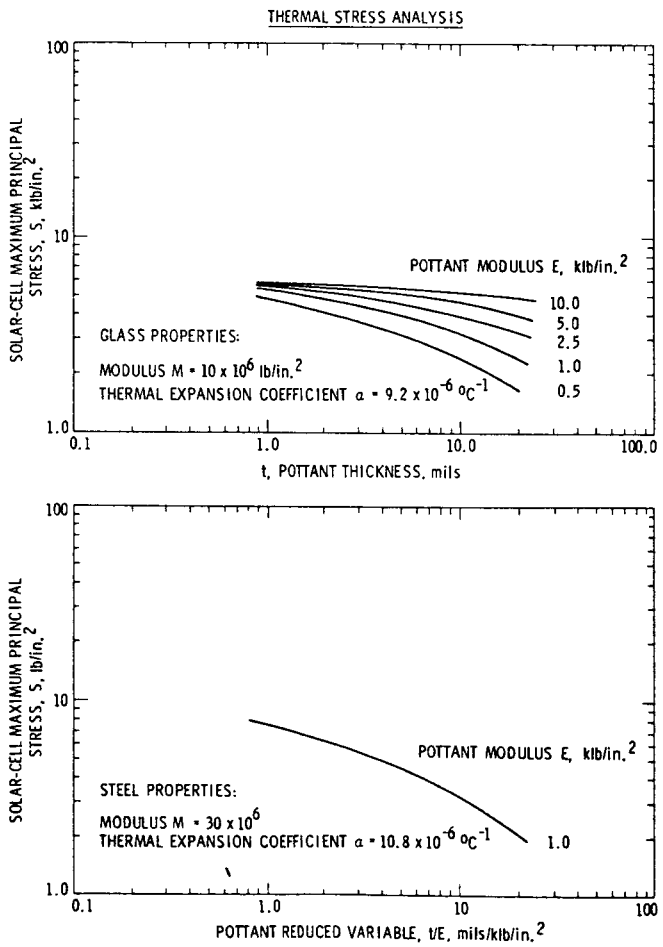

Figure 33. Log-Log Plots of Computer Traces Given in Figure 28 for a Glass-Superstrate Design

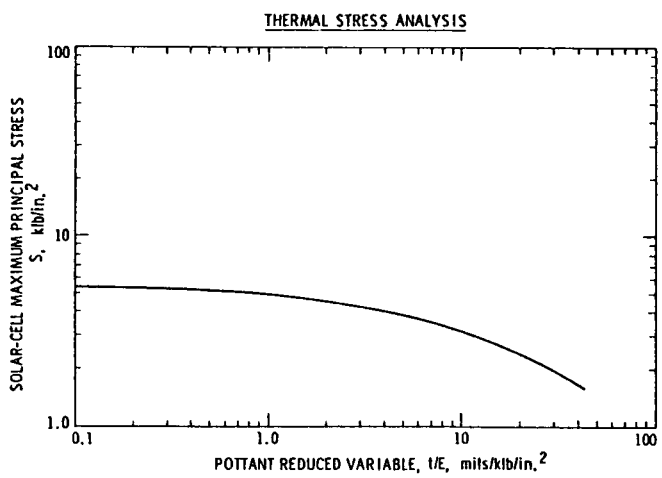

Figure 34. Horizontally Shifted Computer Traces of Figure 33 for Glass Using Reduced Variable, t/E

variable (t/E) for the abscissa, where t and E are respectively the thickness and modulus of the pottant. The traces for the wood and mild steel designs could also be merged with the glass data to yield a combined master curve for thermal stress analysis, as shown in Figure 35. The term "αm" is known as the thermal stiffness, in classical stress analysis. The deflection traces shown in Figures 27, 30, and 32 could also be shifted to a common master curve, but with different reduced variables for the ordinate and abscissa.

Given this general finding, the master-curve concept was expanded to include additional structural parameters relevant to the PV modules. The complete master

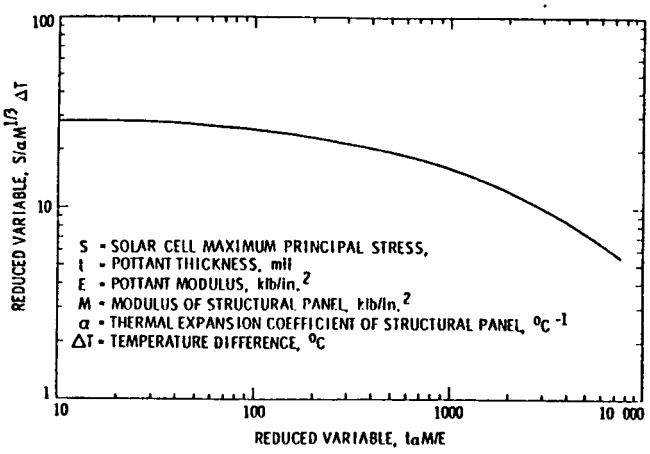

Figure 35. Master Curve for Thermal Stress Analysis

curves for both deflection and thermal analysis are given in Figures 36 and 37. Two applications with use of the thermal stress master curve follow.

5. Aluminum Panel

The Young's modulus M for aluminum is 10×10^6 lb/in.^{2}, and its expansion coefficient α is 24×10^{-6} °C^{-1}. Using these values, log-log traces of solar-cell tensile stress S versus pottant thickness t can be generated from the thermal master curve for $\Delta T = 100$°C. The resulting log-log traces for four levels of the Young's modulus of the pottant, E = 500, 1000, 2000, and 5000 lb/in.^{2}, are given in Figure 38.

Examination of these predicted log-log traces indicates that aluminum generates greater solar cell stresses than glass, wood, or steel because of thermal-expansion differences. The use of a pottant having a Young's modulus of 1000 lb/in.^{2}, such as EVA, would require that the pottant thickness be at least 14 mils, and higher-modulus pottants would have to be used in correspondingly higher thicknesses. The dual handicap for aluminum of a high thermal-expansion coefficient and higher material cost as compared to glass, wood, and steel, makes it an unattractive module substrate-panel material.

6. Wood Panel

The hygroscopic-expansion coefficient for hardboard is 50×10^{-6} in./in. per one percent relative humidity (RH), compared with its thermal-expansion coefficient of 7.2×10^{-6} in./in.°C. These property differences were suspected to be the explanation for a high incidence of fractured solar cells in experimental EVA-hardboard modules. Investigation determined that during vacuum-bag lamination, unprotected hardboards dry out and shrink, and later, in ambient atmosphere, regain moisture and expand, thereby, overstressing the solar cells. The dimensional changes of a hardboard sample in a simulated vacuum laminated process is shown in Figure 39.

A prediction of the tensile stresses developed in solar cells from the hygroscopic expansion of wood can be generated from the master curve by using the hygroscopic-expansion coefficient and 100% RH in place of 100°C. This is equivalent to considering that the wood panel has a thermal-expansion coefficient α of 50×10^{-6} °C^{-1}.

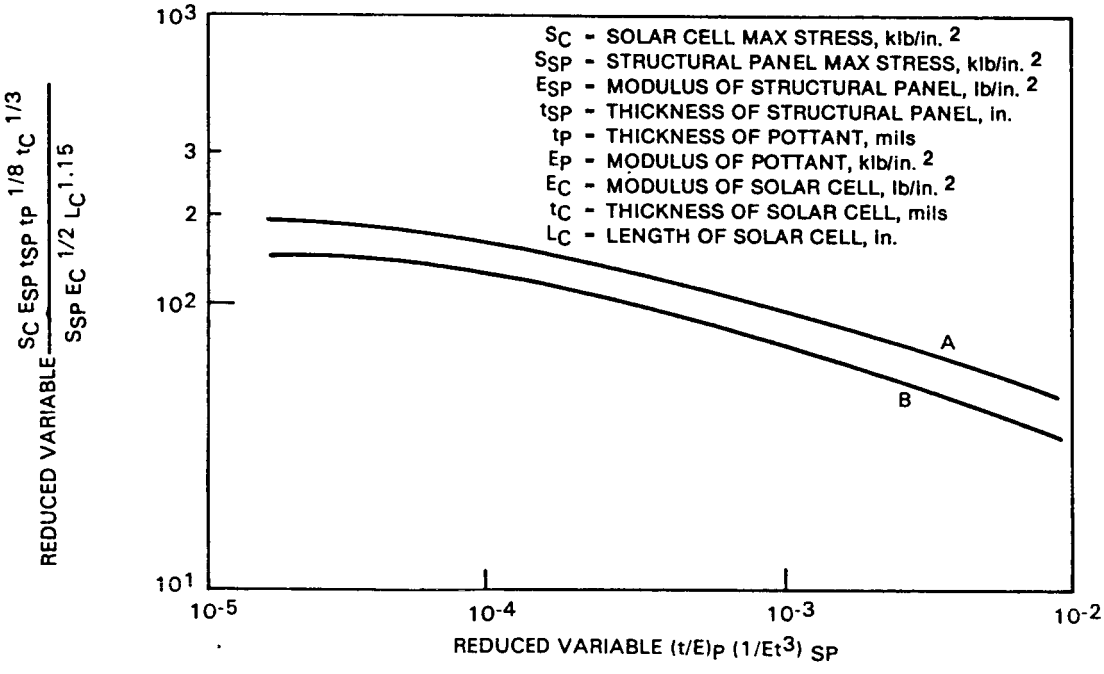

NOTE: USE CURVE A FOR PRESSURE ≤ 10 LB/IN.; USE CURVE B FOR PRESSURE 50 LB/IN.^{2} FOR INTERMEDIATE LOADS. INTERPOLATE LINEARLY BETWEEN A AND B

Figure 36. Master Curve for Deflection Stress Analysis

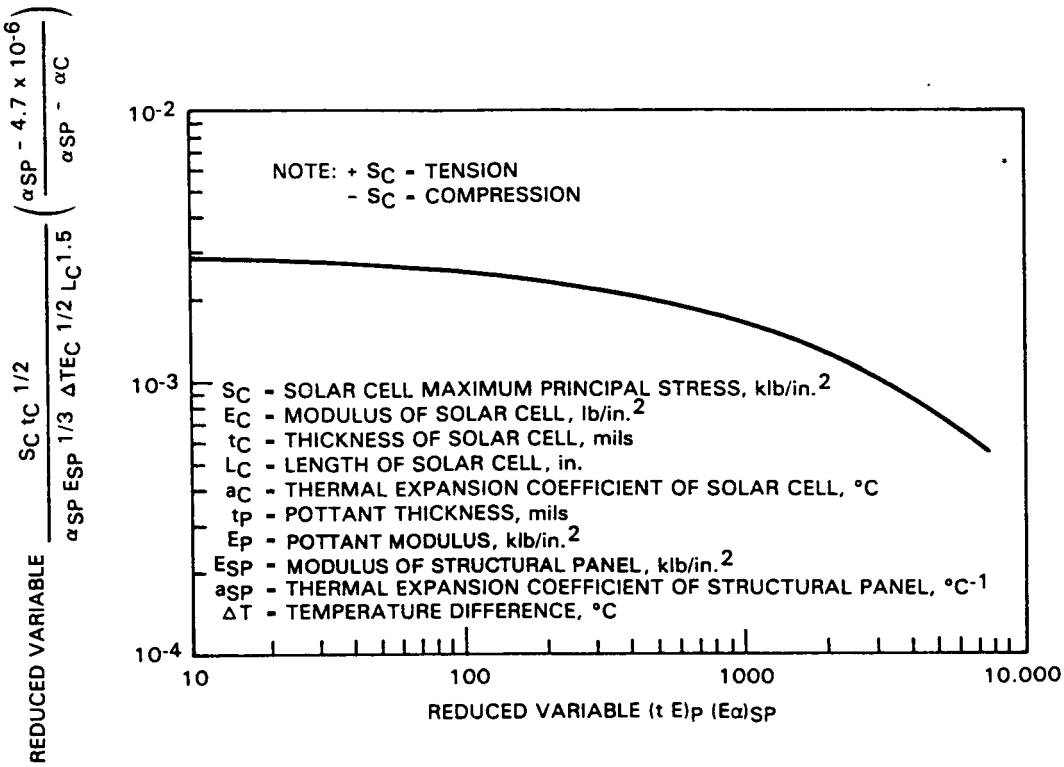

Figure 37. Master Curve for Thermal Stress Analysis

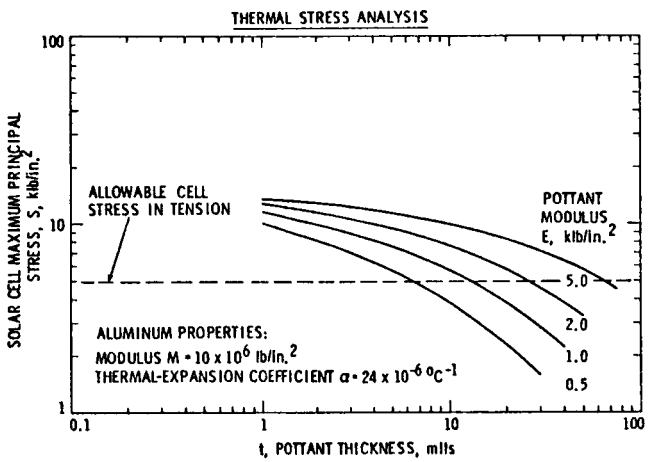

Figure 38. Predicted Stresses of Encapsulated Silicon Solar Cells Resulting from Thermal-Expansion Differences in an Aluminum Substrate Module for a ΔT of 100°C, Using the Thermal Stress Master Curve

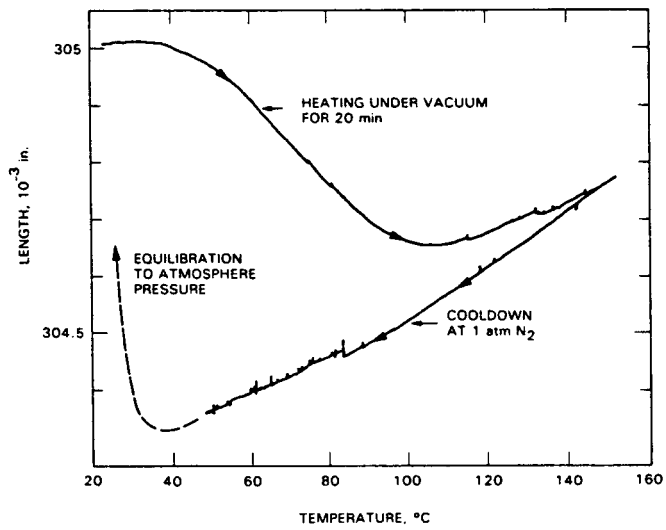

Figure 39. Dimensional Change of Hardboard Under Vacuum-Bag-Lamination Processing Condition

The predicted log-log traces for three levels of Young's modulus of the pottant (E = 500, 1000, and 2000 lb/in.^{2}) are plotted in Figure 40 for a relative-humidity excursion of 100% (i.e., dry wood to saturated wood).

The predicted solar-cell tensile stress response due to humidity requires very thick layers of pottant material to damp the generated expansion stresses down to acceptable levels. A pottant having a Young's modulus of 500 lb/in.^{2} would have to be used at a predicted thickness of about 33 mils, and a pottant, such as EVA having a Young's modulus of near 1000 lb/in.^{2}, would have to be at least 66 mils thick. Even if the relative-humidity excursion after vacuum-bag lamination were only up to 50%, which is more realistic, the thickness of a pottant, such as

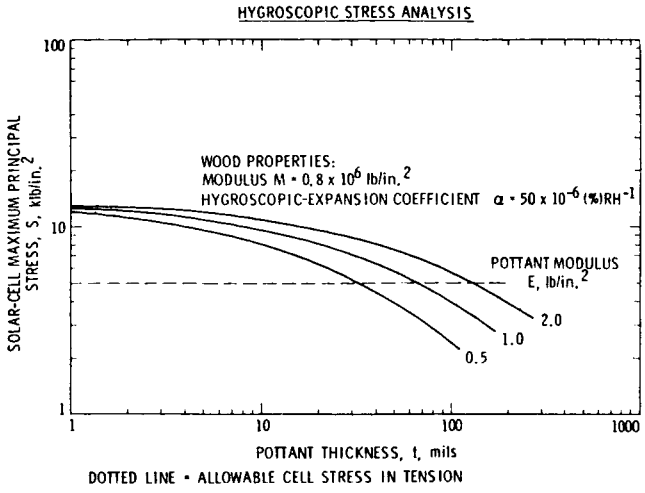

Figure 40. Predicted Stress in Encapsulated Silicon Solar Cells Resulting from Hygroscopic Expansion of a Hardboard Panel from 0% to 100% Relative Humidity, Using the Thermal Stress Master Curve

EVA, would have to be at least 33 mils, which is still very thick compared to practice. The experimental hardboard modules fabricated with EVA used about 18 mils of EVA between the cells and the wood.

The actual observations of a high incidence of broken cells occurring during outdoor exposure of wooden-substrate modules, along with the predictions given in Figure 40, indicate that the estimated cell stress in tension of 5 klb/in.^{2} may be reasonably near the real value.

C. ELECTRICAL INSULATION (SAFETY)

The pottant in a PV module functions as an electrical insulation material, isolating the electrically-active solar cells and associated circuitry from external grounds and/or human contact. In series-connected PV module arrays, circuit voltages above ground may exceed 1000-V DC. Therefore, the long-term (about 30 years) DC electrical insulation qualities of pottant materials such as EVA in outdoor weathering environments is a major concern.

A review of published literature and journal articles revealed that researchers and workers in the field of electrical insulation have been seeking an understanding of electrical aging mechanisms as well as the development of life-prediction methods (see Reference 79). However, despite considerable progress, there are no immediately available methods or techniques to assess the electrical long-term insulation life potential of materials such as EVA, or the other pottant candidates.

Under FSA support, a computer program was developed by Spectrolab to model the level of electrical-field intensities and stresses associated with the thin layer geometries of encapsulated solar cells (see References 52 and 56). This was part of an overall program related to accelerated aging of encapsulation pottant materials, and knowledge of electrical stress levels to which pottants would be subjected in service was sought.

A mathematical analysis of the computer model of the electrical fields led to a possible fundamental definition of an intrinsic dielectric strength of insulation materials that could be stated as a basic material property independent of any test technique, geometry, or service environment. This is similar to other pure material properties such as Young's modulus, index of refraction, and coefficient of thermal expansion.

The model analyzed by Spectrolab is shown in Figure 41, and the computer program yields the electrical field intensity E_{max} as a function of voltage V, radius R, and pottant thickness t. The maximum value of the electrical field intensity E_{max} occurs on the rounded edge of the solar cell. Details of the extensive analysis of the computer modeling results are reported elsewhere (see Reference 57). The key finding is that E_{max}, V, t, and R could be correlated as shown by the following expression:

$$(V/t) = E_{max}(2R)^{1/2}(t + 2R)^{-1/2} \quad (6)$$

or

$$V_a = K(t + a)^{-n} \quad (7)$$

with $V_a = (V/t)$, $K = E_{max}(a)^{-n}$, and $a = 2R$, a term involving the radius of curvature R only. If a is ignored, then the expression reduces to

$$V_a = K(t)^{-n} \quad (8)$$

that has been historically observed (see Reference 80) as a data correlation for electrical-breakdown voltage as a function of sample thickness, which has been explained as a material property. The computer result suggests that this behavior is a consequence of the thickness dependence of the electrical field, and that electrical breakdown occurs whenever a critical value of E_{max} is reached or exceeded. This critical value of E_{max}, herein designated S, is speculated to be the intrinsic dielectric strength of electrical insulation

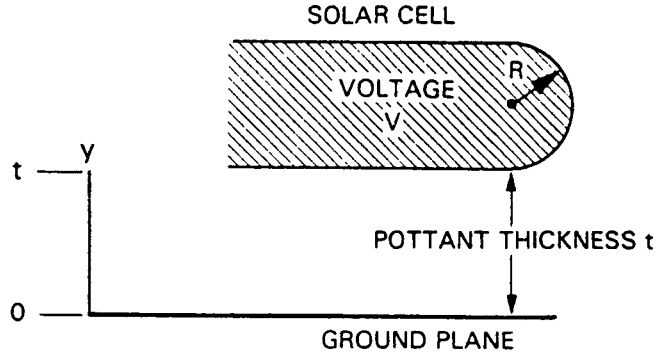

Figure 41. Encapsulation Solar-Cell Geometry

materials. The question then arises if Equation (7) is unique to the geometry analzyed in Figure 41, or is it a description of a general behavior for all electrode geometries of whatever kind.

Table 23 details two analytical solutions of Laplace's field equations for test electrode geometries consisting of a needle tip-to-ground plane configuration, and for a needle tip-to-needle tip configuration (see References 81 and 82). Both of these analytical solutions can be series-expanded (see Reference 57), and when the first two terms of each of their respective series expansions are algebraically combined, the result is:

Tip-to-Tip

$$V_A = E_{max}\,(3R)\,(t + 3R)^{-1} \qquad (9)$$

Tip-to-Ground

$$V_A = E_{max}\,(R)^{2/3}\,(t + R)^{-2/3} \qquad (10)$$

Table 23. Analytical Solutions of Laplace's Field Equations for Needle Electrodes

Tip-to-Ground Plane (Reference 81):

$$(dV/dy)_{max} = 2V_A\,t\,P/Ln\,(Q)$$

$$P = (1 + R/t)^{1/2}/R$$

$$Q = \left[2t + R + 2t^{1/2}\,(t + R)^{1/2}\right]/R$$

Tip-to-Tip Plane (Reference 82):

$$(dV/dy)_{max} = \frac{V_A\,t\,(1 + 2R/t)^{1/2}}{2R\,\tanh^{-1}\,[t/(t + 2R)]^{1/2}}$$

Equations (9) and (10), derived from analytical solutions, are identical in form to Equation (6), that was derived from a computer solution of Laplace's field equation for the geometry in Figure 41. What is different for Equations (9) and (10) are the integer multiplier of R, and the value of the exponent, both of which are being dictated by electrode geometries and pairings. Pairings are the use of two equivalent electrodes as in Equation (9), or two non-equivalent electrodes as in Equations (6) and (10). It is convenient to refer to these electrode pairings as "symmetric" or "asymmetric."

In general, for small values of t or large values of R, Equations (9) and (10) are of the general form

$$V_A = K\,(t + a)^{-n} \qquad (11)$$

where a and n are dictated by electrode geometries and pairings, and when t = 0,

$$V_A = K(a)^{-n} = E_{max} \qquad (12)$$

The experimental observation that V_A decreases with increasing t has been interpreted as a material property. However, the similarity of Equation (8) with these series expanded expressions suggest that, at constant E_{max}, this is a manifestation of the thickness dependence of the spatial distribution of the electrical field. If true, then voltage breakdown of an insulation material is occurring whenever a critical, but constant value of the potential gradient E_{max} is reached or exceeded on a electrode surface. It is suggested that this critical value of E_{max} may be the intrinsic dielectric strength of an insulation material, hereafter designated as S. From experimental voltage breakdown values measured as a function of thickness t, the constants k, a, and n in Equation (8) can be derived by least-squares techniques, and, therefore, for t = 0, $S = K(a)^{-n}$ that is identically equal to E_{max} (Equation 12) as $K = E_{max}(a)^n$.

1. Voltage-Breakdown Data

Flat-Plate Solar Array testing related to dielectric strength and voltage breakdown measurements of encapsulation pottant materials is limited, and to date only one preliminary set of alternating current (AC) voltage-breakdown data has been measured for the EVA pottant. At the time of this preliminary test, it was convenient to use a symmetric pairing of electrodes that was not dictated by any of the concepts or theories being described. It turned out to be a fortuitous choice. The test results measured on three thicknesses of EVA film are given in Table 24, along with the calculated average dielectric strength V_A.

Table 24. Average AC Breakdown Voltage of EVA for Three Film Thicknesses

Thickness (t), mils	Average AC Breakdown Voltage, kV	Average Dielectric Strength V_A = V/t, kV/mil
4.7	11.7	2.49
6.0	13.0	2.17
15.7	17.6	1.12

Using the V_A and t data given in Table 24, Equation 11 was solved for K, a, and n by a least-squares technique to yield the following:

$$V_A = 19{,}173\,(t + 3.74)^{-0.96} \qquad (13)$$

and, therefore, for t = 0

$$S = E_{max} = K(a)^{-n} = 5404\ V/mil \qquad (14)$$

In light of the concept being described, it is tempting to define the value of S = 5404 V/mil as the AC intrinsic dielectric strength of EVA, and to state whenever this electrical field intensity is reached on an electrode surface in contact with EVA, the EVA material will experience voltage breakdown.

Figure 42 is a log-log plot of V_A versus the thickness term (t + 3.74). This is similar to the historically empirical data-correlation technique of plotting V_A versus thickness t on log-log paper, except that here the term a is included along with t in the abscissa. Again, V_A decreases with increasing values of t, not because of any material characteristic, but because of the behavior of the electrical field distribution associated with increasing the gap thickness between electrodes (which happens here to be filled with EVA).

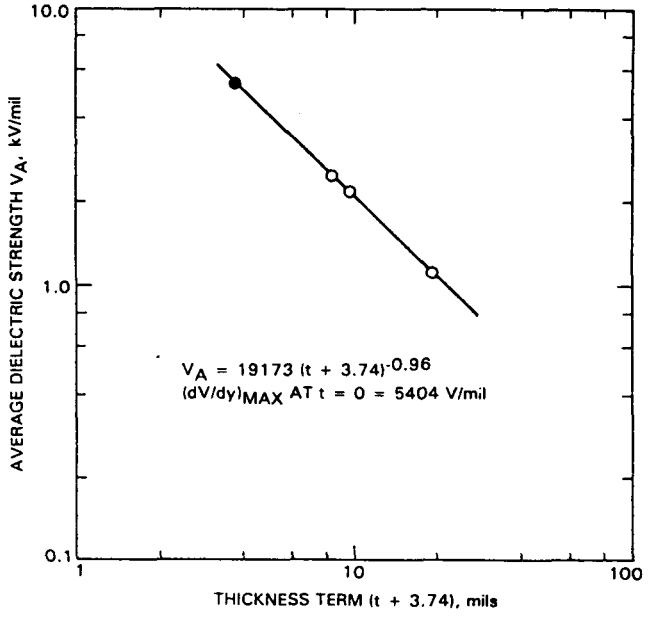

Figure 42. Dielectric Strength of EVA

This EVA test was fortuitously carried out with symmetric electrodes. In Equation 10, the value of the exponent n is 0.96, or very nearly 1. This may be compared with Equation 9, which is the convergence solution for small values of t for symmetric tip-to-tip electrodes, that happens to have an exponent n of 1. If similarities continue, then the effective radius-of-curvature R associated with this voltage breakdown is found in the a value, by dividing by 3. Hence, R is equal to 3.74/3 = 1.24 mils.

In a 1955 paper (see Reference 81), Mason reported experimental results of the measurement of the average dielectric strength V_A of low-density polyethylene as a function of sample thickness. For his test, Mason used an asymmetric electrode pairing, with the ground electrode being a flat plane. Using his published V_A and t data for polyethylene, Equation 11 was solved by a least-squares technique for K, a, and n, yielding the following result:

$$V_A = 8337\ (t + 1.20)^{-0.67} \qquad (15)$$

and, for t = 0

$$S = E_{max} = 7378\ \text{V/mil} \qquad (16)$$

His data, plotted as V_A versus the term (t + 1.20), are shown in Figure 43.

Note the striking similarity of Equation 15 for Mason's polyethylene data measured with asymmetric electrodes and Equation 10, the convergence solution for the asymmetric tip-to-ground electrode configuration. Not only are the values of the exponent n essentially the same, but also, for Mason's data, the value of a, which is equal to R in Equation 10, is the same value of R derived from the EVA data using symmetric electrodes. It is tempting to define the value of S = 7378 V/mil as the intrinsic dielectric strength of polyethylene.

Lastly, data for PMMA are shown in Figure 44, which was extracted from separate technical-data bulletins, and which were also fit to Equation 11 by a least-squares technique, yielding the following:

$$V_A = 8009\ (t + 0.87)^{-0.63} \qquad (17)$$

and, for t = 0

$$S = E_{max} = 8740\ \text{V/mil} \qquad (18)$$

The separate technical bulletins reported that the voltage-breakdown testing was carried out with asymmetric electrodes. With recognized possibilities of some inaccuracy that may result from merging separate experimental data, Equation (17) reflects the behavior expected for asymmetric electrodes.

Comparing the three materials, EVA, polyethylene, and PMMA, they are a soft elastomer, a semi-hard thermoplastic, and a rigid plastic, respectively. It is noted for each that their respective value of S also increases in the same order. In itself, this is not a new observation, as the recognition of a relationship between material hardness and average dielectric strength can be found in early literature on electrical insulation studies (e.g., Whitehead, Reference 83). Thus, if S is the intrinsic dielectric strength, the observations reported here agree with historical observations.

Note, that for the three materials, the range of S values from 5404 to 8740 V/mil is surprisingly narrow, considering that the materials range from a soft elastomer below its glass transition temperature (T_g), to a rigid plastic above its T_g. In 1976, Swanson, et al. (see Reference 84), reported dielectric strength measurements made on a wide variety of polymeric materials, ranging form soft, to semi-hard, to rigid. They concluded that T_g had only a slight effect on dielectric strength values.

2. Electrical Insulation Aging

For PV applications, the DC intrinsic dielectric strength properties are of greater interest than those for AC. The DC intrinsic dielectric strength of EVA was measured to be 3504 V/mil, which is observed to be lower than its AC value of 5404 V/mil.

The effect of aging on the DC intrinsic dielectric strength is being monitored on EVA specimens being aged outdoors on outdoor heating racks at 70, 90, and 105°C, and in UV-accelerated RS/4 chambers at 50°C

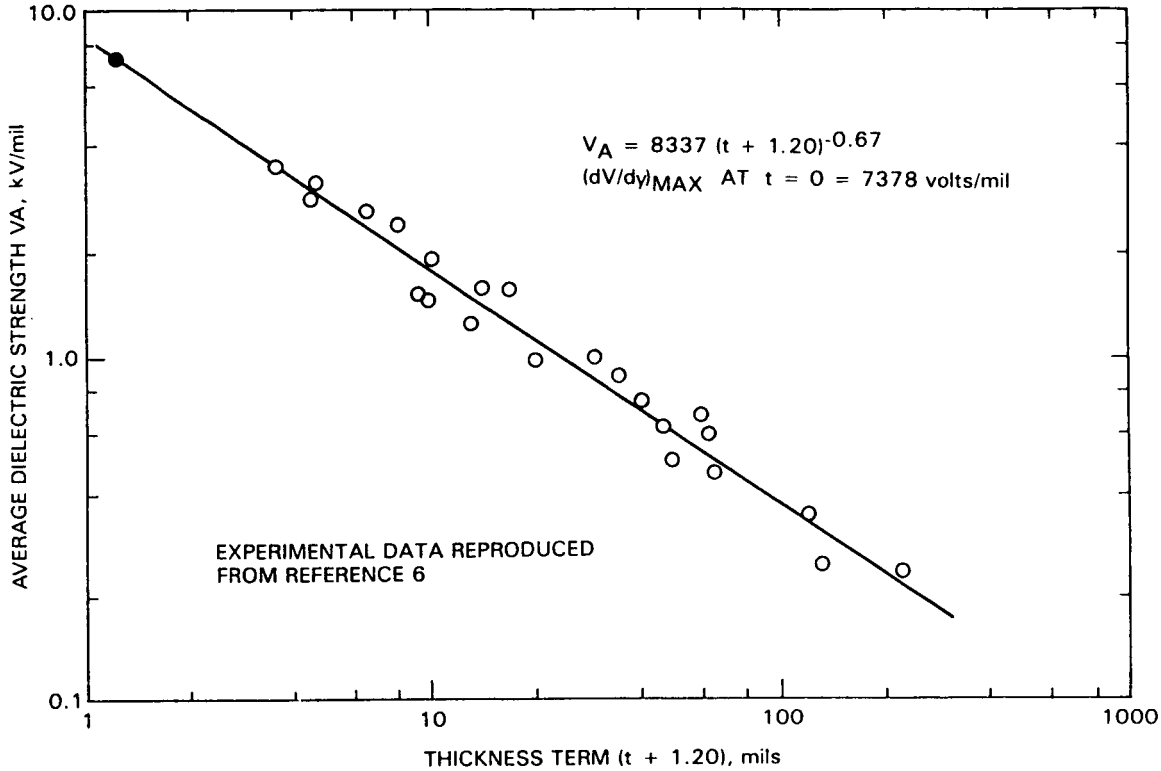

Figure 43. Dielectric Strength of Polyethylene

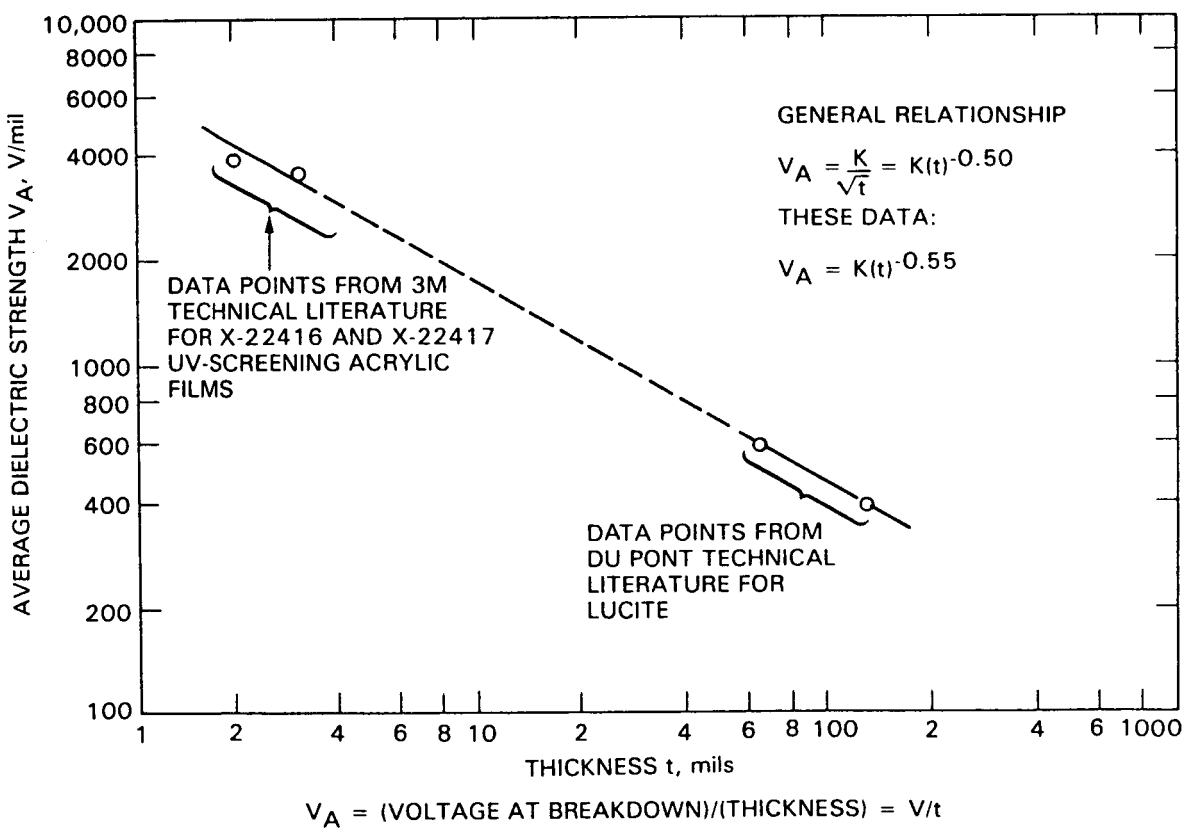

Figure 44. Dielectric Strength of PMMA Acrylic

and at 85 °C. There are two RS/4 chambers being operated at 50 °C; one with, and one without a periodic water spray cycle. These are referred to as RS/4-dry, and RS/4-wet. The unit operating at 85 °C is dry.

Experimental DC dielectric-strength data of A-9918 EVA from RS/4 aging after 2000 h is shown below:

Sample	DC Dielectric Strength, V/mil
Control	3504
RS/4-dry, 50 °C	3065
RS/4-dry, 80 °C	2100
RS/4-wet, 50 °C	3830

The trend indicates a reduction in the DC dielectric strength with dry aging, apparently being accelerated by increasing temperature. However, the data are too preliminary to judge the long-term aging behavior. Interestingly, wet RS/4 aging at 50 °C results in an increase in the DC dielectric strength. One hypothesis is that dry aging may result in an increase in ionic species that could reduce the dielectric strength, whereas the water spray cycle results in extraction of these ionic species. Thus, the DC dielectric strength increases compared to the control sample. The electrical insulation aging study continues beyond the preparation of this document.

SECTION VI

Experimental Aging of Encapsulants

The experimental aging programs were intended to provide an understanding of the outdoor aging characteristics of the encapsulant materials and the module as an integrated package. The results have guided the development and implementation of staged improvements in material and design technologies that have contributed to performance longevity.

Aging programs were primarily carried out in-house at JPL and at Springborn Laboratories in Enfield, Connecticut, with emphasis on EVA, and mini-modules fabricated with electrically active solar cells. As part of the aging program, two new and novel accelerated aging devices were developed and are herein described. One of the devices has been designated controlled environmental reactors (CERs), (see Reference 15) and are operated at JPL, and the other device has been designated outdoor photo-thermal aging racks (OPTAR), and are operated at Springborn Laboratories.

A. EVA AGING PROGRAMS

The aging behavior of both Elvax 150 (the Du Pont base product) and the cured A-9918 EVA formulation were studied at Springborn Laboratories and at JPL. A summary of these separate aging programs and essential findings are first described, and then their results combined to generate an evolving picture of the aging behavior of this material, and an assessment of the materials' service-life potential for array and rooftop-module applications.

1. Springborn Laboratories

Springborn carried out thermal aging (in the dark) of cured A-9918 EVA at 70, 90, and 130 °C in air-circulated ovens, and also exposed Elvax 150 and cured A-9918 EVA to UV light at 55 °C. The UV light source was a General Electric RS/4 sunlamp that was filtered to remove nonterrestrial wavelengths below 295 to 300 nm.

Continuous exposure to these RS/4 sunlamps, operating at 1.4-suns UV intensity for 1300 h, represents about 1 year of outdoor UV exposure (see Reference 85). The UV exposure temperature of 55 °C was selected to match typical array peaking temperatures. Atmospheric moisture in the RS/4 test chambers and in the air-circulated ovens was that associated with the laboratory environment, typically at a relative humidity of about 50 to 60% at 25 °C (77 °F).

Exposure of unprotected Elvax 150 to RS/4 UV at 55 °C results within 1000 h in a visible onset of yellowing that continues and becomes more intense with continued exposure. The surface of this material becomes sticky and tacky, and the physical shape of the specimen eventually manifests slump and a tendency to flow. Progressive deterioration led to termination of this UV aging test at 1500 h. Exposure of an Elvax 150 sample crosslinked with 1.5 parts per hundred (pph) of Lupersol 101, but which contained none of the stabilization additives listed in Tables 4 and 7, essentially paralleled the aging behavior of the uncrosslinked Elvax 150. The primary difference was a general retention of its initial physical form, presumably a result of the effect of crosslinking. Crosslinking of Elvax 150 alone was insufficient to stop or suppress the action of UV photooxidation.

A specimen of uncrosslinked and uncompounded Elvax 150, positioned behind a UV-screening acrylic film, experienced 21,000 h of RS/4 exposure at 55 °C without any visible evidence of yellowing or physical slump, and without any development of surface stickiness or tack. (Aging was terminated at 21,000 h because of equipment failure.) The acrylic film cover filtered out all UV wavelengths shorter than 360 to 365 nm. The evidence, therefore, suggests that to the time limit of this exposure, Elvax 150 exhibits natural resistance to thermal oxidation at 55 °C.

Specimens of cured and fully compounded A-9918 EVA (Table 4) were also directly exposed to RS/4 UV at 55 °C. No UV-screening films or covers were used. The optical and mechanical properties of A-9918 EVA, up to 27,000 h of UV exposure at 55 °C, are given in Table 25. Note that there was very little change in the measured properties of the cured A-9918 EVA. At 35,000 h, the remaining sample[2] was still firm and non-sticky, but had become visibly, but weakly yellow, thus exhibiting the first hints of detectable aging. At this point, testing was stopped.

These RS/4 data trends strongly indicate the potential of 20- to 30-years service life for cured A-9918 EVA, for an array installation having a peaking temperature near 55 °C, when used either in a superstrate or substrate module design. Further, as indicated above, Elvax 150 itself seems to be resistant against purely thermal aging at 55 °C, but will yellow and age at 55 °C when directly exposed to UV. Therefore, the deleterious UV wavelengths activating yellowing and aging by UV photooxidation can be apparently filtered out by UV screening films and also by the Cyasorb UV-531 in the compounded A-9918 EVA.

Thermal aging in dark, air-circulated ovens of cured A-9918 EVA was carried out for 10 months at 70, 90, and 130 °C. The test results for these thermally aged A-9918 EVA specimens are given in Table 26.

[2] This remaining sample was too small for mechanical property testing.

Table 25. Properties of Cured A-9918 EVA as a Function of Exposure Time to RS/4 UV at 55°C

Lot 2 Specimens	Total Integrated Limit Transmission,[a] %	Tensile Strength at Break, lb/in.^{2}	Elongation at Break, %
Control	91.0	1890	510
2,880 h	91.0	1930	631
5,760 h	90.5	1340	550
8,640 h	90.0	1460	590
15,120 h	90.0	1520	570
27,000 h	90.0	1870	560

[a] Measured over the wavelength range of 350 to 800 nm.

Table 26. Thermal Aging of Cured A-9918 EVA in Circulating-Air Ovens

Time	Property	70°C	90°C	130°C
1 wk (168 h)	Tensile, lb/in.^{2}	2685	2200	2000
	Ultimate elongation, %	595	550	550
3 wk (504 h)	Tensile, lb/in.^{2}	1700	1800	1240
	Ultimate elongation, %	670	680	638
2 mo (1344 h)	Tensile, lb/in.^{2}	2370	2660	1320
	Ultimate elongation, %	600	784	647
10 mo (7200 h)	Tensile, lb/in.^{2}	Specimen	2120	144
	Ultimate elongation, %	lost	660	37
	Gel content, %		91%	88%
	Color		Clear, no yellow	Brown/ orange
	Optical transmission, %		91%	74%
	Tangent modulus, lb/in.^{2}		833	335
	Control (unaged)			
	Tensile, lb/in.^{2}	2160		
	Ultimate elongation, %	677		
	Tangent modulus, lb/in.^{2}	890		
	Optical transmission, %	91		
	Gel content, %	91		

After 10 months of thermal aging at 90°C, there was essentially no change in the A-9918 EVA. At 130°C, however, the A-9918 EVA underwent considerable deterioration from thermal oxidation. The material turned brown/orange in color and experienced significant deterioration of both optical and mechanical properties. A trace of visible yellowing was noted after 1 week of thermal aging at 130°C was yellowing and very intense after 2 months.

With respect to rooftop applications and with the module design philosophy of shielding the A-9918 EVA from harmful UV, the thermal aging behavior at 90°C is initially encouraging. The 10 month (7200 h) of thermal

aging at 90°C corresponds roughly to almost 4 years of rooftop service at the higher operating temperatures.

A two-cell mini-module fabricated with glass, EVA, and white Tedlar has been aged up to 18,000 h under RS/4 lamps at 85°C. The EVA was a modified A-9918, having the chemically attachable UV-2098 UV-screening agent in substitution of the Cyasorb UV-531 (see Table 7). This mini-module included a small copper grid encapsulated within the EVA along with two electrically active solar cells connected in series.

Up to 16,000 h at 85°C, there were no visually observable changes, and the cells were still producing the same power as initially measured. At the 18,000 h inspection point, however, there were indications of copper discoloration and pale yellowing of the EVA. Assuming 1300 h of exposure equates to 1 year outdoors, then 18,000 h calculates out to nearly 17 years outdoors at 85°C. This encouraging aging test is continuing.

2. Jet Propulsion Laboratory Testing

JPL has carried out UV aging and thermal aging (in the dark) of both Elvax 150 and cured A-9918 EVA. The UV light source of a CER is a 550-W, Conrad/Hanovia medium-pressure mercury arc lamp surrounded by a Pyrex water jacket for cooling and for removal of IR and non-terrestrial UV wavelengths.

Generally, sample temperature control in photothermal aging is difficult because absorbed radiation causes a rise in temperature, and the higher the acceleration level, the greater is this uncontrollable temperature rise. CER uses an electrical heater and fan system in conjunction with appropriate optical filtering to adjust and control sample temperature precisely (i.e., ±1°C at 50°C, and ±3°C at 135°C).

This device allows UV acceleration of up to 30 suns while maintaining temperature of the absorbing surface at 50 to 135°C. The majority of the testings were carried out at 6 suns of UV intensity at the sample locations. Assuming a 1-sun UV day as 5 h for each 24 h, then about 300 h of exposure to this UV source equates with 1 year of outdoor UV exposure.

The UV-visible IR-absorption spectra of almost all of the test specimens were monitored primarily to detect changes in absorption spectra for chemical information, rather than to determine optical transmission relative to solar-cell performance. Special emphasis was given to the sensitive detection of absorbance at 360 and 400 nm. Absorbance at 360 nm was used to monitor the concentration of Cyasorb UV-531 in the specimens, and absorbance at 400 nm was used to have a more sensitive monitor of material yellowing that may not be readily visible to the human eye.

Such monitoring at 400 nm resulted in the detection of what tentatively seems to be two distinctly different yellowing processes. The first is a transient yellowing, generally at low levels of intensity not detectable by the human eye, which is associated with the decomposition of residual Lupersol 101 peroxide curing agent not consumed during the EVA cure. The second yellowing behavior is associated with thermal and/or UV photooxidation that can eventually become visible to the human eye as was observed in the Springborn aging test.

In general, the EVA aging trends observed at Springborn and JPL were similar. At JPL, exposure of Elvax 150 to 6 suns of UV at 30°C resulted in visible deterioration within 600 h. The material turned yellow and developed a sticky surface. Chemical analysis revealed that some crosslinking had occurred, generating an insoluble gel phase. Specimens of cured A-9918 EVA, exposed to 6 suns UV for 1400 h at 30°C, experienced only two detected changes: depletion of the residual Lupersol 101 peroxide curing agent, and trace formation of hydroxyl groups.

Samples of cured A-9918 EVA exposed to 6 suns of UV for 500 h at 70°C, and for 800 h at 85°C, survived in excellent condition. These results indicate that the Cyasorb UV-531 in the concentration used (0.3 wt %) is adequate to protect the EVA against UV-activated reactions, even at 6 suns of UV intensity.

Control samples of cured A-9918 EVA, thermally aged in the dark for 400 h at 70°C, and for 800 h at 85°C, were in excellent condition with no detection of any yellowing associated with thermal oxidation.

Aging of cured A-9918 EVA up to 800 h at 105°C, however, resulted in measurable and observable changes from which fundamental chemical information on A-9918 EVA aging could be derived. During the time period of this test exposure, no yellowing from either photooxidation or thermal oxidation was detected for the cured A-9918 EVA specimens sandwiched between the Pyrex glass covers that were exposed to 6 suns of UV. Also, chemical analysis of these aged specimens identified the presence of hydroxyl groups, and barely detected minute traces of acetic acid.

However, yellowing of the A-9918 EVA specimens thermally aged in the dark at 105°C began early in the aging test and progressed to become increasingly intense with continued aging, in contrast to the absence of yellowing from the same specimens exposed to 6 suns of UV. The interpretation of these data suggest that UV wavelengths, somewhere between 310 and 370 nm, act in turn to photooxidize the yellow thermal oxidation products. The result of this reaction is yet another degradation product that does not have a visible color; in other words, UV bleaching.

3. EVA Aging Summary

Elvax 150 can be degraded by UV photooxidation, thermal oxidation, and by purely thermal decomposition of the acetate groups to acetic acid. As protection against each of these degradation modes is provided, the life and associated peak service temperature of EVA encapsulant can be extended.

Analysis of Elvax 150 suggests that the UV wavelengths, deleterious to this material and necessary for UV photooxidation, are those shorter than 360 nm. Isolation of Elvax 150 from these UV wavelengths, with UV-filtering outer covers and/or compounding additives such as Cyasorb UV-531, stops UV photooxidation and reduces the aging characteristics of Elvax 150 to thermal effects. This basic and very simple concept was established as a fundamental module design philosophy, and no problem with this concept has been identified in the experimental aging results to date.

For module applications having daytime peaking temperatures near 55°C, it seems that the life of the EVA encapsulant is related more to the life of the UV protection schemes and less to either the thermal behavior of the EVA or thermal protection schemes (for example, antioxidants).

The potential for long service life of EVA in modules at rooftop temperatures (e.g., 85°C) looks encouraging, but predictions of lifetime would be premature. As at 55°C, UV protection and permanence of the UV protection is a must. After that, it is not clearly established which of the thermally driven processes is most critical. These processes include the basic thermal oxidation properties of the Elvax 150, of antioxidants and the associated temperature dependency of their protective induction periods, and the temperature dependence of any physical loss and depletion of the protective compounding additives themselves, such as the UV and thermal stabilization additives.

The phenomenon of the UV bleaching of the yellow thermal oxidation products, observed in accelerated testing at 105°C, suggest possibilities for reducing the amount of UV filtering as currently employed to permit some of the UV bleaching wavelengths to penetrate throughout the EVA. In this way, allowable service temperatures of the EVA might be slightly raised, permitting physical and mechanical deterioration by thermal oxidation to proceed at known rates related to lifetime expectations while maintaining optical clarity by the UV bleaching effect.

B. OUTDOOR HEATING RACKS: OPTARs

A novel accelerated aging technique was developed using outdoor racks on which test materials and modules could be heated to fixed temperature levels above ambient to accelerate aging from exposure to the natural weathering elements, e.g., oxygen, UV, humidity, and pollution. The aging tests were carried out at 70, 90, and 110°C. These outdoor heating racks were given the name OPTARs.

In the OPTAR reactors, natural sunlight is used as the light source and only the specimen temperature is increased. The OPTAR reactors consist of heated aluminum blocks surfaced with stainless steel and mounting hardware to hold the test specimens flush with the surface. The reactors are tilted at 45 deg south, operate at 70, 90, and 110°C, and the devices turn on at sunrise and off at sunset. This approach eliminates the difficulties associated with the irregular spectrum of artificial light sources, exposes the specimens to other environmental conditions such as rain and pollution, and additionally incorporates a dark cycle. The only acceleration, therefore, is in the temperature, all other environmental conditions being present in their natural occurrence and intensity. In summary, the OPTAR device is considered to have the following advantages:

(1) Uses natural sunlight, therefore, avoids the spectral distribution problems encountered with artificial light sources.

(2) Uses temperature to accelerate the photothermal reactions and is easily controllable.

(3) Includes dark-cycle reactions that are a natural part of field exposure.

(4) Includes dew and rain water extraction effects.

(5) More closely resembles the environmental conditions experienced by solar modules.

(6) Easily accommodates both discrete materials and entire modules.

(7) May be set at any temperature desired for the purpose of varying the acceleration rate or extrapolating to lower temperatures.

The initial experiment on these devices using polypropylene as a model polymer was impressively successful. Figure 45 depicts an outdoor aging characteristic of unstabilized polypropylene that is a plot of the materials elongation-at-break (ϵ_B) versus aging time outdoors. The aging is characterized by two stages: an initial induction period during which ϵ_B is virtually unchanged, followed by a second stage that is an almost precipitous drop in ϵ_B. This second

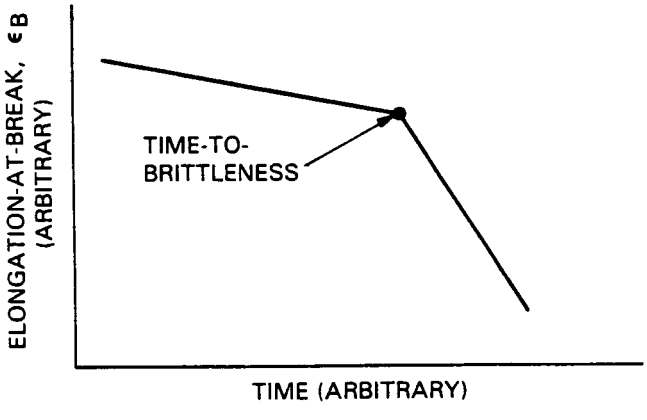

Figure 45. Illustrative Representation of the Natural Outdoor Aging Pattern for Unstabilized Polypropylene

stage reflects brittle failure of the aged polypropylene sample, and the time associated with the onset of this precipitous drop is the time-to-brittleness, which is a function of temperature.

Tensile bars of unstabilized compression-molded polypropylene were placed on the OPTAR devices at the three temperatures and aged until brittle. Figure 46 is an Arrhenius plot of the time-to-brittleness at each of the OPTAR temperatures, and extrapolation of the data line to lower air temperatures predicts the known outdoor aging time of the polypropylene at ambient conditions.

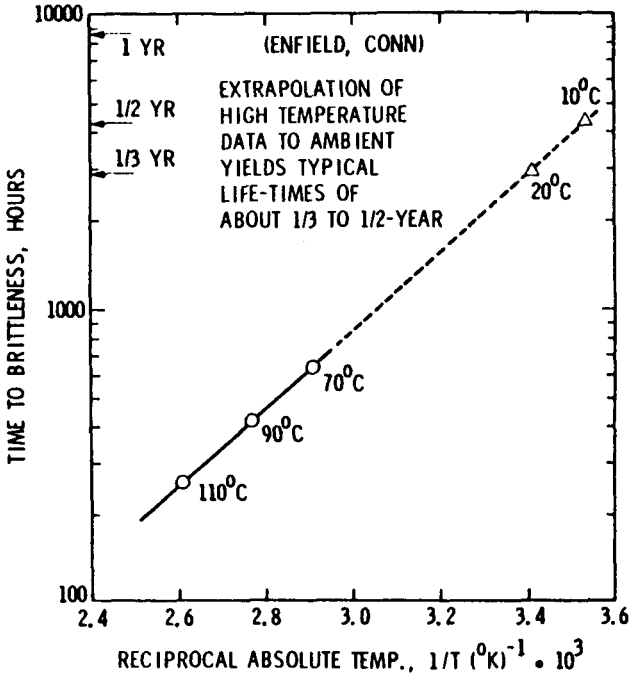

Figure 46. Natural Outdoor Aging of Polypropylene on the Outdoor Heating Racks at 70, 90, and 110°C

1. EVA Testing

Following this impressive initial experiment, cured specimens of both A-9918 EVA and 18170 EVA (see Tables 4 and 7 for formulations) were mounted on the OPTAR devices as free-standing films, and also as composites behind glass, Tedlar, and Teflon FEP. The Tedlar is the UV-screening film, 100BG30UT, which is 1 mil thick. The Teflon FEP is a non-UV screening film which is 1.5 mils thick having one surface that is bondable (the Du Pont designation is FEP-C). This test with FEP addresses the question of whether or not an EVA compounded with weather stabilization additives needs an additional UV-screening outer cover. In this case, FEP, a naturally weatherable transparent film (see Reference 69), functions only to isolate the EVA from direct contact with liquid water (rain, dew, etc.), which should eliminate water extraction effects, and also as a hard, fluorocarbon outer surface for low soil retention.

At this time, the experiment has been ongoing for 7000 h at 70, 90, and 105°C.[3] The free-standing EVA specimens at 90 and 105°C degraded within 2000 h, becoming yellow, tacky, and viscous (loss of mechanical properties).

The mechanical properties of samples removed from the OPTAR devices at a scheduled 3000 h test point were unchanged from unaged controls, including the EVA specimens positioned behind FEP. At 4000 h, the composite samples are observed to be visually and physically unchanged, including the EVA materials behind the non-UV screening FEP film.

2. Module Exposure

Four types of "mini" modules were prepared (5 × 8.25 in.), each containing two interconnected 90-mm-diameter solar cells (Solar Power Corp., Woburn, Massachusetts). Each module consisted of the following components: (1) glass primed with 11861 primer, (2) pottant, (3) the cell pair, and (4) a back-cover film of white Tedlar (200BS30WH) coated with 68040 adhesive. The modules were prepared by a vacuum bag lamination technique with four different pottants to test a formulation variable. The four pottants are listed in Table 27.

Each module was prepared with a 1 x 0.75 in. piece of untreated copper mesh encapsulated in the pottant to determine the severity of copper activation effects. The modules were evaluated by visual inspection.

Table 28 gives the general results of module performance on OPTAR reactors after 12,000 h of exposure.

When aging effects were observed, the first change to be noticed was a slight discoloration in the vicinity of the copper mesh. This was also anticipated to be the first source of degradation. At 70°C, it is barely noticeable after 5000 h and is found in two modules (EVA A9918 and EVA 14747). Apart from this slight effect, there are no other changes that can be observed in any of the modules at the 70°C/12,000 h condition.

At 90°C, the copper discoloration became noticeable in all modules, but more so for those using Lupersol-101 as the curing agent, and at 105°C was dramatically visible in all four. In addition to the strong orange/brown color around the copper mesh, signs of flow of the pottant could also be found, especially in the module using EVA A-9918. In the 90°C/12,000 h condition, a few other effects also became noticeable. Some discoloration (yellowing) of the pottant was found in the module prepared with EVA A-9918 and EVA 14747. Both of these formulations were similarly cured with Lupersol-101, which suggests that this curing agent might result in slightly less photostable compositions

[3]The temperature was lowered to 105°C from 110°C for equipment operating reasons.

Table 27. Modules Under Exposure

Module Number	Pottant Formulation Number	Description
16747-1	EVA A-9918	Standard Formulation (Lupersol 101, UV-531, and Tinuvin 770)
16747-2	EVA 16718A	Experimental EVA Formulation (TBEC, UV-2098, and Tinuvin 770)
16747-3	EVA 16717	Experimental EMA Formulation (TBEC, UV-2098, and Tinuvin 770)
16747-4	EVA 14747	Experimental EVA Formulation (Lupersol 101, UV-2098, and Tinuvin 770)

Table 28. OPTAR Exposure: Modules (12,000 h)

Number	Pottant	Component	At 70°C	At 90°C	At 105°C
16147-1	EVA A-9918	Pottant	1	A2	A4
		Copper	A4	A3, E3	A5, E5
		Glass	1	1	B
		Metallization	1	C2	1
16147-2	EVA 16718A	Pottant	1	D2	A2
		Copper	1	A2	A5
		Glass	1	1	B
		Metallization	1	C2	1
16718-3	EMA 16717	Pottant	1	D2	A4
		Copper	1	A2	A5
		Glass	1	1	B
		Metallization	1	1	1
16718-3	EVA 14747	Pottant	1	A3	A4
		Copper	A2	A4	A5
		Glass	B	B	B
		Metallization	1	C3	C3

A = Discolored
B = Broken/fractured
C = Corrosion (metallization)
D = Delamination
E = Flow/melt

1 = No change
2 = Slight change
3 = Noticeable
4 = Moderate
5 = Severe

than the Lupersol-TBEC used in the other two compositions.

At the 105°C/12,000-h test point, degradative effects were now quite noticeable. The glass outer covers all showed meandering cracks because of thermal shock, the copper catalyzed degradation of the pottant was striking, and all the pottants showed some degree of discoloration. These tests are continuing beyond preparation of this document.

SECTION VII

Evaluation of Alternative Encapsulation Concepts

The emphasis and major focus of the FSA Project was the development, demonstration, and transfer to industry of technology applicable to the design and production of large-scale, long-life, and cost-effective PV solar arrays. In the course of the FSA program, a great variety of candidate materials, processes, and design concepts were proposed, explored, and evaluated. As the FSA Encapsulation Task focused on fewer design approaches, it became necessary to drop development of a number of alternative materials and process concepts. These were dropped based on either their immature technical status or their lacking in comparative cost effectiveness, considering other available design options.

However, these technologies may be well worth developing for a different set of PV module design requirements such as for space, military, or navigation applications in which ruggedness, portability, or weight factors may be overriding. Therefore, several of these advanced encapsulation concepts are summarized in this section for future reference and potential application.

A. ION PLATING

In this technique, developed by ENDUREX, metals are vaporized in a vacuum as positive ions rather than atoms. The ions then stream toward a negatively charged target. Because of this attraction, coverage occurs over all charged surfaces, no matter how inaccessible, in contrast to conventional vapor deposition where the coating is line-of-sight only. The electrical attraction results in the incident ion stream striking the target with sufficient kinetic energy to achieve some subsurface penetration. This results in strong adhesion of the ion-plated coating in contrast to conventional vapor deposition that merely condenses onto a surface.

Early in the encapsulation task, it was recognized that all polymers are permeable to water and, thus, elastomeric pottants and plastic films probably would not isolate encapsulated solar cells from atmospheric moisture. This could be a problem if solar cells were found to be sensitive to loss of performance from exposure to moisture. Therefore, ion plating was investigated as a possible means of applying a thin and transparent conformal coating as an impervious water barrier over all surfaces of a solar cell. The candidate coating material was aluminum oxide (Figure 47), about 1400 Å thick to also function as an AR coating. Further, it was considered that the task of adhesively bonding an elastomeric pottant to a solar cell would be simplified if the solar cell had only one outer surface chemistry.

Experiments revealed that the metallizations on the selected solar cells were extremely porous because of the sintering process, and that although the ion-plated coating penetrated into the pores, it did not function to seal the pores. Thus, water was still able to penetrate to the solar cell through this porous network. Because sintering was a common metallization process, an effort was made at ENDUREX to use their process to first deposit a non-porous metallization grid followed by depositing the impervious aluminum oxide AR coating. There was partial success, but the effort

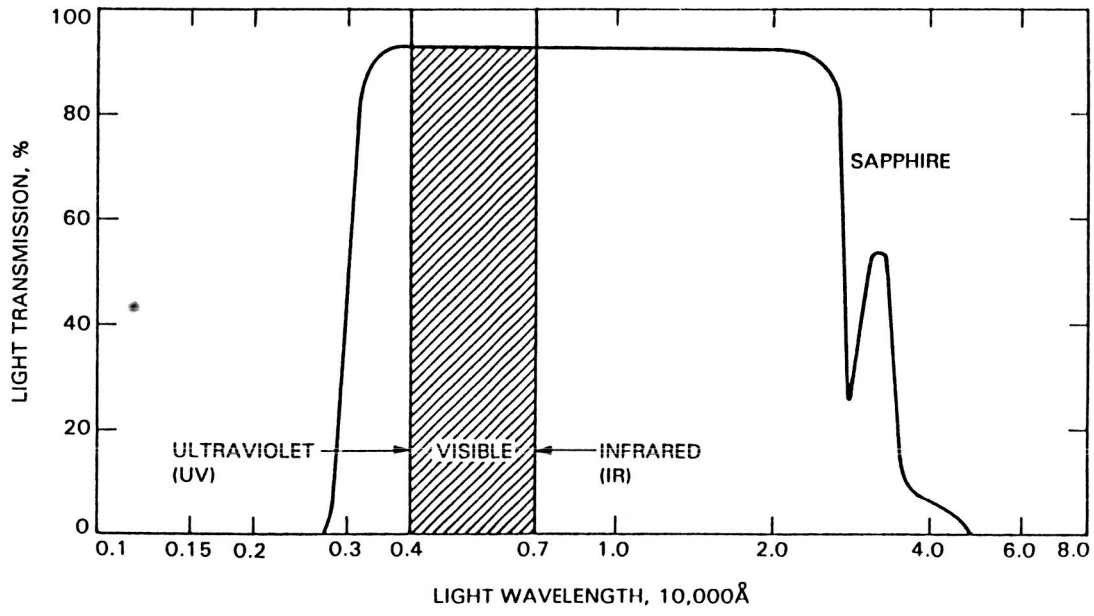

Figure 47. Optical Transmission of Aluminum Oxide

was stopped for two reasons: first, the need for an impervious coating concept vanished when solar cell manufacturers eliminated the root causes for moisture sensitivity and, second, the scale-up and economics of the ion-plating process for high-volume production did not seem attractive at that time.[4]

B. LOW-COST SILICONE ENCAPSULATION CONCEPTS

Silicone materials were popularly used in the 1970s as encapsulation pottants, but their high cost made them noncompetitive with other available polymer systems. Dow Corning was funded to seek approaches to reducing the cost of silicone systems for PV applications (see Reference 17).

Dow Corning identified a commerical silicone resin, Q1-2577, that could be spray coated as a conformal coating pottant. Modules up to 11 × 16 in., that were spray coated with Q1-2577, passed the JPL thermal-cycle test. After spray coating, the modules could be air dried at room temperature for 24 h, or the air drying could be optionally accelerated to a few hours at 75°C.

A white pigment, TiO_2, can be easily dispersed in Q1-2577 that can then be spray coated as a thin layer on substrate panels to provide a light-reflecting white background on module areas not covered by solar cells. The pigmented Q1-2577 can also be used as a back cover for glass superstrate modules.

One Dow Corning innovation to reduce silicon material use (and cost) involved the machining of circular recesses into wood substrates to a depth and diameter slightly larger than the solar cells to be encapsulated. Notches were machined between the circular recesses to accommodate the interconnects. The recessed and notched wood substrate was then spray coated with the white-pigmented Q1-2577 and while still wet (uncured), the interconnected cell string was positioned in the recesses and notches. An overcoat of clear Q1-2577 was sprayed on the entire top surface of the module and cells, and the silicone was cured for a few hours at 75°C.

This module design passed the JPL thermal-cycle test, and one module installed on an outdoor weathering rack at JPL was still functional after 3 years when the rack testing was discontinued for other reasons.

Q1-2577 is commercially available as a solution at a bulk cost of $8.45/lb, which is a 1982 cost quote. The solids content of the solution is 75% by weight, which correspond to a dry-solids cost of $11.26/lb, or 5.8¢/ft^2/mil of thickness, assuming no spray loss.

Dow Corning also developed a silicone/acrylic block copolymer film-forming material to function as a UV screening cover for UV-sensitive pottants. The chemistry of this material permits the incorporation of polymerizable UV screening agents for permanence of the UV screening property. As made, the polymer was dissolved in toluene and the solution then sprayed onto a release paper. After air drying for 30 min at 75°C, the film could be lifted off the release paper.

The polymerizable UV screening monomer that was used was Permasorb-MA from the National Starch and Chemical Corp. in Bridgewater, New Jersey. The acrylic block was a random copolymer of methyl methacrylate (MMA) and n-butyl acrylate (BA), and the silicone block was an acrylic terminated polydimethyl siloxane. The concentration of the acrylics and silicones, as well as the amount of Permasorb-MA, could be varied. From an experimental study relating the relative composition of acrylics and silicones with properties such as mechanical and thermomechanical behavior, the best film composition consisted of 20% by weight silicones and 80% by weight acrylics, with the latter in turn consisting of 50% MMA and 50% BA by weight.

Indications of the UV protection afforded by this film, its inherent weatherability and the permananence of its UV screening property, was assessed in the Dow Corning Atlas Weatherometer. As a UV-degradable control, Dow Corning used cellulose acetate (CA). After 904 h (the accumulated hours), the CA control was virtually destroyed, whereas, CA coated with 3 mils of the film containing 1% by weight Permasorb-MA was visually unchanged. The screening film itself and its level of UV absorption was also unchanged.

The Dow Corning film exhibited good resistance to dirt and soil retention and was also easily cleaned by wiping with a dry or slightly damp cloth. The wiping action did not visually mar or abrade the surface of the film.

Because of the existence of other commercially available UV-screening films, further development of the Dow Corning UV-screening film was suspended, but not forgotten.

C. GLASS-REINFORCED CONCRETE

Glass-fiber reinforced concrete panels as potential PV module substrates were developed and evaluated by MBAssociates of San Ramon, California. The panels were 1/4 in. thick and had integral reinforcing ribs on the back side of the panel. The projected cost was $0.62/ft^2, a 1982 price quote. The glass-reinforced concrete panels were intended to be a part of the solar array field structure in addition to serving as a module substrate, thus making them cost effective by fulfilling two functions.

MBAssociates manufactured a 4- × 8-ft demonstration module with this substrate material, using EVA as

[4]Illinois Tool Works, ENDUREX Division, Elgin, Illinois, LSA Contract 955506.

the encapsulant pottant, and a UV-screening film, Korad 212, as the top cover.[5] The demonstration module was mounted on 6- × 6-in. pressure-treated wood posts, simulating an array field structure. No problems were experienced with these panels.[6]

D. ELECTROSTATIC BONDING

Electrostatic bonding (ESB) is a method of attaching glass sheets to metals or dielectrics without using an additional adhesive. This technology was developed for PV application by Spire Corp. It can be used to attach silicon solar cells to a glass superstrate, or to attach one sheet of glass to another with a dielectric-film interlayer. In the bonding process, the glass is heated to a temperature high enough to allow ion mobility, but lower than the softening point of the glass, typically 350 to 650°C. At this temperature, high voltage is applied across the glass and the object to be bonded. Rearrangement of ions within the glass causes a permanent chemical bond to be formed across the interface. The resulting seal is completely hermetic, and will generally be as strong as the materials being bonded.

Because of the thermal processing involved, the glass used must be a near match in thermal-expansion coefficient to the object to be bonded. For silicon solar cells, Pyrex (Corning Type 7740) or Tempax (Schott Glass 8330) is acceptable up to a process temperature of about 400°C, and Corning Type 7070, Schott Type 8248, or Owens-Illinois Type ES-1 is acceptable up to 650°C.

For adhesion to cells with significant surface metallization, it is necessary to deform the glass around the metal contacts. In this case, process temperatures near the high end of the range are needed and, in some cases, external pressure must be applied to increase the amount of deformation.

Module designs using ESB have several advantages:

(1) The ESB seal is an integral bond between glass and silicon and, thus, is fully hermetic.

(2) There is no pottant between cells and glass cover to be subject to degradation.

(3) Cells are attached to a thermal-expansion-matched glass.

The present process has several requirements:

(1) Thermal expansion of the glass must match that of the silicon.

(2) Glass deformation for bonding solar cells with raised front metallization require temperatures above 500°C. Therefore, the solar cells must be able to withstand at least 5 min of exposure to this temperature without significant thermal degradation.

Figure 48 shows a hybrid module with ESB front lamination and conventional back. This design retains many of the advantages of the fully integral module, at lower cost: no pottant between glass front and cells, expansion-matched superstrate, and hermetic protection of cell-front metallization.[7]

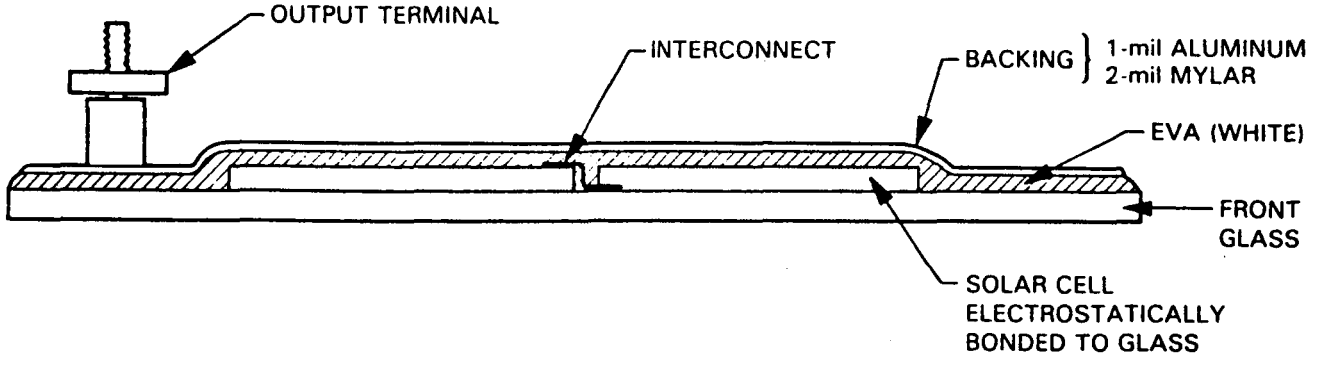

Figure 48. Cross-Sectional View of Integral Front, Electrostatically Bonded Module Assembly

[5]An early FSA UV-screening film candidate.

[6]MBAssociates, San Ramon, California, JPL Contract 954882.

[7]Spire Corp., Bedford, Massachusetts, LSA Contract 954521.

SECTION VIII

Conclusions and Recommendations

The FSA Encapsulation Task has essentially achieved its objectives of identifying, developing, evaluating, and transferring to industry the module encapsulation technology required for the design and manufacture of low-cost, efficient, and durable solar cell modules.

The basic functions of an encapsulation system, which are to provide support, optical coupling, electrical isolation, and physical protection, were translated into required material characteristics. The definition of these material characteristics and desirable properties led to the assessment of available materials. It also led to the development of new materials and combinations of materials and processes that met the performance and economic goals of the FSA Project.

Although the FSA Project was directed toward the development of technology for flat-plate silicon solar cell modules, the Encapsulation Task has also contributed significantly to materials technology for other systems that also need and use environmentally stable polymeric elastomers and plastics.

The Encapsulation Task has succeeded in defining requirements for each of the encapsulation materials for the several different elements of the solar cell module encapsulation package required for achieving 30-year life and high module performance at low cost.

Rapid technical progress, realized during the past several years in solar energy conversion, has established the economic viability of PV modules as a source of electric power. Many alternate avenues of progress have been identified and explored in some detail. However, much remains to be done in establishing an expanded database of design and manufacturing experience for optimizing the economics of solar cell power in terms of module cost, reliability, performance, and safety.

Some of the encapsulation needs and approaches identified and recommended for further R&D by industry and Government are summarized in the following paragraphs.

A. ENCAPSULATION SYSTEM DESIGN ALTERNATIVES

For specialized solar module applications such as military, remote site, limited lifetime, or low-power uses, other material systems than detailed in this report may have advantages of ruggedness, lower weight, resistance to lower or higher temperatures, or lower cost. Therefore, other material systems that have been identified and described in this report, or in other FSA Project reports referenced, may be further evaluated for such special applications.

For most residential and utility applications, tempered glass sheet has been the structural panel material of choice. Alternate materials that have special characteristics of interest include glass fiber-reinforced concrete panels, silicone/acrylic polymer blends, electrostatic bonded modules with no pottant, and wood fiber hardboard for structural substrate panels.

B. MATERIAL AGING RESEARCH

Most concepts for capturing and converting solar energy involve the use of polymeric materials that will be subject to environmental stresses such as heat, cold, moisture, UV radiation, and physical forces. The development of low-cost materials able to operate in these environments reliably for periods of years was a major challenge of the Encapsulation Task.

A major scientific contribution of the Encapsulation Task was the investigation of the mechanisms of long-term polymer degradation and their effects on material optical, structural, and electrical properties. Through research in understanding the processes and mechanisms of aging degradation, it was possible to select the most promising candidate material types and provide criteria for modifying such materials to control degradation and enhance both their performance and fabricability while achieving the FSA Project goals.

Through understanding the degradation mechanisms, it also was possible to develop more valid accelerated testing methods and computer models for predicting material changes with time and exposure conditions. These techniques are now available for more extensive characterization of advanced encapsulation material designs as they are developed.

C. POTTANTS

The testing and chemical modeling studies of the elastomeric pottants EVA, EMA, and PU, as compounded for solar module use, indicate the potential for 30-year durability when used behind glass with sound edge sealing and a plastic film back cover. Defining the limits of temperature and the effects of other adverse environments, the compatibility with various low-cost cell metallization materials, needs further analysis and field test experience.

It has been noted that the hydrocarbon-based polymers are more flammable than the fluorocarbon and silicone materials and, therefore, subject to melting and burning in some of the more severe fire tests applied to roofing materials. Three aspects of this situation

needing further study are: (1) the addition of flame retardants to the pottant, (2) additions to the encapsulant package to shield the pottant or protect the structure under the module from burning, and (3) development of new and appropriate fire safety standards and tests.

Each of these aspects of the situation has been addressed within the FSA Project and the effort should be continued.

D. PRIMERS AND ADHESIVES

Delamination between the pottant material and the structural panel and between the pottant and the solar cell was one of the first identified solar module degradaton modes. As a result, primers and surface preparations were developed and tested that greatly improved interface bonding within the module for the various combinations of materials involved. The long-term bonding integrity under conditions of high temperature and moisture exposure seem adequate, but additional experience is needed to provide a reliability database.

E. ELECTRICAL ISOLATION

The development of a source of electrical power, in which the power generating elements (solar cells) may be at 1000 V potential and separated by only a few thousandths of an inch from a possible short or human contact, presents some special material requirements. Testing has demonstrated that 5.0 mils of EVA will resist up to 12,000 V DC. However, there is little technical data to be able to assess the long-term effects of combined electrical and environmental stress on the dielectric strength of polymeric materials. A fundamental approach to evaluating and quantifying this characteristic has been started and needs to be pursued vigorously.

F. ANTI-SOILING

Treatment of the module cover surfaces, whether of glass, acrylic, or fluorocarbon, with antisoiling chemicals that were defined and evaluated during this effort has increased module long-term performance by 1 to 6%, depending on the cover material and the dirtiness of the environment.

An economical approach is needed to the periodic cleaning and possible recoating of module covers with antisoiling materials. More field testing experience is needed to develop a method for minimizing soiling losses for various solar array locations.

G. THIN-FILM PHOTOVOLTAICS

The encapsulation of thin-film PV modules for long-term, reliable outdoor service represents a future technical challenge similarly as that carried out for crystalline solar cells. This past effort was successfully performed encompassing an integrated team of Government, university, and private research facilities focused on clearly defined research and developmental objectives. It is believed that this same systematic approach and program organization which was effectively used for crystalline solar cells, as well as the technologies described in this report, will serve as a solid basis on which to build a future thin-film encapsulation program.

SECTION IX

References

A. ENCAPSULATION TASK REPORTS

1. *Terrestrial Service Environments for Selected Geographic Locations*, ERDA/JPL-954328-76/5, Battelle Columbus Laboratories, Columbus, Ohio, June 24, 1976.

2. Carmichael, D.C., et al., *Review of World Experiences and Properties of Materials for Encapsulation of Terrestrial Photovoltaic Arrays*, Final Report, Battelle Columbus Laboratories, Columbus, Ohio, July 21, 1976.

3. Cuddihy, E.F., and Carroll, W.F., "Consideration of Encapsulants for Photovoltaic Arrays in Terrestrial Applications," *Proceedings of the 1976 Meeting of the Society of Photo-Optical Instrumentation Engineers*, August 1976.

4. Carrol, W.F., Cuddihy, E.F., and Salama, M., "Material and Design Considerations of Encapsulants for Photovoltaic Arrays in Terrestrial Applications," *Proceedings of the 12th IEEE Photovoltaic Specialists Conference*, November 1976.

5. Willis, P.B., White, R., and Baum, B., *Investigations of Test Methods, Material Properties, and Processes for Solar-cell Encapsulants*, Annual Report, ERDA/JPL-954527, Springborn Laboratories, Inc., Enfield, Connecticut, July 1977.

6. Cuddihy, E.F., *Encapsulation Material Trends Relative to 1986 Cost Goals*, JPL Document 5101-61, Jet Propulsion Laboratory, Pasadena, California, April 13, 1978.

7. Maxwell, H., *Encapsulant Candidate Materials for 1982 Cost Goals*, JPL Document 5101-72, Jet Propulsion Laboratory, Pasadena, California, June 15, 1978.

8. Willis, P.B, Baum, B., and White, R., *Investigations of Test Methods, Material Properties, and Processes for Solar-Cell Encapsulants*, Annual Report, ERDA/JPL-954527, Springborn Laboratories, Inc., Enfield, Connecticut, July 1978.

9. Gupta, A., *Photodegradation of Polymeric Encapsulants of Solar Cell Modules*, JPL Document 5101-77, Jet Propulsion Laboratory, Pasadena, California, August 10, 1978.

10. Gupta, A., *Effect of Photodegradation on Chemical Structure and Surface Characteristics of Silicone Pottants Used in Solar Cell Modules*, JPL Document 5101-79, Jet Propulsion Laboratory, Pasadena, California, August 18, 1978.

11. Gupta, A., Moacanin, J., Smith, T., and Kaelble, D.H., "Effect of Outdoor Exposure on Adhesion of Silicone Pottants to Solar Cell Module Substrates," *Polymer Preprints*, Vol. 19, p. 702, 1978.

12. Cuddihy, E.F., Baum, B., and Willis, P.B, *Low-Cost Encapsulation Materials for Terrestrial Solar Cell Modules*, JPL Document 5101-78, Jet Propulsion Laboratory, Pasadena, California, September 1978, and *Solar Energy*, Vol. 22, p. 389, 1979.

13. Willis, P.B., and Baum, B., *Investigations of Test Methods, Material Properties, and Processes for Solar-Cell Encapsulants*, Annual Report, ERDA/JPL-954527, Springborn Laboratories, Inc., Enfield, Connecticut, July 1979.

14. Baum, B., Parker, C.H., Cuddihy, E.F., and Willis, P.B., "Weathering Properties of Plastics for the Construction Industry," *Plastics in Building Construction*, Vol. III, No. II, Technomic Publishing Company, August 1979.

15. Laue, E., and Gupta, A., *Reactor for Simulation and Acceleration of Solar Ultraviolet Damage*, JPL Document 5101-135, Jet Propulsion Laboratory, September 21, 1979.

16. Plueddemann, E.P., *Chemical Bonding Technology for Terrestrial Solar Cell Modules*, LSA Project Task Report, JPL Document 5101-132, Jet Propulsion Laboratory, Pasadena, California, September 1, 1979.

17. *Develop Silicone Encapsulation Systems for Terrestrial Silicon Solar Arrays*, Final Report, DOE/JPL 945995-80/6, Dow Corning Corp., Midland, Michigan, December 1979.

18. Cuddihy, E.F., *Encapsulation Materials Status to December 1979*, JPL Document 5101-144, Jet Propulsion Laboratory, Pasadena, California, January 15, 1980.

19. Bouquet, F.L., *Glass for Low-Cost Photovoltaic Solar Arrays*, JPL Publication 80-12, JPL Document 5101-147, DOE/JPL-1012-40, Jet Propulsion Laboratory, Pasadena, California, February 1, 1980.

20. Willis, P.B., and Baum, B., *Investigations of Test Methods, Material Properties, and Pro-*

cesses for Solar-Cell Encapsulants, Annual Report, ERDA/JPL-954527, Springborn Laboratories, Inc., Enfield, Connecticut, July 1980.

21. Gupta, A., and Di Stefano, S., "Photocatalytic Degradation of a Cross-Linked Ethylene Vinyl Acetate (EVA) Elastomer," *Polymer Preprints*, Vol. 21, p. 178, August 1980.

22. Cuddihy, E.F., "Theoretical Considerations of Soil Retention," *Solar Energy Materials*, Vol. 3, pp. 21-33, 1980.

23. Baum, B., Willis, P.B., and Cuddihy, E.F., "Photovoltaic Encapsulation Materials," *Proceedings of the Symposium on Materials and New Processing Technologies for Photovoltaics*, Sponsored by the Electrochemical Society, Inc., Vol. 81-3, January 1981.

24. Garcia, A., Minning, C.P., and Cuddihy, E.F., "A Quantitative Method for Photovoltaic Encapsulation System Optimization," *Proceedings of the 26th National SAMPE Meeting*, April 28-30, 1981, Los Angeles, California.

25. Garcia, A., Minning, C.P., and Cuddihy, E.F., "An Analytical Approach to Photovoltaic Encapsulation System Design," *Proceedings of the 15th IEEE Photovoltaic Specialists Conference*, May 1981.

26. Liang, R.H., Tsay, F.D., Moacanin, J., and Gupta, A., "Photodegradation of Poly (n-Butylacrylate), A Candidate Encapsulant Material for Photovoltaic Modules," *Proceedings of the Symposium on Applications of Spectroscopy to Problems in Polymer Engineering and Science*, 90th National Meeting of AICHE, Houston, Texas, April 1981.

27. Minning, C.P., Coakley, J.F., Perrygo, C.M., Garcia, A., and Cuddihy, E.F., "Thermal and Optical Performance of Encapsulation Systems for Flat-Plate Photovoltaic Modules," *Proceedings of the 15th IEEE Photovoltaic Specialists Conference*, May 1981.

28. Willis, P.B., and Baum, B., *Investigations of Test Methods, Material Properties, and Processes for Solar-Cell Encapsulants*, Annual Report, Springborn Laboratories, Inc., Enfield, Connecticut, DOE/JPL 954527-81-15, July 1981.

29. Cuddihy, E.F., *Development of Reduced-Variable Master Curves for Estimating Tensile Stresses of Encapsulated Solar Cells Caused by Module Deflection or Thermal Expansion*, JPL Document 5101-182, Jet Propulsion Laboratory, Pasadena, California, October 1, 1981.

30. *Phase I Technical Report for Flat-Plate Solar Array Project Contract 955567*, Spectrolab, Inc., Sylmar, California, November 1981.

31. Liang, R.H., Yavrouian, A., and Gupta, A., "Development of a Weatherable Acrylic Elastomer for Solar Cell Encapsulation," *Proceedings of the 158th Meeting of the Electrochemical Society*, Hollywood, Florida, Vol. 81-3, pp. 261-265, 1981.

32. Cuddihy, E.F., Coulbert, C.D., Willis, P.B., Baum, B., Garcia, A., and Minning, C.P., "Polymeric Encapsulation Materials for Low-Cost Terrestrial Photovoltaic Modules," Paper No. 22 in *Polymers in Solar Energy Utilization*, ACS Symposium Series No. 22, Symposium Series No. 220, March 1982.

33. Burger, D., and Cuddihy, E.F., "Vacuum Lamination of Photovoltaic Modules," Paper No. 25 in *Polymers in Solar Energy Utilization*, ACS Symposium Series No. 220, March 1982.

34. Cuddihy, E.F., Carroll, W.F., Coulbert, C.D., Gupta, A., and Liang, R.H., *Photovoltaic Module Encapsulation Design and Materials Selection: Volume I*, JPL Publication 81-102, JPL Document 5101-177, DOE/JPL-1012-56, Jet Propulsion Laboratory, Pasadena, California, June 1, 1982.

35. Liang, R.H., Gupta, A., and Di Stefano, S., *Photothermal Characterization of Encapsulant Materials for Photovoltaic Modules*, JPL Publication 82-42, JPL Document 5101-210, DOE/JPL-1012-72, Jet Propulsion Laboratory, Pasadena, California, June 1, 1982.

36. Willis, P.B., and Baum, B., *Investigation of Test Methods, Material Properties, and Processes for Solar Cell Encapsulants*, Annual Report, DOE/JPL-954527-82/83, Springborn Laboratories, Inc., Enfield, Connecticut, July 1982.

37. Borsing, E., Li, S., Nir, Z., Vogl, O., and Gupta, A., "Polymerizable [2(2-Hydroxyphenyl) 2H-Benzotriazole] Ultraviolet Stabilizers," *Proceedings of the IUPAC 28th Macromolecular Symposium*, p. 298, July 12-16, 1982, Amherst, Massachusetts.

38. Duncan, L.B., Minning, C.P., Garcia, A., and Cuddihy, E.F., "Empirical Testing of Structural Deflection Modeling of Large Photovoltaic Modules," *Proceedings of the 16th IEEE Photovoltaic Specialists Conference*, September 1982.

39. Gupta, A., Liang, R.H., and Vogl, O., "Photo-oxidative Degradation of Clear Ultraviolet

Absorbing Acrylic Copolymer Surfaces," *Physicochemical Aspects of Polymer Surfaces*, Vol. 1, p. 293, 1982.

40. Coulbert, C.D., *The Application of Encapsulation Material Stability Data to Photovoltaic Module Life Assessment*, JPL Publication 83-27, JPL Document 5101-224, DOE/JPL-1012-84, Jet Propulsion Laboratory, Pasadena, California, April 1, 1983.

41. Cuddihy, E.F., Coulbert, C.D, Liang, R.H., Gupta, A., Willis, P.B., and Baum, B., *Applications of Ethylene Vinyl Acetate as an Encapsulation Material for Terrestrial Photovoltaic Modules*, JPL Publication 85-35, JPL Document 5101-220, Jet Propulsion Laboratory, Pasadena, California, April 15, 1983.

42. Maxwell, H.G, et al., *FSA Field Test Report 1980-1982*, JPL Publication 83-29, JPL Document 5101-215, DOE/JPL-1012-85, Jet Propulsion Laboratory, Pasadena, California, April 15, 1983.

43. Liang, R.H., Oda, K., Chung, S., Smith, M., and Gupta, A., *Handbook of Photothermal Test Data on Encapsulant Materials*, JPL Publication 83-32, JPL Document 5101-230, DOE/JPL-1012-86, Jet Propulsion Laboratory, Pasadena, California, May 1, 1983.

44. Cuddihy, E.F., "Surface Soiling: Theoretical Mechanisms and Evaluation of Low-Soiling Coatings," in *Proceedings of the Flat-Plate Solar Array Project Research Forum on Quantifying Degradation*, E.F. Cuddihy Chairman, JPL Publication 83-52, JPL Document 5101-231, DOE/JPL-1012-89, Jet Propulsion Laboratory, Pasadena, California, June 1, 1983.

45. Willis, P.B., and Baum, B., *Investigations of Test Methods, Material Properties, and Processes for Solar-Cell Encapsulants*, Annual Report, DOE/JPL-954527-83/24, Springborn Laboratories, Inc., Enfield, Connecticut, July 1983.

46. Coulter, D.R., Cuddihy, E.F., and Plueddemann, E.P., *Chemical Bonding Technology for Terrestrial Photovoltaic Modules*, JPL Publication 83-86, JPL Document 5101-232, DOE/JPL-1012-91, Jet Propulsion Laboratory, Pasadena, California, November 15, 1983.

47. Cuddihy, E.F., "Breakdown of Organic Insulators," in *Proceedings of the Flat-Plate Solar Array Project Research Forum on the Design of Flat-Plate Photovoltaic Arrays for Central Stations*, R. Ross, Chairman, JPL Publication 84-44, JPL Document 5101-247, DOE/JPL-1012-98, Jet Propulsion Laboratory, Pasadena, California, December 1983.

48. *Design and Analysis of Advanced Encapsulation Systems for Terrestrial Photovoltaic Modules*, 1983 Annual Report, Spectrolab, Inc., Sylmar, California.

49. Liang, R.H., Chung, S., Clayton, A., Di Stefano, S., Oda, K., Hong, S.D., and Gupta, A., "Photothermal Degradation of Ethylene/Vinylacetate Copolymer," *Polymer Alloys*, Vol. III, pp. 267-278, 1983.

50. Liang, R.H., Coulter, D.R., Dao, C., and Gupta, A., "Novel Diagnostic Techniques for Early Detection of Photooxidation in Polymers," *ACS Sym. Series*, No. 220, *Polymers in Solar Energy Utilization*, pp. 265-273, 1983.

51. Coakely, J.E., Kallis, J.M., Jones, I.R., Cuddihy, E.F., and Garcia, A., "Cell Temperatures in Terrestrial Photovoltaic Modules-Effect of Designs Factors," *Proceedings of the 17th IEEE Photovoltaic Specialists Conference*, May 1984.

52. Kallis, J.M., Trucker, D.C., Szeto, R.K., Cuddihy, E.F., and Garcia, A., "Electrical Isolation Design of Photovoltaic Modules," *Proceedings of the 17th IEEE Photovoltaic Specialists Conference*, May 1984.

53. Cuddihy, E.F., *Photovoltaic Module Encapsulation Design and Materials Selection: Vol. II*, JPL Publication 84-34, JPL Document 5101-237, DOE/JPL-1012-97, Jet Propulsion Laboratory, Pasadena, California, June 1, 1984.

54. Willis, P.B., and Baum, B., *Investigations of Test Methods, Material Properties, and Processes for Solar-Cell Encapsulants*, Annual Report, DOE/JPL-954527-84-27, Springborn Laboratories, Enfield, Connecticut, July 1984.

55. Cuddihy, E.F., and Willis, P.B., *Antisoiling Technology: Theories of Surface Soiling and Performance of Antisoiling Surface Coatings*, JPL Publication 84-72, JPL Document 5101-25, DOE/JPL-1012-102, Jet Propulsion Laboratory, Pasadena, California, November 15, 1984.

56. Kallis, J.M., Trucker, D.C., Cuddihy, E.F., and Garcia, A., "Method For Calculating Multidimensional Electrical Fields in Photovoltaic Modules," *Solar Cells*, Vol, 11, pp. 309-330, 1984.

57. Cuddihy, E.F., *A Concept for the Intrinsic Dielectric Strength of Electrical Insulation Materials*, JPL Publication 85-30, JPL Document 5102-252, DOE/JPL-1012-105, Jet Propulsion Laboratory, Pasadena, California, April 15, 1985.

58. Gomez, P.M., Fu, S.K., Gupta, A., and Vogl, O, "New 2(2-Hydroxyphenyl)2H-Benzotriazole Ultraviolet Absorbers and Their Incorporation into Addition and Condensation Polymers," *Polymer Preprints*, Vol. 26, No. 1, pp. 100-101, April 1985.

59. Willis, P.B., *Investigation of Test Methods, Material Properties, and Processes for Solar Cell Encapsulants, Ninth Annual Report*, DOE/JPL 954527-85-28, Springborn Laboratories, Inc., Enfield, Connecticut, July 1985.

60. Cuddihy, E.F., "Encapsulant Selection and Durability Testing Experience," in *Reliability and Engineering of Thin-Film Photovoltaic Modules*, R. Ross and E. Royal, Editors, JPL Publication 85-73, JPL Document 5101-264, DOE/JPL-1012-111, Jet Propulsion Laboratory, Pasadena, California, October 1, 1985.

61. Garcia, A., Final Technical Report for FSA Contract 955567, *Design, Analysis and Test Verification of Advanced Encapsulation Systems*, Spectrolab, Inc., Sylmar, California, DOE/JPL 955567-85-16, November 1985.

62. Koenig, J.L., Boerio, F.J., Plueddemann, E.P., Miller, J., Willis, P.B., and Cuddihy, E.F., *Chemical Bonding Technology: Direct Investigation of Interfacial Bonds*, JPL Publication 86-6," JPL Document 5101-284, DOE/JPL-1012-120, Jet Propulsion Laboratory, Pasadena, California, January 1986.

63. Cuddihy, E.F., *The Aging Correlation (RH+t): Relative Humidity (%) + Temperature (°C)*, JPL Publication 86-7, JPL Document 5101-283, DOE/JPL-1012-121, Jet Propulsion Laboratory, Pasadena, California, January 15, 1986.

64. Willis, P.B., *Investigation of Materials and Processes for Solar Cell Encapsulation*, Final Report for FSA Contract 954527, DOE/JPL 954527-86-29, Springborn Laboratories, Inc., Enfield, Connecticut, August 1986.

B. LITERATURE CITATIONS

65. Roark, R.J., *Formulas for Stress and Strain*, 4th edition, McGraw-Hill, p. 225, 1965.

66. Stultz, J.W., and Wen, L.C., *Thermal Performance Testing and Analysis of Photovoltaic Modules in Natural Sunlight*, JPL Document 5101-31, Jet Propulsion Laboratory, Pasadena, California, July 29, 1977.

67. Stultz, J.W., *Thermal and Other Tests of Photovoltaic Modules Performed in Natural Sunlight*, JPL Document 5101-76, DOE/JPL-1012-78/9, Jet Propulsion Laboratory, Pasadena, California, July 31, 1978.

68. Rainhart, L.G., and Schimmel, Jr., W.P., "Effect of Outdoor Aging on Acrylic Sheet," *Solar Energy*, Vol. 17, p. 259, 1975.

69. *Weatherability of Teflon Film*, Du Pont Technical Information Bulletin T-6C, undated.

70. Rogers, C., "Permeability and Chemical Resistance," Chapter 9 in *Engineering Design for Plastics*, E. Baer, Editor, Reinhold Publishing Co., New York, 1964.

71. Brendlay, W.H., Jr., "Fundamentals of Acrylic Polymers," *Paint and Varnish Production*, Vol. 63, No. 7, pp. 19-27, July 1973.

72. Boerio, F.J., Gosselin, C.A., Dillingham, R.G., and Liu, H.W., Analysis of Thin Films on Metal Surfaces, *J. Adhesion*, Vol. 13, pp. 159-176, 1981.

73. Hoffman, A.R., and Maag, C.R., "Airborne Particulate Soiling of Terrestrial Photovoltaic Modules and Cover Materials," *Proceedings of the Institute of Environmental Sciences*, Philadelphia, Pennsylvania, May 11-14, 1980, Institute of Environmental Sciences, Mt. Prospect, Illinois, 1980.

74. Hoffman, A.R., and Maag, C.R., *Photovoltaic Module Soiling Studies, May 1978 to October 1980*, JPL Publication 80-87, JPL Document 5101-131, DOE/JPL-1012-49, Jet Propulsion Laboratory, Pasadena, California, November 1, 1980.

75. Wen, L., *An Investigation of the Effect of Wind Cooling on Photovoltaic Arrays*, JPL Publication 82-28, JPL Document 5101-201, DOE/JPL-1012-69, Jet Propulsion Laboratory, Pasadena, California, March 1982.

76. Raithby, G.D., and Hollands, H.G.T., "A General Method of Obtaining Approximate Solutions to Laminar and Turbulent Free-Convection Problems," *Advances in Heat Transfer*, Vol. II, pp. 265-315, ed. T.F. Irvine and J.P. Hartnett, Academic Press, 1975.

77. McAdams, W.H., *Heat Transmission*, 3rd Edition, McGraw-Hill Book Co., Inc., New York, 1954.

78. Chen, C.P., *Fracture Strength of Silicon Solar Cells*, JPL Document 5101-137, JPL Publication 79-102, DOE/JPL-1012-32, Jet Propulsion Laboratory, Pasadena, California, October 15, 1979.

79. *Conference Records of the IEEE International Symposia on Electrical Insulation for the Years 1976 to 1982*, published and sponsored by the IEEE Electrical Insulation Society.

80. *Tests for Dielectric Breakdown Voltage and Dielectric Strength of Electrical Insulating Materials at Commercial Power Frequencies*, ASTM-D-149-64, American Society for Testing Materials, 1970.

81. Mason, J.H., "Breakdown of Solid Dielectrics in Divergent Fields," Proceedings IEEE, Monograph 127M, 102C, p. 254, Institution of Electrical Engineers, London, 1955.

82. Ashcraft, A.C., Eichhorn, R.M., and Shaw, R.G., "Laboratory Studies of Treeing in Solid Dielectrics and Voltage Stabilization of Polyethylene," Conference Record of 1976 IEEE International Symposium on Electrical Insulation, Sponsored by the IEEE Electrical Insulation Society, p. 213, Institute of Electrical and Electronics Engineers, Inc., New York, 1976.

83. Whitehead, S., *Dielectric Breakdown of Solids*, Oxford at the Clarendon Press, London 1951.

84. Swanson, J.W., and Dall, F.C., "On the Dielectric Strength of Synthetic Electrical Insulating Materials," Conference Record of 1976 IEEE International Symposium of Electrical Insulation, Sponsored by the IEEE Electrical Insulation Society, p. 196, Institute of Electrical and Electronics Engineers, Inc., New York, 1976.

85. Estey, R.S., *Measurement of Solar and Simulator Ultraviolet Spectral Irradiance*, JPL Document 5101-58, Jet Propulsion Laboratory, Pasadena, California, March 15, 1978.

86. Ware, J.C., "Clear Sky Temperature," presented at ISES Meeting, Fort Collins, Colorado, August 1974.

APPENDIX

Glossary

AR	antireflective
n-BA	n-butyl acrylate
CA	cellulose acetate
CER	controlled environmental reactor
DRIFT	diffuse reflectance infrared spectroscopy
EMA	ethylene methyl acrylate
EPDM	ethylene propylene (diene monomer) rubber
ESB	electrostatic bonding
EVA	ethylene vinyl acetate
FSA	Flat-Plate Solar Array (Project)
HALS	hindered amine light stabilizer
IPN	interpenetrating network
IR	infrared
I_{sc}	short-circuit current
JPL	Jet Propulsion Laboratory
MMA	methyl methacrylate
NOCT	normal operating cell temperature
OPTAR	outdoor photo-thermal aging racks
PMMA	polymethyl methacrylate
P-n-BA	poly-n-butyl acrylate
PU	polyurethane
PV	photovoltaic(s)
PVB	polyvinyl butyral
PVF	polyvinyl fluoride
R&D	research and development
RH	relative humidity
RTV	room-temperature vulcanized
UV	ultraviolet
V DC	volt direct current

Prepared by the Jet Propulsion Laboratory, California Institute of Technology, for the U.S. Department of Energy through an agreement with the National Aeronautics and Space Administration.

The JPL Flat-Plate Solar Array Project is sponsored by the U.S. Department of Energy and is part of the National Photovoltaics Program to initiate a major effort toward the development of cost-competitive solar arrays.

More Technology Advancements

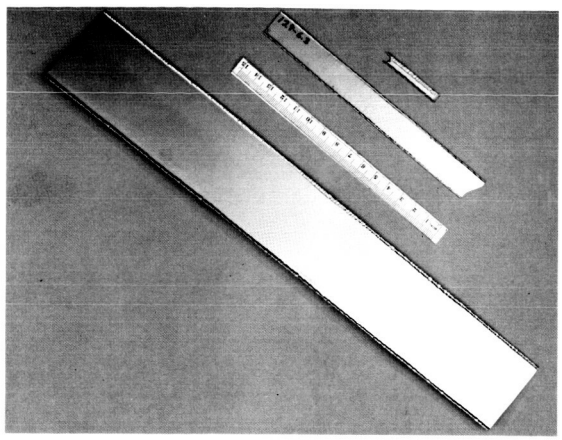

Dendritic web silicon ribbons are grown to solar-cell thickness. Progress is shown by experimental ribbons grown in 1976 and 1978 and a ribbon grown in a Westinghouse Electric Corporation pilot plant.

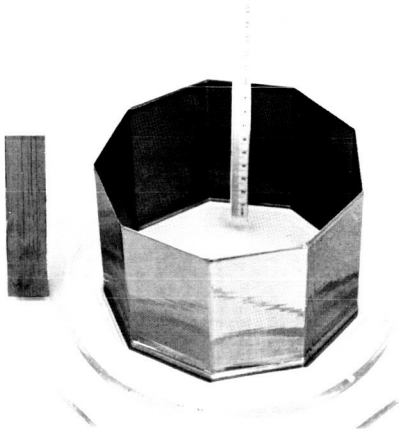

The edge-defined film-fed growth silicon ribbons are grown to solar-cell thickness. A DOE/FSA-sponsored research ribbon grown in 1976 is shown next to a nine-sided ribbon grown in a Mobil Solar Energy Corporation funded configuration.

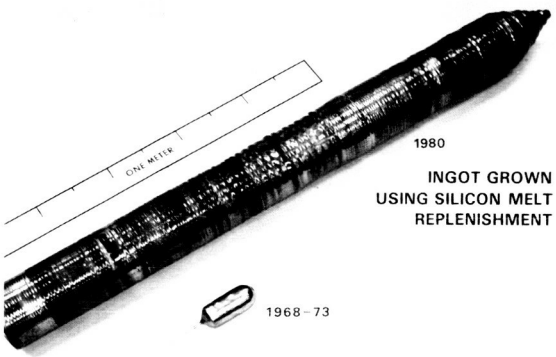

Czochralski silicon crystals as grown are sawed into thin circular wafers. (Support for this effort was completed in 1981.)

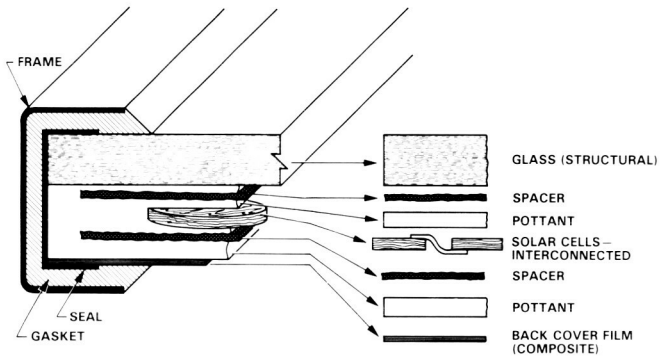

Typical superstrate module design is shown with the electrically interconnected solar cells embedded in a laminate that is structurally supported by glass. Materials and processes suitable for mass production have been developed using this laminated design.

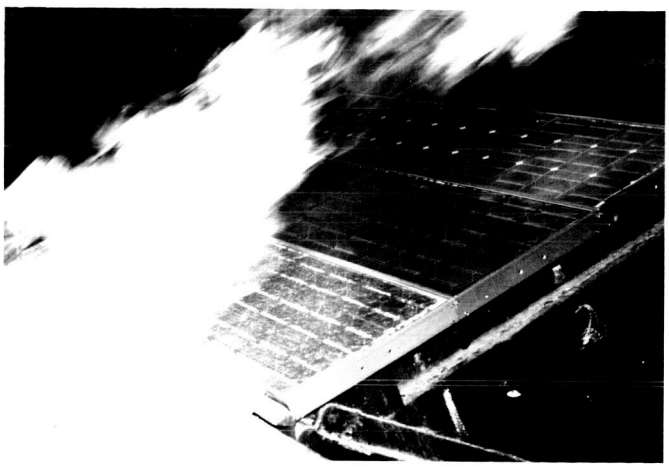

Prototype modules have passed UL 790 Class A burning brand tests which are more severe than this spread of flame test.

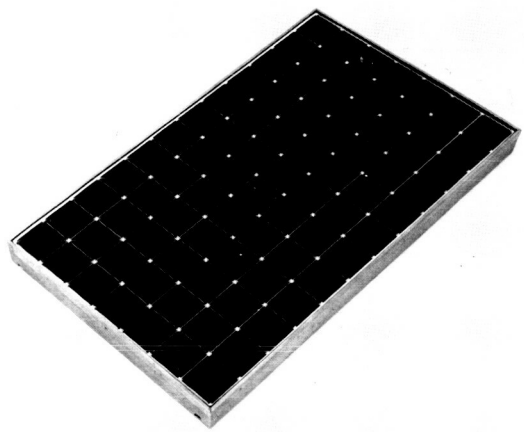

A 15.2% efficiency prototype module (21 x 36 in.) was made by Spire Corp. using float-zone silicon wafers. Recently, similarly efficient modules were fabricated from Czochralski silicon wafers.

Photovoltaic Applications

1975

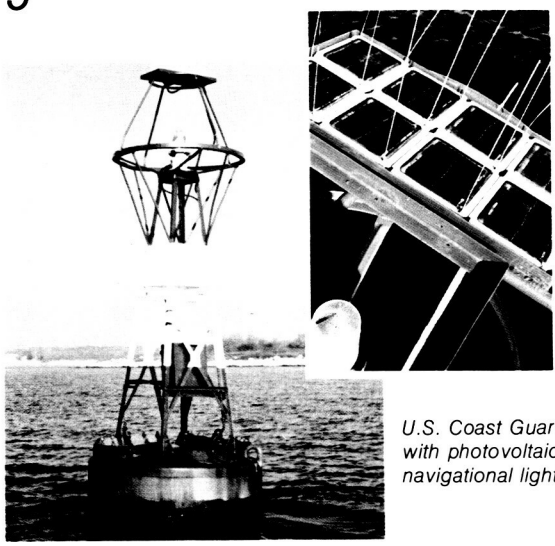

U.S. Coast Guard buoy with photovoltaic-powered navigational light.

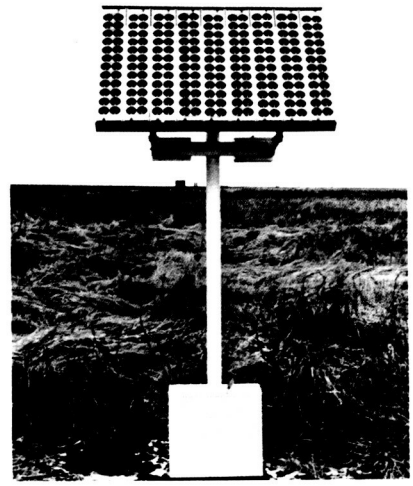

Photovoltaic-powered corrosion protection of underground pipes and wells.

Later...

House in Carlisle, Massachusetts, with a 7.3-kW photovoltaic rooftop array. Excess photovoltaic-generated power is sold to the utility. Power is automatically supplied by the utility as needed.

A 28-kW array of solar cells for crop irrigation during summer, and crop drying during winter (a DOE/University of Nebraska cooperative project).

1985

1.2 MW of photovoltaic peaking-power generation capacity for the Sacramento Municipal Utility District. (The 8 x 16 ft panels are mounted on a north-south axis for tracking the sun.)